SALP Service Altimetrie & Localisation Precise

CLS Collecte Localisation Satellites

cnes Centre National d'Études Spatiales

CalVal Jason-2

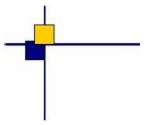

Jason-2 reprocessing impact on ocean data (cycles 001 to 145).

Comparison of Jason-2 Gdr-D with Gdr-T, as well as with Jason-1 Gdr-C and Envisat Gdr v2.1

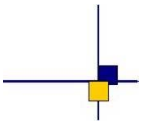

Reference : CLS.DOS/NT/12.222

Nomenclature : SALP-RP-MA-EA-22140-CLS

Issue : 2rev 1

Date : September 30, 2013

CLS - 8-10 Rue Hermès - Parc Technologique du Canal - 31520 Ramonville St-Agne - FRANCE
Phone 33 5 61 39 47 00 / Fax 33 5 61 75 10 14

Chronology Issues :		
Issue :	Date :	Reason for change :
1.0	15/12/2012	document created
1.1	25/02/2013	Updated after CNES review (Nicolas Picot)
2.0	29/03/2013	Updated with MLE3 vs MLE4 retracking results
2.1	30/09/2013	Updated after CNES review (Nicolas Picot)

People involved in this issue:				
	AUTHORS	**COMPANY**	**DATE**	**INITIALS**
WRITTEN BY	H. Roinard S. Philipps	CLS CLS		
CHECKED BY	S. D'Alessio	CLS		
APPROVED BY	J.P. Dumont	CLS CLS		
APPLICATION AUTHORISED BY				

Index sheet :	
Context	
Keywords	Jason-2, Jason-1, Calval, Reprocessing
hyperlink	

Distribution :		
Company	Means of distribution	Names
CLS/DOS	electronic copy	G. Dibarboure V. Rosmorduc J.P. Dumont
CNES	electronic copy	emilie.bronner@cnes.fr francoise.bailly-poirot@cnes.fr nicolas.picot@cnes.fr thierry.guinle@cnes.fr aqgp_rs@cnes.fr

List of tables and figures :

List of Tables

List of Figures

Contents

LIST OF ACRONYMS

AMR	Advanced Microwave Radiometer
DEM	Digital Elevation Model
ECMWF	European Center for Medium range Weather Forecasts
GDR-D	Geophysical Data Record version D
GDR-T	Geophysical Data Record version T
GMSL	Global Mean Sea Level
JMR	Jason-1 Microwave Radiometer
LTM	Long Term Monitoring
MQE	Mean Quadratic Error
MSL	Mean Sea Level
MSS	Mean Sea Surface
MWT	Model Wet Troposphere
POE	Precise Orbit Ephemeris
PRF	Pulse Repetition Frequency
RWT	Radiometer Wet Troposphere
SLA	Sea Level Anomalies
SSB	Sea State Bias
SSH	Sea Surface Height
SWH	Significant Wave Height

1. Introduction

Since the launch of the Jason-2 satellite on 20th of June 2008, the Gdr (Geophysical Data Record) data were distributed in version T (see GdrT product disclaimer [7]). The OSTST community requested (during the OSTST meetings of 2009, 2010, and 2011) several modifications in order to correct for some problems in the GdrT and to improve several standards. After taking into account these requests, the reprocessing of the Jason-2 mission in Gdr-D version started in April 2012. It has been performed within the frame of the CNES Altimetry Ground Segment (SALP) activities (SALP contract N ° 104685/00).
A first overview of the impact of the GdrD version of Jason-2 altimeter system over ocean was performed over the formation flight phase (cycles 001 to 020) spanning the period from 12th of July 2008 to 26th of January 2009 [14]. The present global report deals with the complete reprocessed period (cycles 1 to 145) of the Jason-2 mission, thanks to comparison with previous Jason-2 GdrT standard, as well as comparison with Jason-1 and Envisat data. It also contains the impact of the reprocessing on the mean sea level trend. Note that the operational version of Jason-2 GDR switched to standard D from cycle 146 onwards (for IGDR, from cycle 150 onwards).

The report is split into 6 main sections, after this introduction describing the keys of the reprocessing campaign:

- first, the **data used** are presented, with a status of the geophysical content of the fields that have changed between GdrT and GdrD.
- the **data coverage** and measurement validity issues are then presented.
- a global **overview** of the performances improvement is then synthetized.
- then, the **impact of the reprocessing on the main altimeter and radiometer parameters** is presented.
- and finally the impact of the reprocessing on **Mean Sea Level** issues, through cross calibration results, is detailed on the **global** and **regional** drift
- An additional part concerns the analysis of the differences between the MLE3 and MLE4 retracking data.

Though Jason-2 GdrD products contain (in addition to the MLE4 retracking algorithm outputs) also outputs from the MLE3 retracking algorithm, except on the dedicated MLE3 retracking analysis chapter, only the data from MLE4 retracking algorithm are analysed.

2. Data used and processing

2.1. Data used

This document deals with the global impact of Jason-2 altimeter mission reprocessing (cycle 001 to 145 covering the period from 12th of July 2008 to 18th of June 2012). Yet, for any information concerning the historical data, please refer to the Jason-2 yearly reports [13]. From cycle 146 onwards, the operational version of the Jason-2 GDR products have only been computed in version D.

2.2. Particular WARNINGS for this standards version:

Note: several (especially) ascending passes have a time tag shifted (compared to GdrT version) by about 0.051 seconds. Positions (latitude, longitude) are also different. This implies that altimeter and radiometer parameters are also different for these passes. Performances of GdrD version are good, number of edited measurements is slightly higher than in GdrT version. But when comparing both versions, differences are not only due to evolutions from GdrT to GdrD version, but also due to the time tag and position differences. The compression of 20 Hz data to 1 Hz data is shifted by a 20 Hz measurement. Note that time tag differences (shift of elementary 20 Hz measurements used for 1 Hz data) are regularly observed between Ogdr and Igdr data. Note that from cycle 52 onwards, the number of passes with this kind of time tag differences between GdrT and GdrD is lower than from cycles 1 to 51: it is probably due to a more coherent SPA software version (GdrT were computed using SPA version 2 until cycle 51, and in SPA version 3 afterwards).

Note: as in GdrT version, some passes are impacted by low signal tracking anomaly before upload of correction on 2008-12-10 (Cycle 016 - pass 073).

2.3. GDR Standards

The Jason-2 GdrD data are generated using the SPA software version 3-4-1p2.

Model	Product Version "T"	Product Version "D"
Orbit	EIGEN-GL04S with time-varying gravity (annual and semi-annual terms up to deg/ord 50) + ITRF 2005 DORIS+SLR+GPS	EIGEN-GRGS_RL02bis_MEAN_FIELD with time-varying gravity (annual, semi-annual, and drifts up to deg/ord 50) + ITRF 2008 DORIS+SLR+GPS (increased weight for GPS)
Altimeter Retracking	MLE4 + 2nd order Brown model : MLE4 simultaneously retrieves the 4 parameters that can be inverted from the altimeter waveforms: epoch, SWH, Sigma0 and mispointing angle. This algorithm is more robust for large off-nadir angles (up to 0.8°).	Identical to version "T", in addition altimeter parameters are also available using MLE3 retracking
Altimeter Instrument Corrections	Consistent with MLE4 retracking algorithm.	One consistent with MLE4 retracking + One consistent with MLE3 retracking
Jason-2 Microwave Radiometer Parameters	Using calibration parameters derived from long term calibration tool developed and operated by NASA/JPL	Using calibration parameters derived from long term calibration tool developed and operated by NASA/JPL + enhancement in coastal regions + correction of anomaly in 34 GHz channel addition of radiometer rain and ice flag addition of radiometer 18.7 GHz/ 23.8 GHz/ 34 GHz antenna gain weighted land fraction in main beam
Dry Troposphere Range Correction	From ECMWF atmospheric pressures and model for S1 and S2 atmospheric tides.	Identical to version "T"
Wet Troposphere Range Correction from Model	From ECMWF model.	Identical to version "T"
Back up model for Ku-band ionospheric range correction.	Derived from JPL's Global Ionosphere Model (GIM) maps	Identical to version "T"

.../...

Model	Product Version "T"	Product Version "D"
Sea State Bias Model	Empirical model derived from 3 years of Jason-1 MLE4 altimeter data with version "b" geophysical models	Empirical models derived from Jason-2 data (One consistent with MLE4 retracking + One consistent with MLE3 retracking)
Mean Sea Surface Model	CLS01	CNES_CLS_2011
Geoid	EGM96	Identical to version "T"
Bathymetry Model	DTM2000.1	Identical to version "T"
Mean Dynamic Topography	Rio 2005 solution	CNES_CLS2009 solution
Inverse Barometer Correction	Computed from ECMWF atmospheric pressures after removing model for S1 and S2 atmospheric tides.	Identical to version "T"
Non-tidal High-frequency De-aliasing Correction	Mog2D high resolution ocean model. Ocean model forced by ECMWF atmospheric pressures after removing model for S1 and S2 atmospheric tides.	Identical to version "T"
Tide Solution 1	GOT00.2 + S1 ocean tide . S1 load tide ignored.	GOT4.8 (S1 ocean tide and S1 load tide are included).
Tide Solution 2	FES2004 + S1 and M4 ocean tides. S1 and M4 load tides ignored	Identical to version "T"
Equilibrium long-period ocean tide model.	From Cartwright and Taylor tidal potential.	Identical to version "T"
Non-equilibrium long-period ocean tide model.	Mm, Mf, Mtm, and Msqm from FES2004.	Mm, Mf, Mtm, and Msqm from FES2004 + correction for a bug
Solid Earth Tide Model	From Cartwright and Taylor tidal potential.	Identical to version "T"
Pole Tide Model	Equilibrium model.	Equilibrium model + correction of error which was present over lakes and enclosed seas.
Wind Speed from Model	ECMWF model	Identical to version "T"

.../...

Model	Product Version "T"	Product Version "D"
Altimeter Wind Speed	Table derived from Jason-1 GDR data.	Table is identical to version "T", but the inputs differ.
Altimeter Rain Flag	Set to default values	Derived from Jason-2 sigma naught MLE3 values
Altimeter Ice Flag	Flag based on the comparison of the model wet tropospheric correction and of a radiometer bi frequency wet tropospheric correction (derived from 23.8 GHz and 34.0 GHz), accounting for a backup solution based on climatologic estimates of the latitudinal boundary of the ice shelf, and from altimeter wind speed.	Identical to version "T"
Update of the altimeter characterization file		PRF value is no longer truncated (2058.513239 Hz) Bias of 18.092 cm applied for Ku- and C-band range (corrects the value of the distance between center of gravity and the reference point of the altimeter antenna). Note that this bias is not applied on ice retracking. Antenna aperture angle (at 3 dB) changed to 1.29 deg MQE setting is applied during 20 Hz to 1 Hz compression Tracker_range_res at a more precise value
other	LTM calculated over 1 day	LTM calculated over 7 days (sliding window) and applied for one day. the origin of the constant part of the time tag bias was found and is directly corrected in the Gdr-D datation.

Table 1: *M*odels and standards adopted for the Jason-2 product version "T", and "D"

2.4. Jason-1 data used for comparison

The formation flight phase (cycles 001 to 020) is specially suited for intercomparison between Jason-2 and Jason-1, as both satellites were only 55 seconds apart on the same ground track. A special report, dedicated to the formation flight phase analysis has been written in July 2012 [14]. In the current report, Jason-1 GdrC standard was used to compare to Jason-2, but several corrections for Jason-1 were as much as possible updated to be as homogeneous as possible with the Jason-2 reprocessed data. The following corrections were therefore updated for Jason-1 (when compared to Jason-2 GdrD):

- POE orbit standard D provided by CNES
- GOT 4.8 ocean tide
- Mean Sea Surface CNES_CLS_2011
- Use of JMR replacement products (which correct for stabilization problems that occured just after the August 2008 safe-hold, for Jason-1 cycles 228 to 259)

Note that sea state bias correction is the one of the product, not the latest version presented in [18]. Note, that for several cycles, comparisons between Jason-2 and Jason-1 are not relevant, as Jason-1 data were absent (satellite safe-hold mode or altimeter switched off during the period of ground track change). This is for example the case for Jason-2 cycles 003, 004, 044, and 045 where Jason-1 was several days (or the whole cycle) in safe-hold mode.

2.5. Envisat data used for comparison

In this report, Envisat Gdr v2.1 standard (from 2011 Envisat RA-2 reprocessing) was used to compare to Jason-2, but several corrections for Envisat were as much as possible updated to be as homogeneous as possible with the Jason-2 reprocessed data. The following corrections were therefore updated for Envisat (when compared to Jason-2 GdrD):

- POE orbit standard D provided by CNES
- GOT 4.8 ocean tide
- Mean Sea Surface CNES_CLS_2011
- Use of PTR computed by F-Pac team, similar to the one available from isardSAT computation at the following adress: ftp://diss-nas-fp.eo.esa.int under the directory : altimetry_dataset_v2.1. [9]

Note that sea state bias correction is the one of the product, not the latest version presented in [18]. Note that wet troposphere correction is the one of the product. For further information of the Envisat Gdr v2.1 standard, see the validation report of the Envisat RA-2 reprocessing [11].

3. Missing and edited measurements

This part consists in analyzing the availability of data for level 2 products over oceans before and after the reprocessing exercise. Furthermore the edited (invalidated) measurements are monitored.

3.1. Missing measurements

The reprocessed GdrD data are globally as available as the GdrT data set (see figure 1). Most missing data during the formation flight phase were and are still missing due to acquisition stations problems, as explained on the cyclic validation reports [see Tab 2].

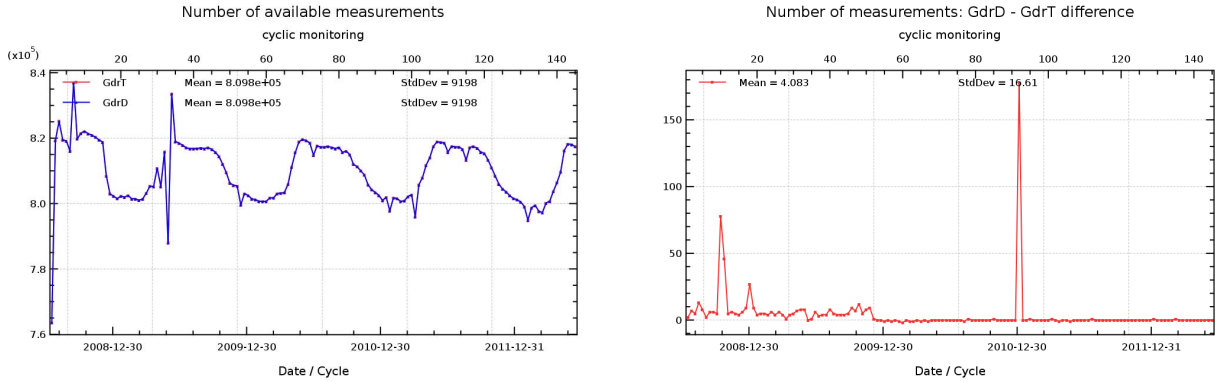

Figure 1: ***Left:*** *Number of data available.* ***Right:*** *Number of data difference GdrD - GdrT.*

As there was a change on SPA Processing Pilot on cycle 52 during GdrT processing (from V2-3 to V3-0), the number of measurements is more coherent between GdrT and GdrD (using SPA Processing Pilot V3-4-1) data from cycle 52 onwards (see the right side of figure 1).

For some cycles there are more data in the GdrD product than in the GdrT products. These **additional data** concern:

- On cycle 010, there are 0.02% of missing points versus 0.04% with previous product.
  On pass 177 (near Indonesia) there are a few missing measurements over ocean (several times approximately 10 seconds). This was already the case in Gdr-T. Nevertheless a small portion of these missing measurements is now available in Gdr-D. Note that pass 176 (South Atlantic) in Gdr-T had also a few missing ocean measurements (several times approximately 10 seconds). These data are now available in Gdr-D.
- On cycle 011, there are 0.04% of missing points versus 0.05% with previous product.
  On several passes there are a few missing measurements over ocean (several times approximately 10 seconds) (already encountered in Gdr-T). Nevertheless on pass 049 the few measurements which were missing in Gdr-T, are now present in Gdr-D.
- On cycle 018, less than 0.01% of additional points compared to the previous product.
- On cycle 092, additional available points on GdrD on pass 001 (mostly over land), and on pass 016.

Jason-2 Cycles		Events leading to missing data
Cycle 001		Passes 45 and 49 are completely missing, several passes are partly missing. This was already the case for GdrT products. Hereafter some details :
	2008-07-13 between 17:40:00 and 19:37:30	Missing telemetry : Usingen acquisition station problem. Pass 045 is completely missing, and passes 044 and 046 are partly missing with respectively 97% and 12% of missing measurements over ocean.
	2008-07-13 between 21:38:29 and 23:30:00	Missing telemetry : NOAA acquisition station problem. Pass 049 is completely missing and passes 048 and 050 are partly missing with respectively 85% and 6% of missing measurements over ocean.
	2008-07-16 and 2008-07-17	upload of DEM on 16th and 17th July (plannified unavailability), in consequence several passes between pass 109 and 139 are partly missing (over North Atlantic ocean and Europe)
	2008-07-17 between 13:22:21 and 13:31:56	there is a data gap at the transition between passes 141 and 142 due to altimeter restart
	2008-07-17 between 15:19:01 and 15:30:22	there is a data gap in pass 144 due to altimeter restart (just before start of Median mode)
Cycle 003	2008-08-02 between 02:23:57 and 05:46:54	Due to missing telemetry :Usingen acquisition station problem, passes 33 and 34 are completely missing and passes 32 and 35 are partially missing with respectively 100% and 91.5% of missing ocean measurements. This was already the case for GDR-T data.
Cycle 005	2008-08-29 21:47:26 and 2008-08-30 02:52:06	Due to missing telemetry : Usingen acquisition station problem, passes 237 to 240 are completely missing and passes 236 and 241 are partly missing with respectively 67.9% and 80.6% of missing measurements over ocean. This was already the case for GdrT.
Cycle 006		Due to calibrations, 2 passes are partly missing :
	2008-09-08 between 15:48:00 and 16:21:21	pass 232 has 65.5% of missing measurements over ocean due to altimeter calibration (long LPF)
	2008-09-08 between 18:53:00 and 19:19:09	pass 235 has 8.3% of missing measurements over ocean due to altimeter calibration (CNG step)
	.../...	

Jason-2 Cycles		Events leading to missing data
Cycle 010		No missing pass, but on pass 177 (near Indonesia) there are a few missing measurements over ocean (several times approximately 10 seconds). This was already the case in Gdr-T. Nevertheless a small portion of these missing measurements is now available in Gdr-D. Note that pass 176 (South Atlantic) in Gdr-T had also a few missing ocean measurements (several times approximately 10 seconds). These data are now available in Gdr-D.
Cycle 011		No missing pass, but on several passes there are a few missing measurements over ocean (several times approximately 10 seconds) (already encountered in Gdr-T). Nevertheless on pass 049 the few measurements which were missing in Gdr-T, are now present in Gdr-D.
Cycle 016	10/12/2008 between 15:11:19 and 15:13:27	No missing pass, but pass 073 is partly missing (as in Gdr-T) on 2008-12-10 due to upload of correction for low signal tracking anomaly and following memory dumps (planned unavailability).
Cycle 026	18/03/2009 between 05:09:15 and 05:10:44	pass 33 has approximatly 90 seconds of missing ocean measurements (4.54%) in gulf of guinea (probably due to missing telemetry)
Cycle 029	23/04/2009 between 20:18:36 and 20:35:11	data gap over land (on transition between passes 209 and 210) due to missing telemetry
Cycle 031	11/05/2009 12:09 to 14/05/2009 13:09	Upload of new DEM leading to missing portions (northern hemisphere) for passes 154 to 231
Cycle 033	02/06/2009 between 06:55:11 and 15:58:05	Passes 205 to 212 are completely missing. Passes 204 and 213 are partly missing with respectively 100% and 96% of missing measurements over ocean. This is due to software upload to Poseidon-3.
Cycle 034	13/06/2009 between 07:07:03 and 07:40:23 13/06/2009 between 10:11:41 and 10:37:50	Due to long calibration, pass 232 is partly missing with 65% of missing measurements over ocean. Due to calibration CNG step, pass 235 is partly missing with 8% of missing measurements over ocean.
Cycle 037	06/07/2009 between 02:33:12 and 02:34:33	pass 054 has a small data gap due to missing PLTM
Cycle 039		pass 105 has a 20seconds data gap in indian ocean due to missing telemetry
Cycle 053	11/12/2009 between 20:38:19 and 21:29:43	passes 57 and 58 have a data gap due to Gyro calibration

.../...

Jason-2 Cycles		Events leading to missing data
	18/12/2009 between 16:39 and 17:12	pass 232 has a data gap due to CAL2 calibration (65% of missing ocean measurements)
	18/12/2009 19:43	pass 235 has a data gap due to CNG calibration (mostly over land, 8% of missing ocean measurements)
Cycle 066		As in GdrT, there is a few data gaps on pass 249 (West of New-Zealand)
Cycle 072	23/06/2010 between 19:15:37 and 19:16:59	pass 199 has small data gap due to missing telemetry
Cycle 073	05/07/2010 between 00:09:33 and 00:42:54	pass 232 has a data gap due to CAL2 calibration (65.43% of missing ocean measurements)
	05/07/2010 between 03:14:11 and 03:40:20	pass 235 has a data gap due to CNG calibration (mostly over land, 8.33% of missing ocean measurements)
Cycle 081	16/09/2010 between 16:40:22 and 16:52:48	pass 087 has a data gap (16.04% of missing ocean measurements) due to upload of DEM update (for GAVDOS transponder calibration)
	22/09/2010 between 13:07:27 and 13:18:12	pass 237 has a data gap (7.47% of missing ocean measurements) due to upload of DEM update (for GAVDOS transponder calibration)
Cycle 084	14/10/2010 between 06:02 and 06:21:15	pass 031 and 032 have a data gap due to calibrations (8.2% of missing ocean measurements)
	14/10/2010 between 17:00:57 and 17:02:39	pass 043 has a small data gap due to missing PLTM (3.8% of missing ocean measurement)
Cycle 086	03/11/2010	pass 034 has a data gap due to missing PLTM (3.78% of missing ocean measurements)
Cycle 094	29/01/2011 between 04:50 and 04:55	pass 231 : Calibration CAL1 (14% of missing ocean data)
	29/01/2011 between 05:38 and 06:11	pass 232 : Calibration CAL2 (65% of missing ocean data)
	29/01/2011 between 08:37 and 09:03	pass 235 : Calibration CNG (mostly over land, 9% of missing ocean data)
Cycle 101	04/04/2011 between 18:49:08 and 21:03:48	Telemery outage at Usingen, passes 133 to 135 have respectively 23%, 100%, and 91% of missing ocean data
Cycle 110	04/07/2011 between 00:27:29 and 01:27:29	Gyro calibration. Passes 158 and 159 have respectively 18% and 88% of missing ocean data
	.../...	

Jason-2 Cycles		Events leading to missing data
Cycle 115	25/08/2011 between 11:07:35 and 11:40:56	pass 232 : Calibration CAL2: 65% of missing ocean data
	25/08/2011 between 14:12 and 14:38	pass 235 : Calibration CNG: mostly over land, 8% of missing ocean data
Cycle 132	10/02/2012 between 00:42:26 and 01:14:03	pass 232 : Calibration CAL2: 65.43% of missing ocean data
	10/02/2012 between 03:47:11 and 04:13:20	pass 235 : Calibration CNG: mostly over land, 8.33% of missing ocean data
Cycle 135		pass 105 is partly missing: 53.77% of global missing measurements, 24.80% over ocean, due to technical problem and operator error
Cycle 136	19/03/2012 between 02:01:49 and 02:58:01	A part of pass 191 is missing (55.86% of missing measuremetns over sea) due to a problem of ACK.
Cycle 145	14/06/2012 between 11:41:15 and 11:42:58	pass 143 partly missing due to missing PLTM
	18/06/2012 between 13:20:10 and 13:21:29	pass 248 partly missing

Table 2: *M*issing passes, from cycle 001 to cycle 145

3.2. Edited measurements

3.2.1. Overview

Data editing is necessary to remove altimeter measurements having lower accuracy. Once data over land are excluded, it consists in:

- First: removing the data corrupted by sea ice and ice.
- Then, removing the measurements out of thresholds tuned for several parameters. The applied thresholds can be found in the Jason-2 User Handbook ([6]).
- The third step uses cubic splines adjustments to the Jason-2 Sea Surface Height (SSH) to detect remaining spurious measurements.
- The last step consists in removing an entire pass if SSH-MSS mean and standard deviation have higher values than a certain threshold. This criterium is used to detect problems such as bad orbit quality or time tag problems. Nevertheless for Jason-2 GDR it has never edited data.

The percentage of edited data per cycle is monitored for GdrT and GdrD products on the left panel of figure 2. Note that the peak at cycle 019 is due to AMR unavailability (radiometer parameters set to default values).
The number of edited measurements is slightly increased for GdrD compared to GdrT (see right panel of figure 2). The number of measurements edited by sea ice flag is increased (left panel of figure 3). This is probably related to the use of MQE setting during 20 Hz to 1 Hz data compression (see chapter 5.4.1.). This can modify the number of elementary 20 Hz measurements. The modification of brightness temperatures might also impact the sea ice flag. Both radiometer wet troposphere correction and number of elementary range measurements are used in the sea ice algorithm.
Furthermore the number of measurements edited by altimeter parameters are higher in GdrD than in GdrT (such as on right panel of figure 3). This concerns especially regions with disturbed sea state like around Indonesia. This is probably related to the use of MQE thresholds during 20 Hz to 1 Hz compression. For GdrD, range_numval_ku has around Indonesia more often less than 10 values than for GdrT. In this case, range_ku is often at default value (see figure 4).

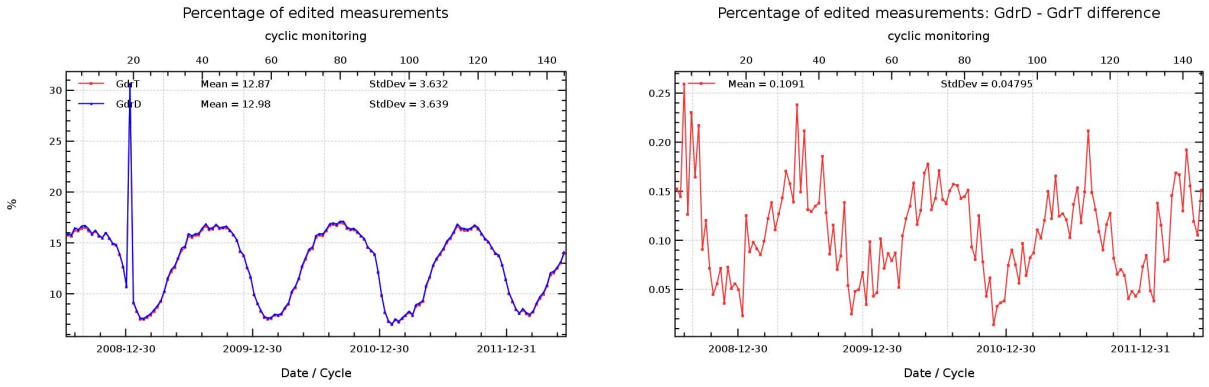

Figure 2: ***Left:*** *Percentage per cycle of rejected data in GdrT and GdrD.* ***Right:*** *Difference of percentage of rejected data (GdrD - GdrT).*

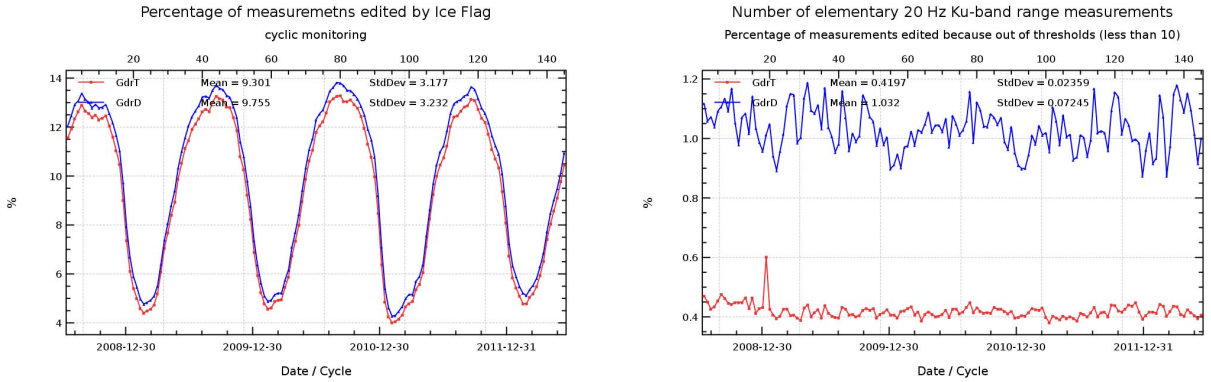

Figure 3: *Percentage per cycle of rejected data in GdrT and GdrD:* ***Left:*** *due to sea ice presence* ***Right:*** *due to number of elementary 20 Hz Ku-band range measurements out of threshold (less than 10).*

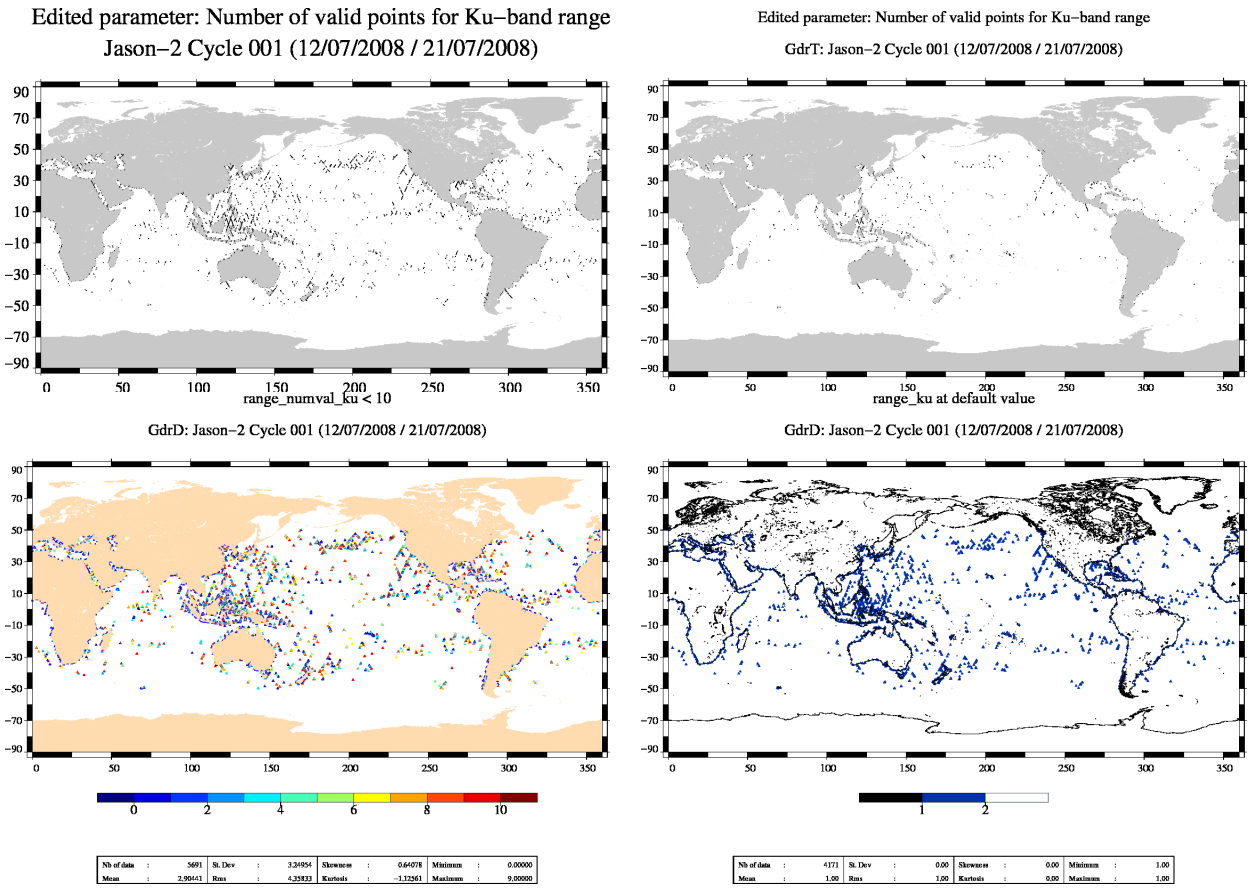

Figure 4: ***Top:*** *Maps of invalidated range_numval_ku for GdrD (left) and GdrT (right) for cycle 001.* ***Bottom left:*** *: Map where range_numval_ku has values less than 10 for GdrD.* ***Bottom right:*** *Map where range_ku for GdrD has default values.*

3.2.2. Particular editing events

Note: as in GdrT version, some passes are impacted by low signal tracking anomaly before the upload of a correction on 2008-12-10 (Cycle 016 - pass 073). During the low signal tracking anomaly the altimeter parameters are edited as they are out of thresholds. For more information see the Jason-2 annual report ([13]). In addition, because of meteorological conditions, some parts of passes are sometimes rejected because of parameters out of thresholds; and because of meteorological conditions, maneuvers and star tracker anomalies, some parts of passes have sometimes parameter values higher than usual, but still within thresholds.

Jason-2 Cycles	Events
Cycle 001	As in GdrT, some passes are impacted by low signal tracking anomaly Jason-2 used DIODE/SGT mode till 2008-07-17 15 :30 (pass 144), after this time it used DIODE/Median mode
Cycle 002	As in GdrT, some passes are impacted by low signal tracking anomaly
Cycle 003	**Jason-2 used DEM mode during this cycle**.
Cycle 004	As in GdrT, some passes are impacted by low signal tracking anomaly
Cycle 005	**Jason-2 used DEM mode during this cycle**.
Cycle 006	As in GdrT, some passes are impacted by low signal tracking anomaly
Cycle 007	**Jason-2 used DEM mode during this cycle**.
Cycle 008	As in GdrT, some passes are impacted by low signal tracking anomaly
Cycle 009	As in GdrT, some passes are impacted by low signal tracking anomaly
Cycle 010	As in GdrT, some passes are impacted by low signal tracking anomaly
Cycle 011	As in GdrT, some passes are impacted by low signal tracking anomaly
Cycle 012	As in GdrT, some passes are impacted by low signal tracking anomaly
Cycle 013	As in GdrT, some passes are impacted by low signal tracking anomaly
Cycle 014	As in GdrT, some passes are impacted by low signal tracking anomaly
Cycle 015	As in GdrT, some passes are impacted by low signal tracking anomaly
Cycle 016	As in GdrT, some passes are impacted by low signal tracking anomaly
Cycle 019	from 2009-01-07 11:00:35 to 2009-01-08 03:23:34, passes 024-042 completely edited and passes 24 and 42 are partly edited because of radiometer wet troposphere correction at default value due to AMR unavailability

.../...

Jason-2 Cycles	Events
	from 2009-01-11 03:56:38 to 2009-01-12 19:26:14, passes 120-160 completely edited and passes 119 and 161 are partly edited because of radiometer wet troposphere correction at default value due to AMR unavailability
Cycle 034	**Jason-2 used DEM mode during this cycle**. (new version of DEM was uploaded during cycle 031).
Cycle 045	a part of pass 112 has default radiometer wet troposphere correction and defaulted 34GHz brightness temperature during a very short time (it was not the case in GdrT)
Cycle 047	a part of pass 112 has default radiometer wet troposphere correction during a very short time
Cycle 048	a part of passes 047 and 112 have default radiometer wet troposphere correction during a very short time
Cycle 051	a part of pass 112 has defaulted radiometer wet troposphere correction and defaulted 34 GHz brightness temperature during a very short time
Cycle 057	a part of pass 112 has defaulted radiometer wet troposphere correction and defaulted 34 GHz brightness temperature during a very short time (it was not the case in GdrT)
Cycle 060	as for GdrT products, the DORIS datation has been replaced by the GPS datation from 5am up to 10:35 am on the 18th of February.
Cycle 110	as in GdrT, a portion of pass 47 is edited by radiometer wet troposphere correction out of threshold or at default values (radio-frequency interference from a ground based source)

Table 3: *C*alVal output

3.2.3. Conclusion

Data availability of GdrD products is equivalent to the data availability of GdrT products. For some cycles, data which were missing in GdrT version, are present in GdrD version. Percentage of invalidated data is similar between GdrT and GdrD. Nevertheless, GdrD products have more edited data likely due to the use of MQE criterium during the 20 Hz to 1 Hz compression.

4. Quality overview/Performances

In this chapter the performances of Jason-2 GdrD data are analyzed at crossovers and along-track. Therefore comparison to previous GdrT version and Jason-1 data are done. Globally, the reprocessed data are improved in terms of availability (see Figure 1 in part 3.1.), homogeneity and performances (see Figure 5).

4.1. Performances at crossovers

Ascending / descending SSH (Sea Surface height) differences are computed at crossover points. These differences are computed for time differences less than 10 days between ascending and descending tracks. This allows us to minimize the contribution of the oceanic variability (mesoscale). Therefore the variance of the SSH differences at crossover points gives an information of the performance of the altimeter system. Computing the differences of these variances (using on the one hand GdrD data and on the other hand GdrT data), allows to measure the ability of the GdrD data to improve the computation of the SSH.

The main SSH calculation for Jason-2 are defined below:

$$SSH_{GdrD} = Orbit_{GdrD} - Altimeter\ Range_{GdrD} - \sum_{i=1}^{n} Correction\ GdrD_i$$

$$\begin{aligned}\sum_{i=1}^{n} Correction\ GdrD_i \quad = \quad & Dry\ troposphere\ correction \\ + \quad & Dynamical\ atmospheric\ correction \\ + \quad & Radiometer\ wet\ troposphere\ correction_{GdrD} \\ + \quad & Dual\ frequency\ ionospheric\ correction_{GdrD}\ (filter\ 250\ km) \\ + \quad & Non\ parametric\ sea\ state\ bias\ correction_{GdrD} \\ + \quad & GOT4.8\ ocean\ tide\ correction\ (including\ loading\ tide) \\ + \quad & Earth\ tide\ height \\ + \quad & Pole\ tide\ height\end{aligned}$$

$$SSH_{GdrT} = Orbit_{GdrC} - Altimeter\ Range_{GdrT} - \sum_{i=1}^{n} Correction\ GdrT_i$$

$$\begin{aligned}\sum_{i=1}^{n} Correction\ GdrT_i &= Dry\ troposphere\ correction \\ &+ Dynamical\ atmospheric\ correction \\ &+ Radiometer\ wet\ troposphere\ correction_{GdrT} \\ &+ Dual\ frequency\ ionospheric\ correction_{GdrT}\ (filter\ 250\ km) \\ &+ Non\ parametric\ sea\ state\ bias\ correction_{GdrT} \\ &+ GOT00\ ocean\ tide\ correction\ (including\ loading\ tide) \\ &+ Earth\ tide\ height \\ &+ Pole\ tide\ height\end{aligned}$$

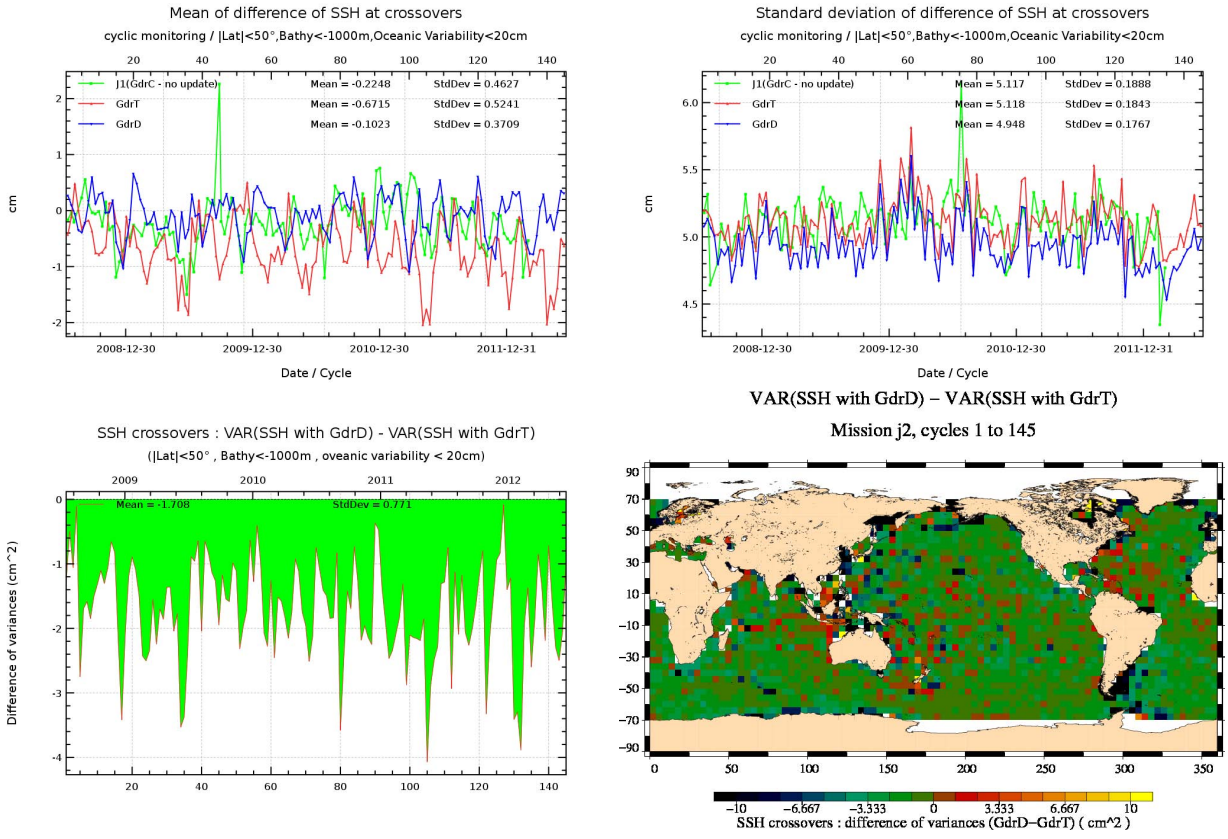

Figure 5: ***Top:*** *Cycle per cycle monitoring of mean* ***(left)*** *and standard deviation* ***(right)*** *of SSH difference at crossovers with GdrD (blue), GdrT (red) standards and Jason-1 GdrC standards (green).* ***Bottom left:*** *Difference of SSH variance at crossovers between GdrD and GdrT. Crossovers are only selected for open ocean (latitude less than ± 50°, bathymetry less than -1000 m and oceanic variability less than 20 cm).* ***Bottom right:*** *Map of difference of SSH variances (variance SSH_{GdrD} - variance SSH_{GdrT}).*

On Figure 5 (except for the map), a selection on $|latitude| < 50deg$, $bathy < -1000m$ and low variability areas has been done. The standard deviation of SSH differences is systematically lower

for GdrD than GdrT data, thus improving the coherence between ascending and descending passes (at time scales less than 10 days). The global SSH variance reduction (bottom of figure 5) is about 1.7 cm^2, with occasionnally reductions up to 3 cm^2. On Figure 6, showing the mean of ascending/descending SSH difference, the GdrD data improve also the coherence of ascending/descending SSH differences (geographic patterns are reduced). These improvements (variance reduction and a mean close to zero with reduced geographical patterns, which are signs of an improved coherence of ascending/descending passes) are mainly due to the new orbit solution (chapter 5.2.), the use of GOT4.8 tide instead of GOT00 tide (chapter 5.5.1.), and the modified datation used for GdrD data (chapters 4.1.2. and 5.1.).

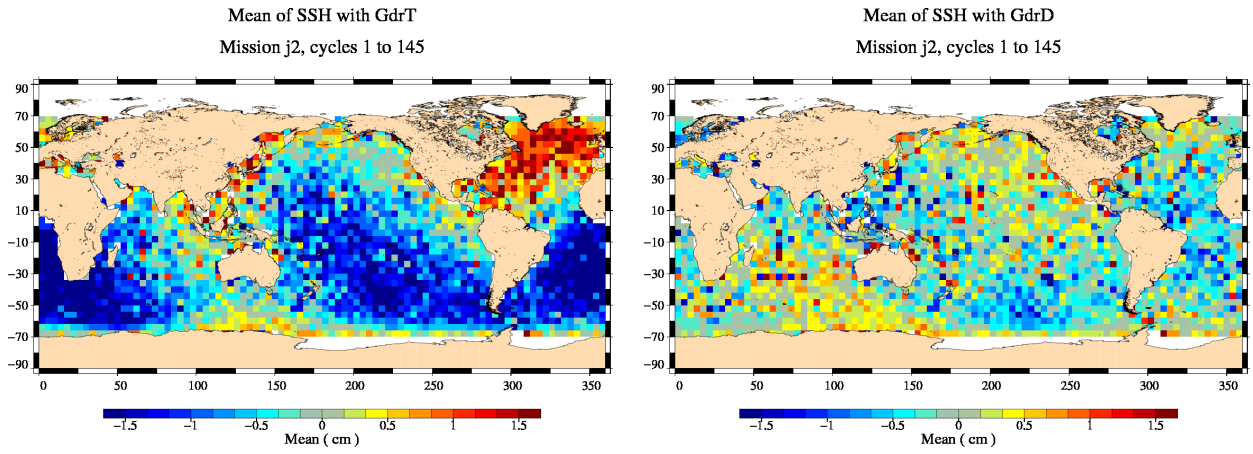

Figure 6: *Mean ssh crossovers differences:* ***Right:*** *with GdrD standards,* ***Left:*** *with GdrT standards*

4.1.1. Jason-1/Jason-2 and Envisat/Jason-2 SSH crossover differences

Figure 7 shows monitoring of multi-mission crossovers (between Jason-1 and Jason-2) using GdrT/GdrC standards for Jason-2/Jason-1 (red curve) or GdrD standard for Jason-2 and updated Jason-1 standards (GdrC product + GdrD orbit + GOT 4.8 ocean tide + JMR replacement product) for the blue curves (using radiometer wet troposphere for dark blue curve, and ECMWF model wet troposphere concerning light blue curve). The standard deviation between JA1/JA2 SSH crossovers (right of the figure) is reduced when using Jason-2 GdrD standards (+ updated Jason-1 standards). The mean of Jason-1 minus Jason-2 SSH crossover differences stays quite stable over the analyzed period, but on the left of figure 7, the jump that was visible for GdrT/GdrC data about Jason-2 cycle 69 is reduced. Instead, a small drift seems to appear between cycles 69 to 133. Using model wet troposphere instead of radiometer wet troposphere to compute Jason-1 minus Jason-2 differences of SSH crossovers, tends to be slightly lower and quite more stable.
Note that the change in the relative bias between Jason-1 and Jason-2 (-7.6 cm for GdrT/GdrC standards and +10.2 cm for GdrD/updated Jason-1 standards) comes mainly from the Jason-2 GdrD range (correction for 18.092 cm bias, as well as more precise PRF), but also from Jason-2 GdrD sea state bias and to a much lesser extent from Jason-2 GdrD dual-frequancy ionosphere correction.
Since Jason-1 move to a geodetic orbit, the mean of Jason-1 minus Jason-2 SSH difference shows a jump of about 7mm. It is mainly due to a more precise PRF value for Jason-1 since may 2012

(3.16mm), but also partly due to new JMR calibration file (about 1mm). Nevertheless, some millimeters of this jump remain unexplained, this is under investigation.

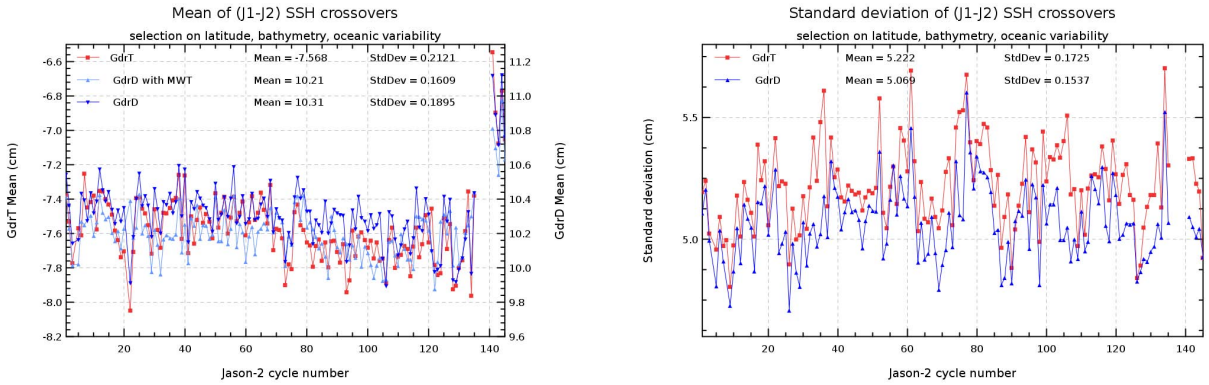

Figure 7: *Monitoring of mean* ***(left)*** *and standard deviation* ***(right)*** *of JA1-JA2 SSH crossovers.*

Figure 8 shows monitoring of multi-mission crossovers (between Jason-2 and Envisat) using $GdrT/Gdr_{beforeenvisatreprocessing}$ standards for Jason-2/Envisat (red curve) or GdrD standard for Jason-2 and updated Envisat standards (v2.1 product (from 2011 Envisat reprocessing) + POE orbit standard D + GOT 4.8 ocean tide + PTR corrected) for the blue curve. In order to allow comparison, the green curve represent cyclic mean of difference at J1/J2 crossovers computed with GdrCupdated Jason-1 data and GdrD Jason-2 data. The red curve shows a great variability as Envisat is not homogeneous before the reprocessing of the Envisat data (see [11]). After the Jason-2 and especially Envisat reprocessing, the cycle per cycle mean of SSH differences at Envisat/Jason-2 crossovers is much more homogeneous (blue curve), but shows still more variability than the curve from Jason-1/Jason-2 crossovers. Furthermore, the Envisat/Jason-2 curve after reprocessing of both satellite (blue curves) reveals a trough during year 2009 that is due to the PTR correction (see [9]). Note that there were geographical patterns on maps of difference of SSH at J2/EN crossovers that are greatly reduced using the most recent standards. This improvement is mainly due to the POE-D orbit solutions, see chapter 5.2..

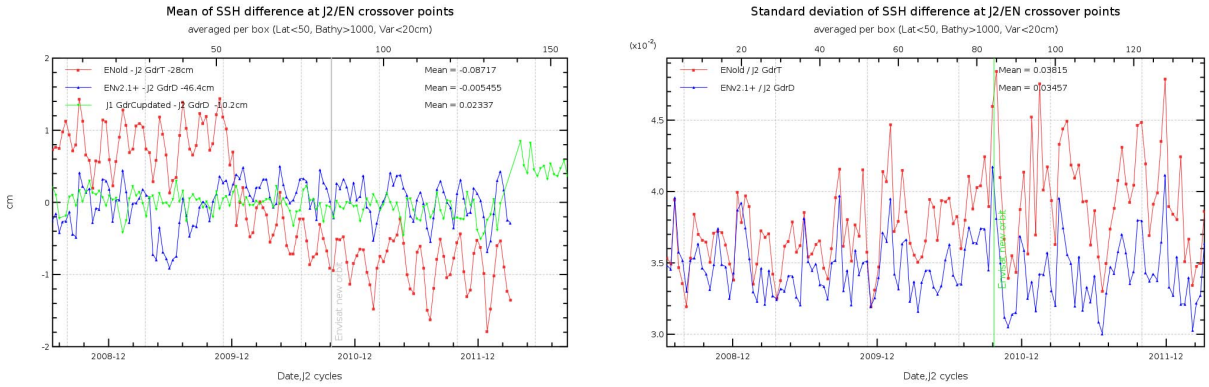

Figure 8: *Monitoring of mean* ***(left)*** *and standard deviation* ***(right)*** *of JA2-EN SSH crossovers. The curves on the left figure are centered around zero.*

4.1.2. Estimation of pseudo time-tag bias

The pseudo time tag bias (α) is found by computing at SSH crossovers a regression between SSH and orbital altitude rate ($\dot{H}$), also called satellite radial speed:

$$SSH = \alpha \dot{H}$$

This empirical method allows us to estimate the potential real time tag bias but it can also absorb other errors correlated with $\dot{H}$. Therefore it is called "pseudo" time tag bias. The monitoring of this coefficient estimated at each cycle is performed for Jason-1 and Jason-2 in figure 9. The curves are very similar highlighting an unexplained almost 59-day signal. The bias for Jason-2 GdrT is close to -0.29 ms. This bias explains a part of the geographical pattern visible on GdrT SSH crossover differences (left panel of figure 6): notably the small (north/south) hemispheric differences with maximal differences close to 8 mm where $\dot{H}$ is maximal (15 $m.s^{-1}$) at medium latitudes ($\pm 50^{\circ}$). The origin of this pseudo time tag bias was found by CNES [2], nevertheless the 59 day-signal is still unexplained (right of figure 9, see also dedicated splinter at OSTST 2010 [22]). However, a correction containing $\alpha\dot{H}$ in Jason-1 GDR-C products ([1]) has been already added to improve the Jason-1 SSH calculation, therefore the mean pseudo time tag bias for Jason-1 is close to zero. For Jason-2 GdrD data, the datation was directly modified in order to correct it properly. As shown on the left of figure 9, Jason-2 GdrD pseudo time tag bias is also close to zero (mean value).

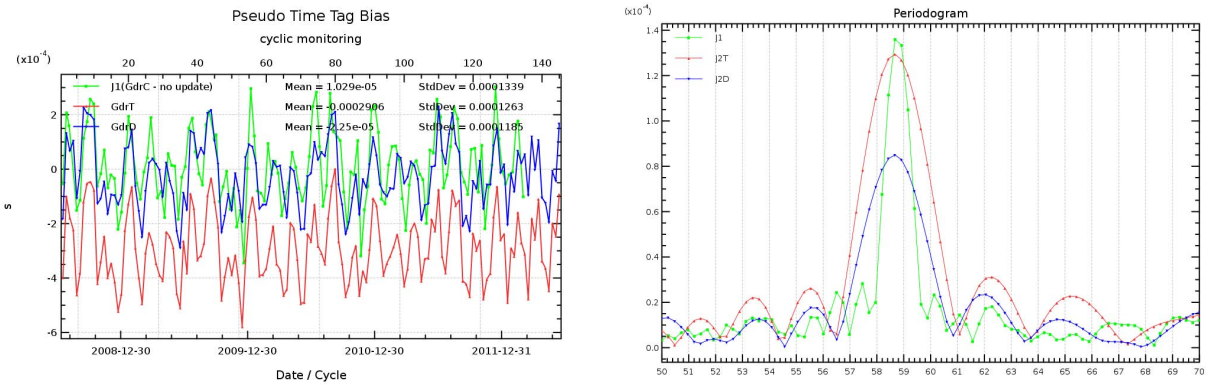

Figure 9: ***Left:*** *Cycle per cycle monitoring of pseudo time-tag bias estimated cycle by cycle from GDR products for Jason-2 (GdrT and GdrD) and Jason-1 (GdrC). Unit is in seconds.* ***Right:*** *Periodogram of pseudo time tag bias signal around 59days.*

4.2. Along-track performances of Sea Level Anomaly

4.2.1. SLA differences between GdrD and GdrT

The Sea Level Anomaly corresponds to the Sea Surface Height where the mean sea surface is removed (SLA = SSH - MSS). Due to the numberous changes (e.g. range, orbit, sea state bias, ...) between GdrT and GdrD data, their SLA are different.
The global difference between GdrD and GdrT SLA is around -18.1 cm. Figure 10 shows that the SLA was 20.7 cm for GdrT and is 2.6 cm with GdrD data. This difference is mainly due to a more precise PRF (more digits are taken into account), the bias of 18.092 cm (which corrects the value of the distance between center of gravity and the reference point of the altimeter antenna), as well as new sea state bias and modified dual-frequency ionosphere correction. On the right of the figure, the difference between SLA computed thanks to GdrD standards and SLA computed using GdrT standards shows an approximatively 60days signal mainly due to the change of ocean tide solution (tide got4.8 for GdrD versus got00 for GdrT).

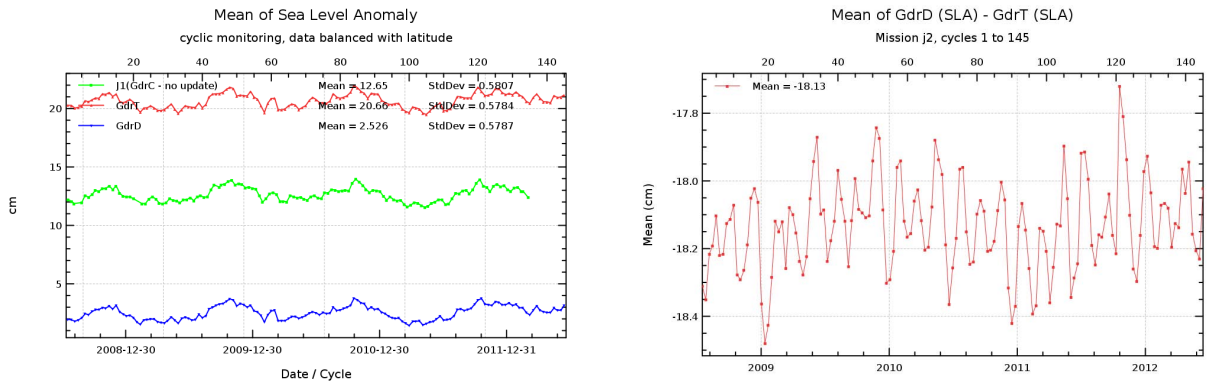

Figure 10: ***Left:*** *Cycle per cycle mean of SLA with GdrD (blue), GdrT (red) standards and Jason-1 standards (green).* ***Right:*** *Monitoring per cycle of the difference of GdrD SLA and GdrT SLA (data balanced according to the latitude).*

Mainly thanks to the new mean sea surface and the GOT4.8 global tide model, the standard deviation of GdrD SLA is reduced (figure 11, see also chapter 5.5.1. dedicated to the ocean tide).

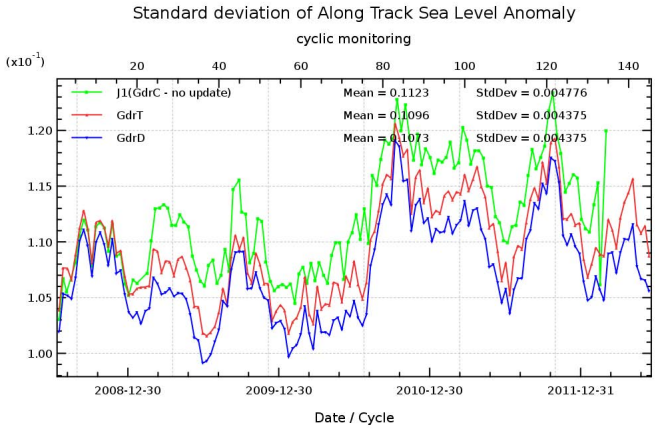

Figure 11: *Cycle per cycle standard deviation of along track SLA with GdrD (blue), GdrT (red) standards and Jason-1 standards (green).*

Besides the global bias between SLA of GdrT and GdrD, there are also geographical differences, which come mainly from orbit and sea state bias, see left panel of figure 12. Table 4 gives an overview of the global biases between GdrD and GdrT data for several parameters/corrections used in the SLA computation.

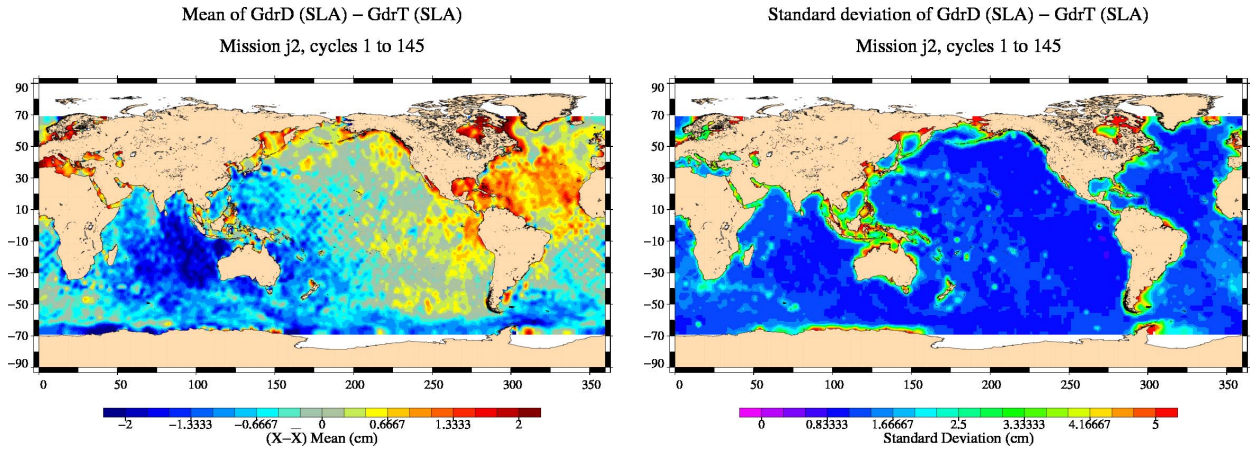

Figure 12: *GdrD-GdrT mean* ***(left)*** *and standard deviation* ***(right)*** *difference of SLA over cycles 001 to 145. Note that the map showing the mean difference between GdrD and GdrT SLA is centered around -18.1 cm.*

	Global (GdrD-GdrT) bias computed over 145 cycles	Regional bias
SLA	-18.13 cm	± 2cm
Orbit	$< 1mm$	± 1cm
Range	+15.34 cm	
Ionosphere	- 0.57 cm	± 0.2cm
Radiometer wet troposphere	$< 1mm$	-6mm near coasts ± 1mm far from coasts
Sea State Bias	+2.95 cm	-1cm / +0.4cm
Tide	$< 1mm$	low
Pole Tide Model		Impact over lakes and enclosed seas
MSS	+ 0.44 cm	± 1cm

Table 4: *M*ain biases of parameters/ corrections used in SLA between Jason-2 versions (GdrD - GdrT) for cycles 001 to 145.

4.2.2. SLA differences between JA1 and JA2

When comparing Jason-2 and Jason-1 SLA over the formation flight phase (cycle 001 to 020), using on the one hand Jason-2 GdrD and updated Jason-1 GdrC standards (right side of figure 13) and on the other hand Jason-2 GdrT and Jason-1 GdrC standards (without updates) (left side of figure 13), the differences between Jason-2 and Jason-1 are increased for the reprocessed data. The main geographical correlated differences between the two satellites come from the orbit (though for both, POE standard D was used) and the sea state bias (which is quite different for Jason-2 GdrD, see also chapter 5.4.8.). Indeed, when computing the SLA difference using an updated SSB correction for both satellites (from N. Tran [18] presented at OSTST 2012 meeting), the differences are slightly reduced (see bottom of figure 13), but still higher than for GdrT (JA2)/GdrC (JA2) comparisons.

As during the formation flight phase, both satellites were on the same ground track with only 55 seconds apart, the satellites observe the same ocean under the same environmental conditions and differences of uncorrected SLA (Orbit -Range - MSS) can directly be made between Jason-1 and Jason-2. This is shown on figure 14. For GdrD standard the differences between Jason-2 and Jason-1 are reduced when only considering uncorrected SLA in comparison to differences of corrected SLA (right side of figure 13), proving that most of the differences of Jason-2 and Jason-1 come from the different standards of corrections used for Jason-2 and Jason-1, especially the sea

state bias. Nevertheless, also for uncorrected SLA, the difference between Jason-2 and Jason-1 increases when using Jason-2 GdrD and updated Jason-1 GdrC (updated with MSS 2011 and POE-D orbit). A small part of the differences is probably due to the approximation in pseudo time tag bias for Jason-1, whereas the correction is correctly applied for Jason-2 data (see 4.1.2.). Note that due to reduced GPS availability, Jason-1 orbit is for this time period rather a Doris/ Laser orbit, than a Doris/ Laser/ GPS orbit. The bottom of figure 14 shows a difference map using a dedicated Doris/Laser POE for Jason-2, in order to put Jason-2 in the same conditions as Jason-1 (no GPS for this period). The map shows reduced patterns when compared to the use of the DORIS/Laser/GPS orbit (GdrD) for Jason-2 (right of figure 14), but has still increased patterns when compared to GdrT (JA2)/GdrC (JA1) difference map which used the POE-C standard (left of figure 14).

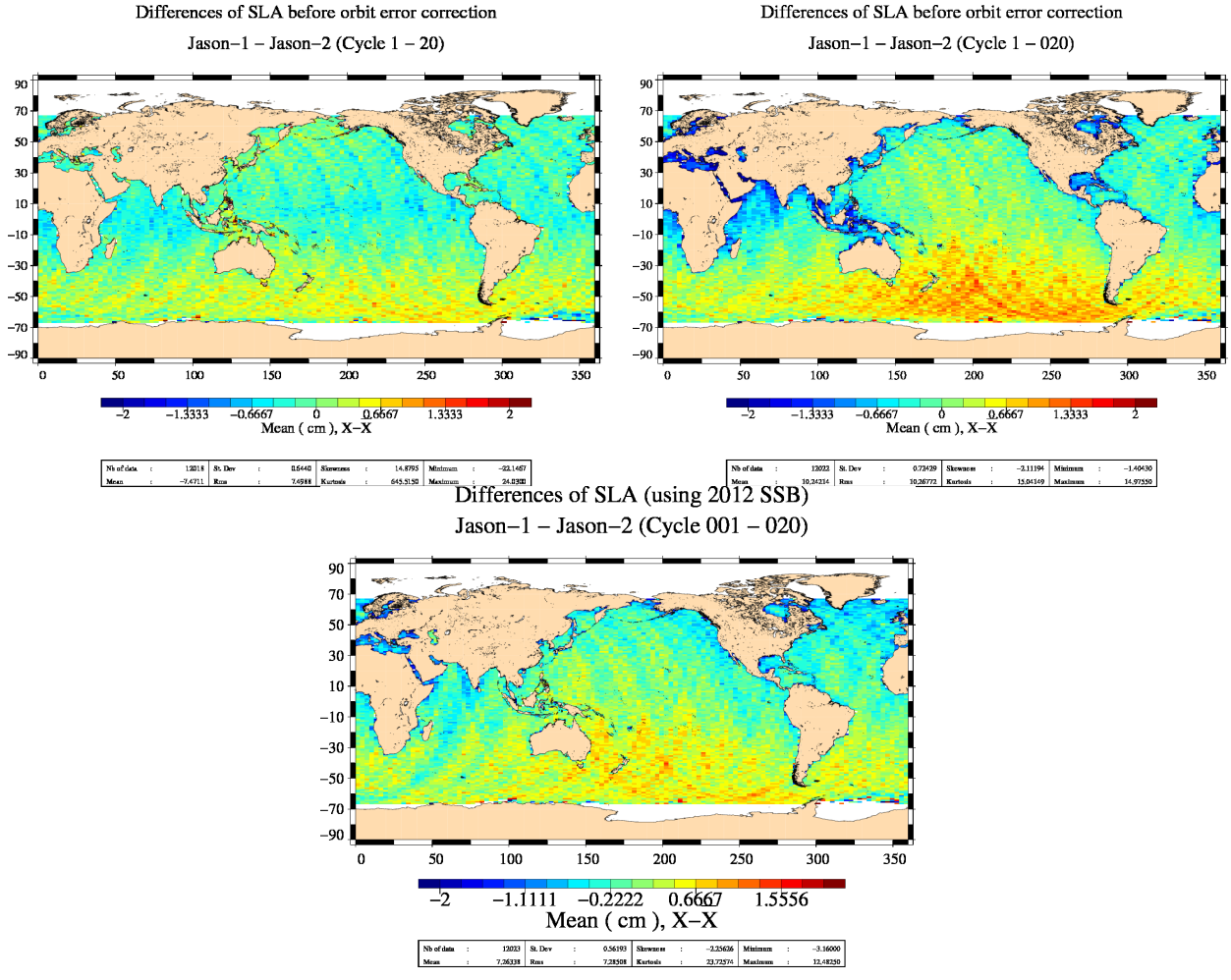

Figure 13: *SLA differences between JA1 and JA2 (before applying orbit error correction),* ***Right:*** *with GdrD standards for Jason-2 and updated GdrC standards for Jason-1,* ***Left:*** *with GdrT standards for Jason-2 and GdrC standards for Jason-1.* ***Bottom:*** *with GdrD standards for Jason-2 and updated GdrC standards for Jason-1, accounting for sea state bias correction updated for both missions from [18]. The maps are centered around the mean value (left: mean=-7.47cm, right:mean=10.24cm, bottom: mean=7.26cm).*

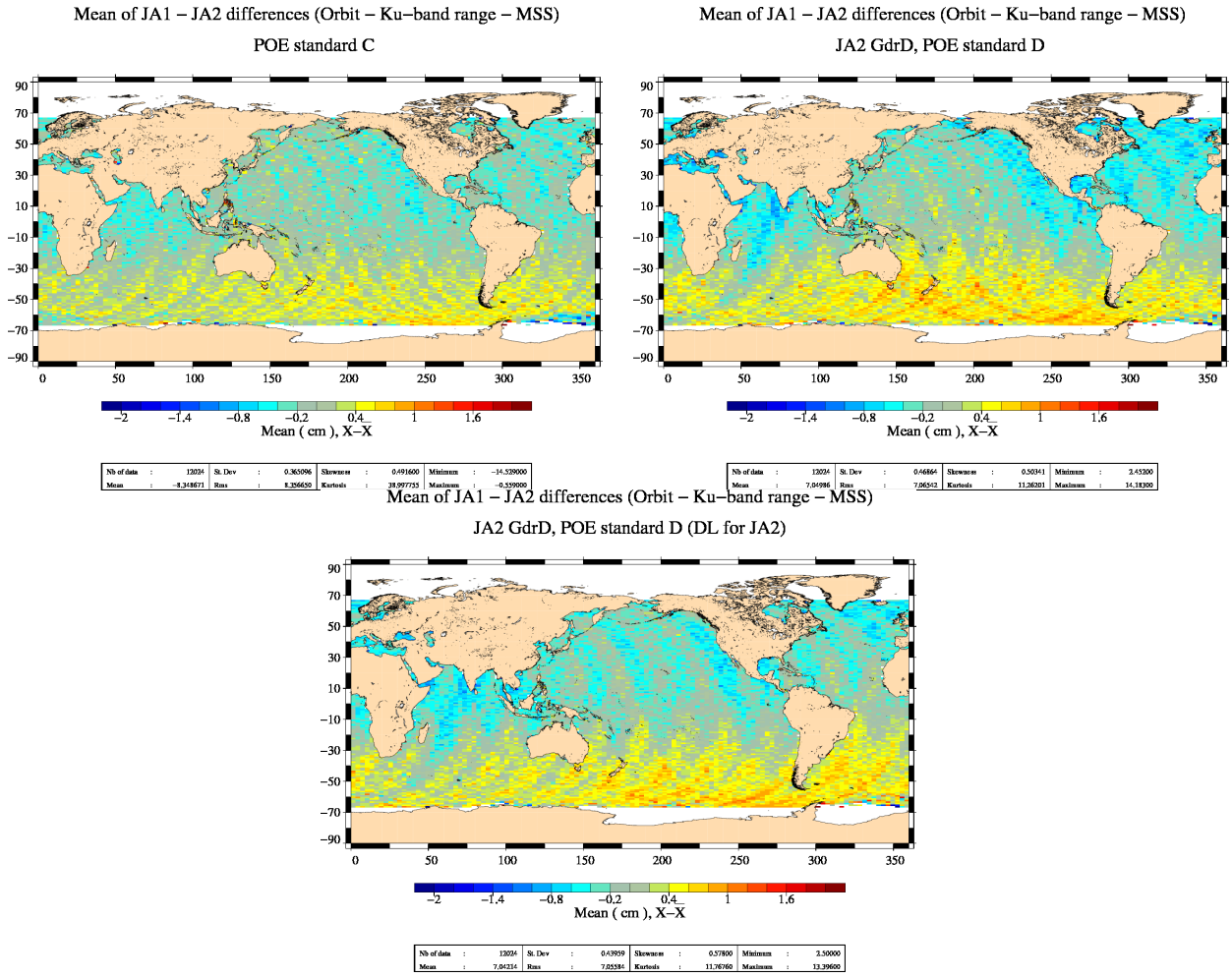

Figure 14: *SLA differences between JA1 and JA2 (without any correction),* ***Right:*** *with GdrD standards,* ***Left:*** *with GdrT standards,* ***Bottom:*** *with GdrD standards, but orbit Doris/Laser for JA2. The maps are centered around the mean value (left: mean=-8.35cm, right:mean=7.05cm, bottom: mean=7.04cm).*

5. Details of the changes in GdrD standard

In the following chapter the changes of the GdrD standard (compared to GdrT) are detailed. Therefore comparisons between Jason-2 GdrD and GdrT are done, but also between Jason-2 and Jason-1. As several passes have time tag differences of about 51 milli-seconds between Jason-2 GdrD and GdrT versions (see 5.1.), several comparisons between GdrD and GdrT exclude these data with such a large time difference (especially when comparing variables such as orbit and range).

The following points are adressed:

- the datation
- the orbit standard
- the radiometer related parameters
- the altimeter related parameters
- the other corrections

5.1. Concerning the datation of GdrD products

Until recently Jason-1 or Jason-2 data contained a pseudo time tag bias close to 0.3 milli-seconds. This was especially visible through a small north/south bias on ascending/descending mono-mission crossover points (see also right panel of figure 6). In Jason-1 GdrC products, a pseudo altimeter datation bias correction is available which was determined empirically (see also chapter 4.1.2.). The origin of this pseudo time tag bias was found by CNES [2] in 2010. It has a mean of about 0.25 milli-seconds and is dependent on the altitude of the satellite. For Jason-2 GdrD data, the datation was directly modified in order to correct it properly. As shown on figure 9, Jason-2 GdrD pseudo time tag bias is now close to zero (mean value).

The datation between Jason-2 GdrD and GdrT differs therefore by approximatly 0.25 milli-seconds and is dependent on the latitude, as shown on the bottom of figure 15. In addition, several (especially) ascending passes that have a time tag shifted (compared to GdrT version) by about 0.051 seconds (see top of figure 15). These differences of 51 milli-seconds appear especially for cycles in DEM mode. Positions (latitude, longitude), as well as altimeter and radiometer parameters are also different for these passes. The compression of 20 Hz data to 1 Hz data seems to be shifted by a 20 Hz measurement. Generally these time tag differences disappear after encounter of land (but not in DEM mode). Note that time tag differences (shift of elementary 20 Hz measurements used for 1 Hz data) are regularly observed between Ogdr and Igdr data. Note that from cycle 52 onwards, the number of passes with this kind of time tag bias between GdrT and GdrD is lower than for cycles 1 to 51: it is probably due to a more coherent SPA software version (GdrT were computed in SPA version 2 until cycle 51, and in SPA version 3 after).

On the bottom panel of figure 15, some passes of cycle 34 with an intermediary value of time tag are visible (three passes are concerned, with a bias of -1.6ms et -1.0ms and 0.0ms: analysis is still ongoing), it has no significant impact on results.

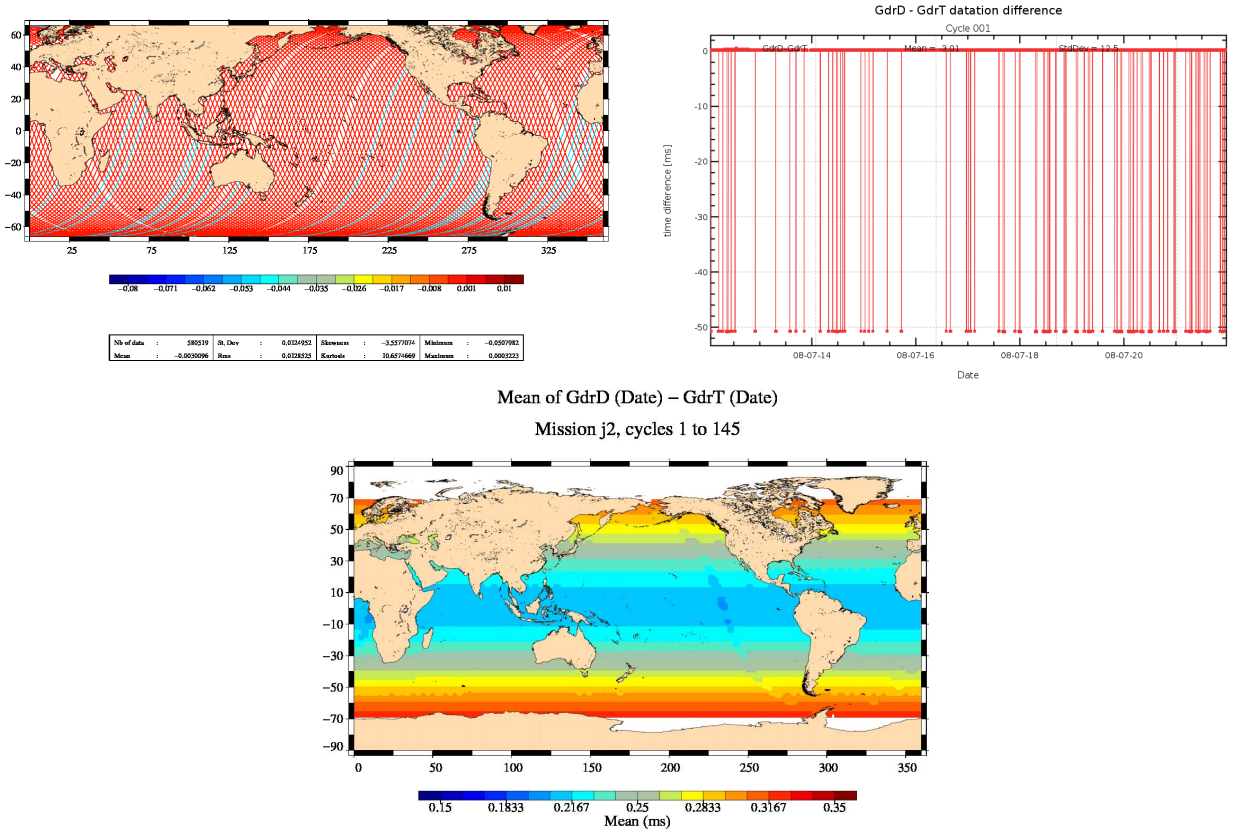

Figure 15: ***Top:*** *Difference between time tag of GdrD and GdrT for cycle 001 (left: map, right: along track).* ***Bottom:*** *Map of time tag differences between GdrD - GdrT (only measurements with time differences less than 0.01 s are selected) over cycles 001 to 145.*

5.2. Concerning the standard of GdrD Precise Orbit Ephemeris (POE-D)

The GdrD data contain the Precise Orbit Ephemeris standard D. This POE-D orbit standard uses the ITRF2008 and a new gravity field (EIGEN-GRGS_RL02bis_MEAN_FIELD), as well as non-tidal TVG (time variable gravity field) for annual and semi-annual variations, and drifts up to deg/ord 50 (see Cerri et al. [5]).

The difference between orbit standard D and C (Jason-2 GdrT products contain POE-C orbit standard) shows mostly an hemispheric $east_{(longitudebetween-180^{\circ}and0^{\circ})}/west_{(longitudebetween0^{\circ}and180^{\circ})}$ pattern of about $\pm$ 1 cm amplitude (with positive values over american continent and negative values over indian ocean), as shown on figure 16. This pattern is mostly due to the different gravity fields used in the POE-D and POE-C standards. The amplitude of the orbit difference increases over time (figure 17), as POE-C standard only used annual and semi-annual variations of the gravity field, whereas POE-D standard uses also drift of the gravity field.

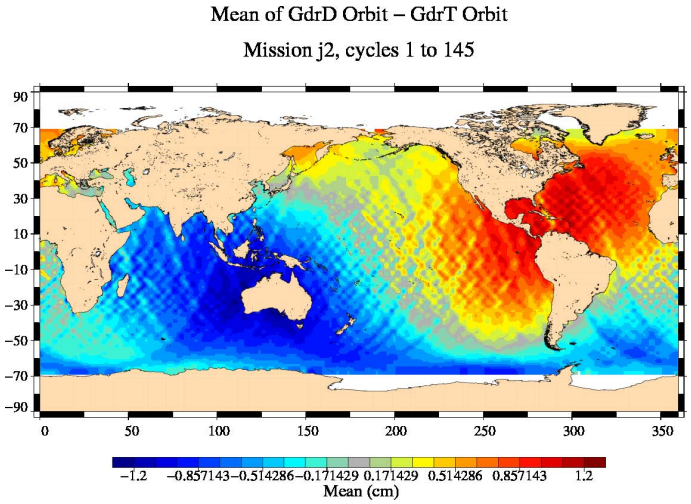

Figure 16: *Mean difference between GdrD and GdrT orbit over Jason-2 cycles 001 to 145 (only measurements with time differences less than 0.01 s are shown).*

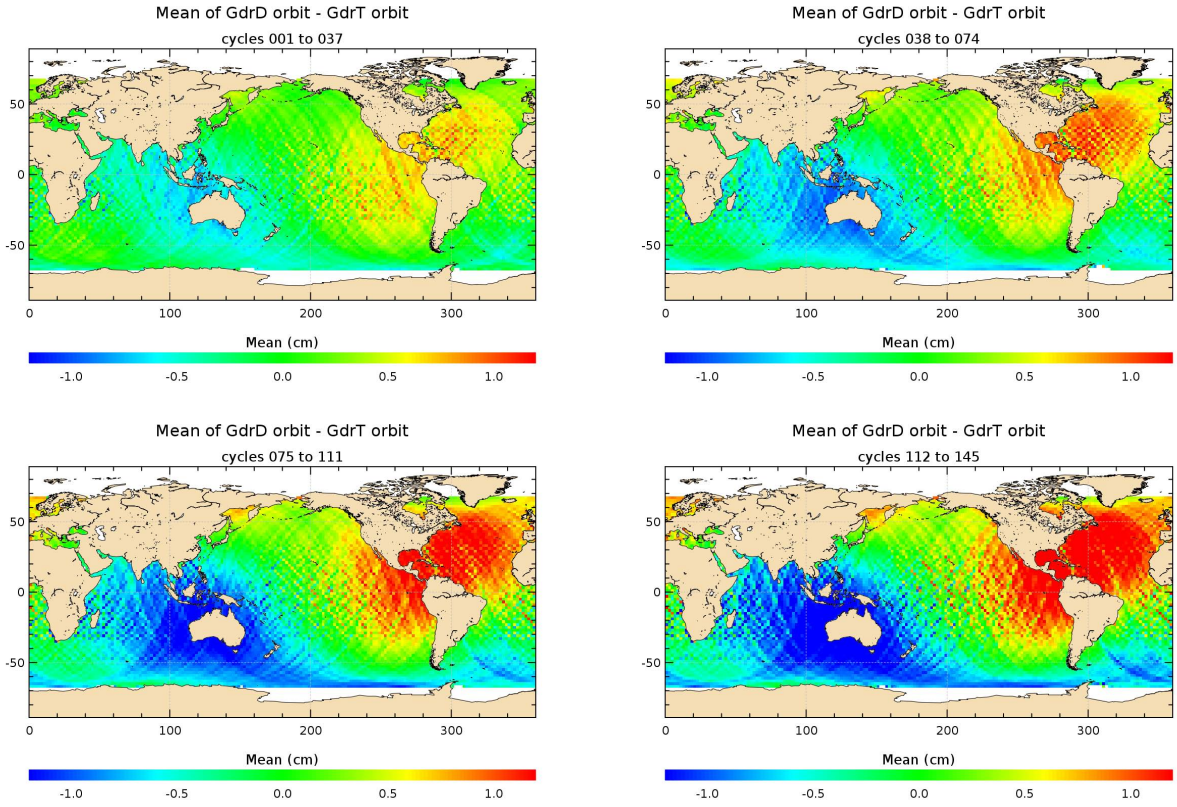

Figure 17: *Mean difference between GdrD and GdrT orbit per year over Jason-2 cycles 001 to 145 (only measurements with time differences less than 0.01 s are shown).*

Analysis of ascending/descending SSH crossover differences show that with POE-D, the systematic differences between ascending and descending passes are strongly reduced. The red curve (using

POE-D orbit) on the right side of figure 18 is more centered around zero than the blue curve (using orbit from GdrT). Furthermore, the geographical pattern observable on the map of Jason-2 SSH crossover differences when using POE-C (left side of figure 19) are strongly reduced when using POE-D (right side of figure 19). The POE-D standard increases therefore the homogeneity of ascending and descending passes.
Finally, the variance of SSH crossover differences is reduced using POE-D compared to POE-C standard, as shown on left side of figure 18 (the difference is negative). The mean variance reduction is about -1.2 cm^2, which is a main contributor to the total SSH variance reduction of the GdrD versus GdrT product (about - 1.7 cm^2).

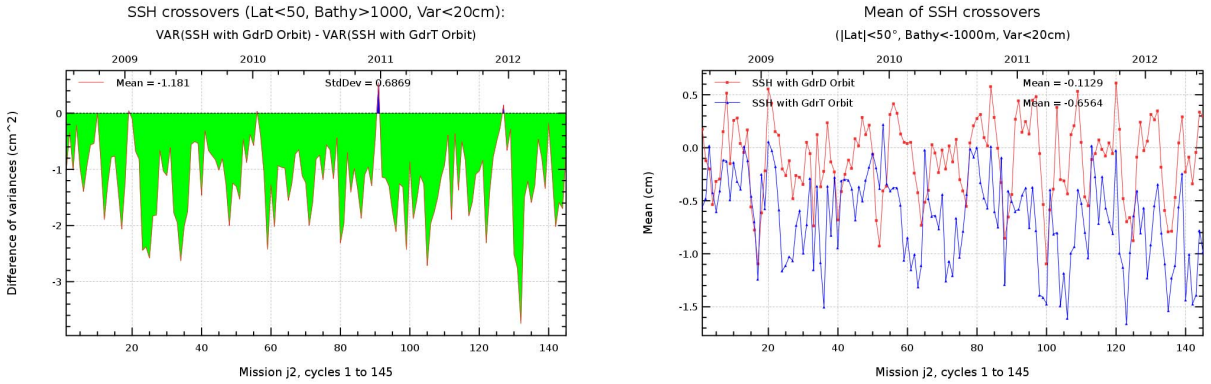

Figure 18: ***Left:*** *Cycle per cycle monitoring of difference of SSH crossover variance using either POE-D or POE-C.* ***Right:*** *Cycle per cycle monitoring of the mean of ascending/descending SSH differences using either POE-D or POE-C. Jason-2 data are from GdrD products (only the orbit standard changes). Only crossover points with |latitude| < 50°, bathymetry < -1000m and oceanic variablity less than 20 cm are chosen (only measurements with time differences less than 0.01 s are shown).*

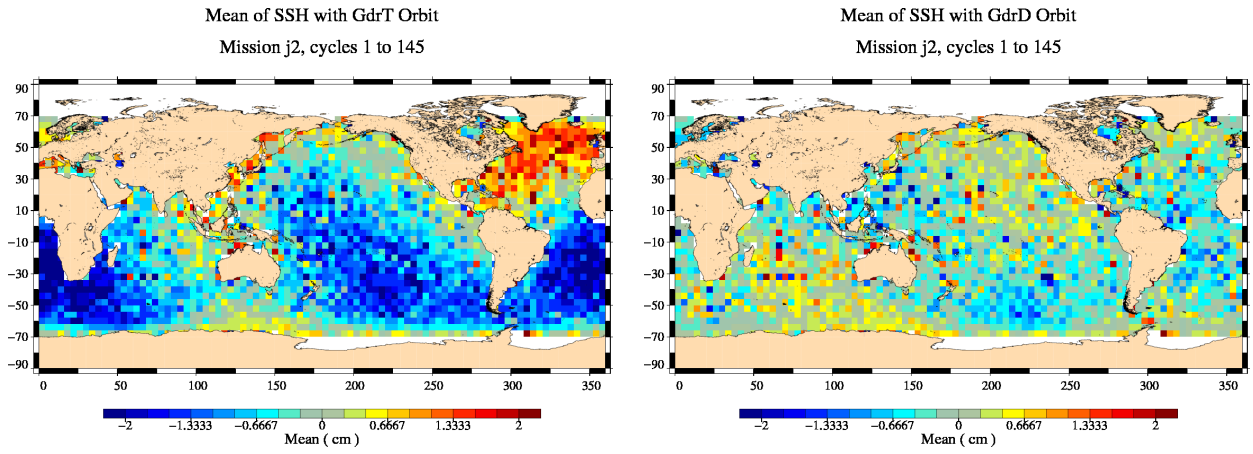

Figure 19: *Cycle difference between ssh crossovers differences:* ***Right:*** *with POE-D standard,* ***Left:*** *POE-C standard (only measurements with time differences less than 0.01 s are shown).*

Comparing SSH multi-mission crossover maps (Envisat - Jason-2) shows a large east/west bias when using POE-C standards for both satellites (left of figure 20). When using POE-D orbit standard, this east/west bias disappears and smaller previously hidden structures appear (right of figure 20). This improvement is mainly due to the new gravity field used in the POE-D solution. The remaining structures on the right of the figure are slightly reduced when using new SSB solution for both Jason-2 and Envisat data (presented at OSTST 2012 meeting, by Tran et al. [18]). Furthermore some of the differences come also from the ionospheric correction (as for this period Envisat has no longer a dual-frequency ionosphere correction available, but only GIM). Nevertheless some pattern of differences are still unexplained. Note that similar structures can be observed between Jason-1/Envisat crossover maps (see Envisat data validation report 2012 [12]).

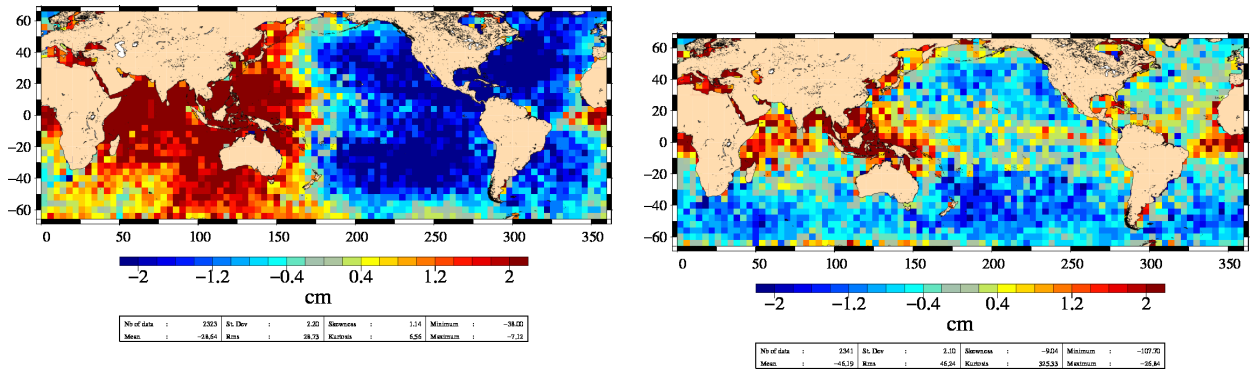

Figure 20: *Maps of ssh crossovers differences over the year 2011:* ***Left:*** *POE-C standard used with Jason-2 GdrT and Envisat V2.1 data (radiometer wet troposphere correction applied),* ***Right:*** *POE-D standard used with Jason-2 GdrD and Envisat V2.1 data (ecmwf model wet troposphere instead of radiometer wet troposphere used).*

The POE-D orbit solution lowers the Jason-2 global mean sea level trend by 0.1 mm/yr. When computing the mean sea level separatly for ascending and descending passes, the values are much more closer when using POE-D orbit (ascending/descending trend differences are less than 0.1 mm/yr), than when using POE-C orbit (ascending/descending differences of about 0.7 mm/yr).

5.3. Concerning the radiometer related parameters

For the GdrD product, JPL has provided the following inputs (see also [4]):

- new AMR caracterization file
- correction of the 34 GHz anomaly
- new wet path-delay retrieval algorithm for coastal areas
- new radiometer related flags (rain, sea ice)
- all-weather ocean sigma0 attenuation correction

5.3.1. New radiometer flags

Rain flag, previously not set in GdrT, is now available in GdrD. Furthermore a radiometer rain flag (left side of figure 22), as well as a radiometer sea ice flag (top left of figure 21) are also available. There are also other new radiometer related parameters available, such as radiometer 18.7 GHz, 23.8 GHz and 34 GHz antenna gain weighted land fraction in main beam. Furthermore, the radiometer surface type has in GdrD 3 states (whereas it had only 2 states in GdrT).

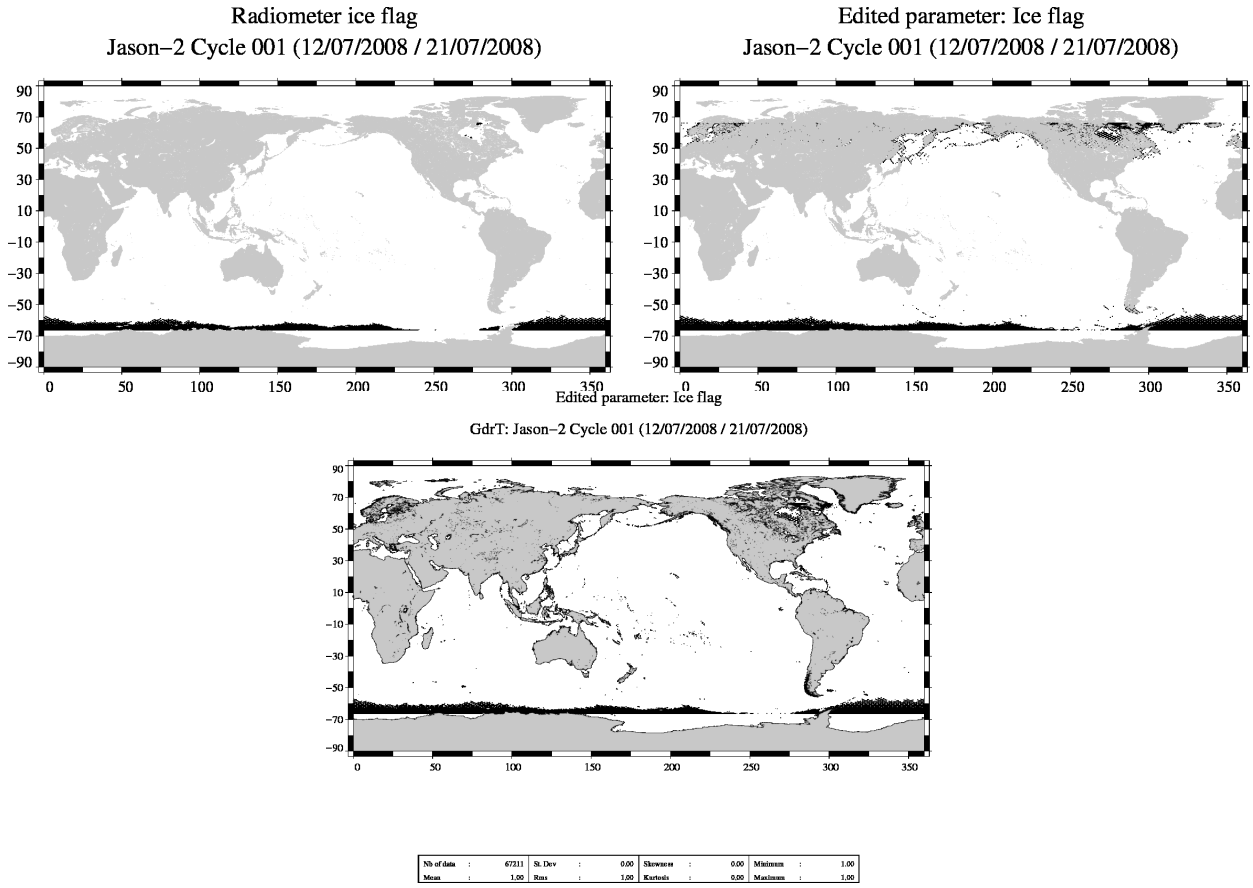

Figure 21: ***Top:*** *Maps of rad_sea_ice_flag* ***(left)*** *and ice_flag* ***(right)*** *for GdrD cycle 001.* ***Bottom:*** *ice_flag for GdrT.*

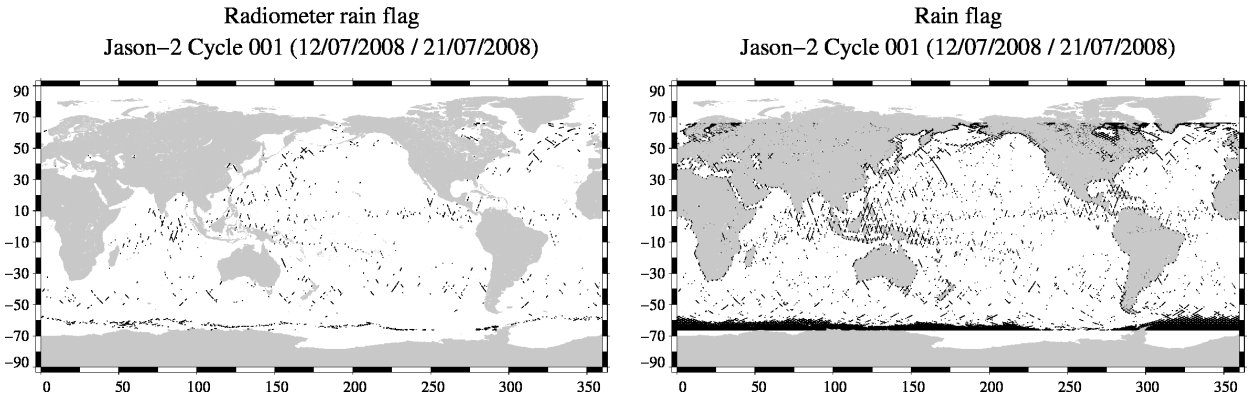

Figure 22: *Maps of rad_rain_flag* ***(left)*** *and rain_flag* ***(right)*** *for GdrD cycle 001.*

5.3.2. Correction of the 34 GHz brightness temperature correction

In GdrT, the histogram of the 34 GHz brightness temperature showed often an anomalous behaviour as shown on red curve on figure 23. This anomaly is corrected for the GdrD data (blue curve) on figure 23.

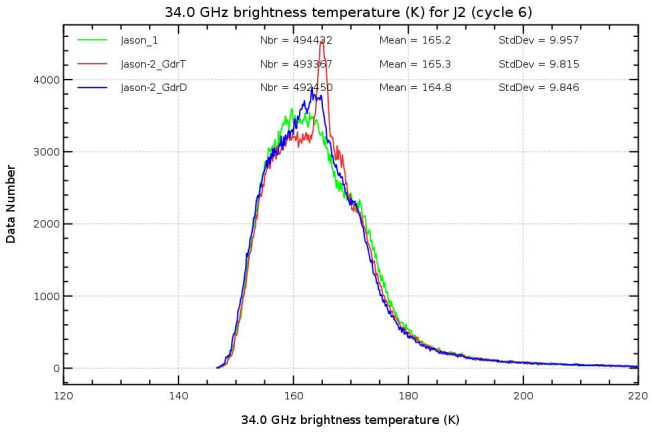

Figure 23: *Histogram of 34 GHz brightness temperature for Cycle 006. Only valid data are selected.*

5.3.3. Radiometer wet troposphere correction

The differences of radiometer wet troposphere correction between GdrD and GdrT come from :

- new coastal algorithm (see [3])
- correction of the anomaly of 34 GHz channel
- use of new calibration coefficients

Note that the GDR-D AMR radiometer wet troposphere correction has (according to S. Brown) several level of calibration:

- Cycles 1-113 - Climate data record quality calibration Cycles
- 114-140 - Intermediate quality calibration (somewhere between climate quality and operational(ARCS) quality)
- Cycle 141 onward - Operational(ARCS) quality calibration

The new coastal retrieval algorithm improves the quality of the radiometer wet troposphere correction, as on the one hand difference of radiometer minus ECMWF model wet troposphere stays for GdrD quite stable when approaching the coast (left side of figure 24) and on the other hand the variance of SLA is reduced especially near coasts when using GdrD instead of GdrT radiometer wet troposphere correction (right side of figure 24).

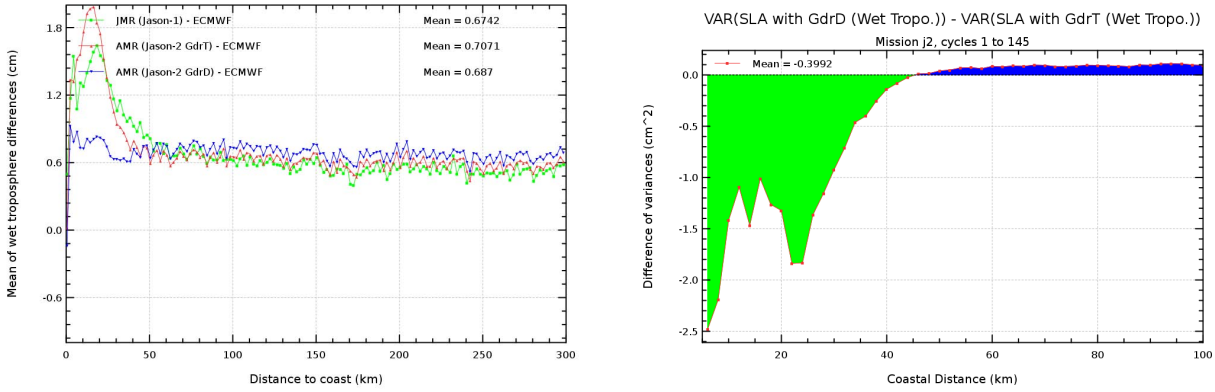

Figure 24: ***Left:*** *Difference of radiometer minus ECMWF model wet troposphere correction in fonction of coast distance for cycle 001.* ***Right:*** *Difference of SLA variances - computed by using successively GdrD and GdrT radiometer wet troposphere - plotted in function of coastal distances between 0 and 100 km.*

Differences near coasts are also visible on left side figure 25, which represents the mean of GdrD-GdrT radiometer wet troposphere differences over the 145 cycles. Furthermore, there are also small differences in tropical regions. Daily mean of direct Jason-1 minus Jason-2 radiometer wet troposphere correction (bottom of figure 25) are much more homogeneous when using Jason-2 GdrD radiometer correction and Jason-1 JMR replacement correction. This homogenisation is mostly due to the JMR replacement product which corrects the instability problems of the JMR which occured after the August 2009 Jason-1 safehold. The standard deviation of the differences increases using

new standard instead of the elder. This is mainly due to near coast changes, as blue and pink curves are closer on the bottom right side than of the bottom left side of figure 25.
The GdrD-GdrT difference of the radiometer wet troposphere correction (right of figure 25) changed of about -1.5mm over the 4 years. Note that the global mean sea level trend using the radiometer wet troposphere correction from GdrD data instead from GdrT data is increased by about 0.35 mm/yr.

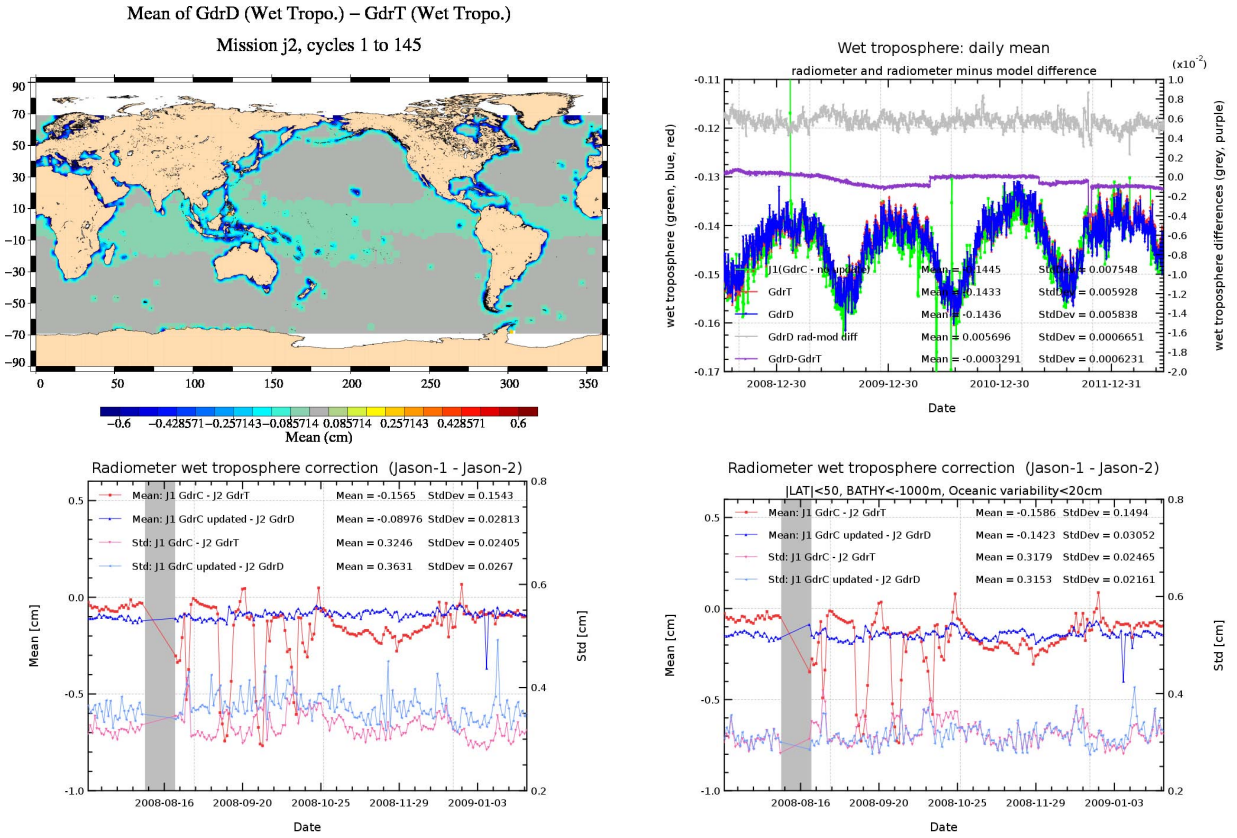

Figure 25: ***Top left:*** *Map of differences between GdrD - GdrT radiometer wet troposphere (rad_wet_tropo_corr) over cycles 1 to 145 (only measurements with time differences less than 0.01s are shown).* ***Top right:*** *Daily mean of Jason1, Jason2 radiometer wet troposphere correction, GdrD minus GdrT radiometer wet troposphere, and radiometer minus model wet troposphere correction versionD difference.* ***Bottom:*** *Daily mean and standard deviation of Jason1 minus Jason2 radiometer wet troposphere correction difference during the formation flight phase [**Left:** all data ,**Right:** restricted to open ocean].*

5.3.4. Atmospheric attenuation

As the atmospheric attenuation is derived from radiometer parameters, which have changed in GdrD version, it is also different between GdrD and GdrT product version (see figure 26). Furthermore, for GdrD the atmospheric attenuation algorithm was updated to be valid for all ocean scenes ([4]). As backscattering coefficient is corrected for the atmospheric attenuation, this difference of about -0.015dB between GdrD and GdrT atmospheric attenuation will also impact the Sigma0 (figure 5.4.5.).

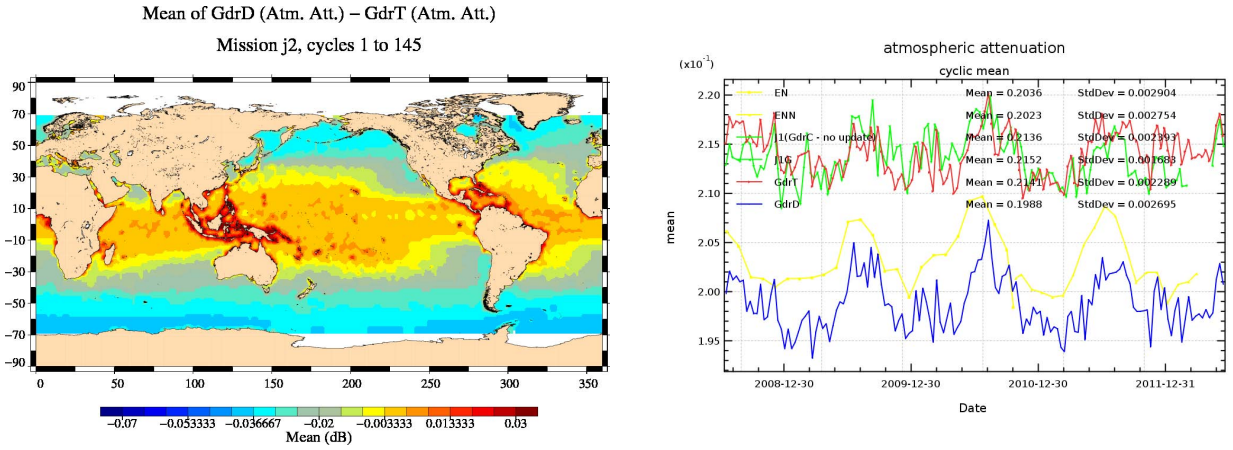

Figure 26: ***Left :*** *Difference between GdrD - GdrT atmospheric attenuation (only measurements with time differences less than 0.01 s are shown.* ***Right :*** *Cycle mean of atmospheric attenuation.)*

5.4. Concerning the altimeter related parameters and corrections derived from the altimeter related parameters

5.4.1. Use of MQE setting

For Jason-2 GdrT data, no threshold was used for MQE (Mean Quadratic Error) editing during the 1 Hz compression (step which passes from 20 Hz data to 1 Hz data), since the threshold from Jason-1 was not applicable to Jason-2. Therefore, Jason-2 GdrT products had more elementary 20 Hz data used for 1 Hz compression than Jason-1. Meanwhile the MQE thresholds were specially determined for Jason-2 data and are applied during 1 Hz compression for GdrD products.
In consequence, the number of elementary measurements decreases slightly for Jason-2 GdrD (see left side of figure 27). This is particularly the case for regions with disturbed sea states (near Indonesia, over sea ice, ...), as expected and shown on right side of figure 27.

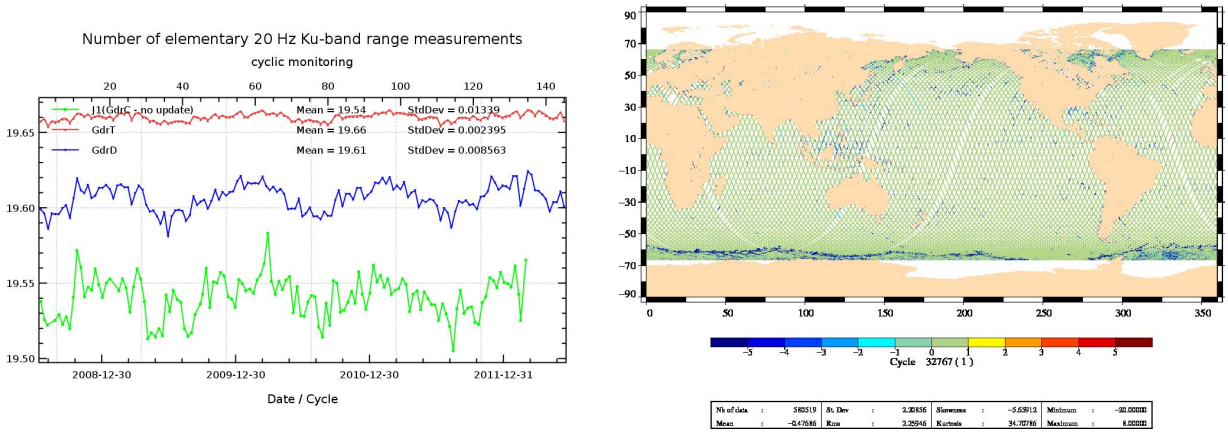

Figure 27: ***Left:*** *Mean per cycle of elementary 20 Hz Ku-band range (range_numval_ku) for cycles 1 to 145.* ***Right:*** *Maps of differences of number of elementary 20 Hz Ku-band range (range_numval_ku) measurements between GdrD and GdrT in Ku-band for Cycle 001.*

5.4.2. Altimeter Ku-band range

In the histogram (left side of figure 28), GdrD - GdrT Ku-band range difference shows a peak around 15.3 cm. This large difference between GdrD and GdrT range comes mainly from:

- The absolute bias of 18.092 cm applied for Ku- and C-band range (this corrects the value of the distance between center of gravity and the reference point of the altimeter antenna, see [8]).
- The PRF value (2058.513239 Hz) used in the altimeter caracterization file is no longer truncated (see [8]). This results in a bias of about -2.48 cm.
- The use of new LUT (altimeter instrumental corrections tables).

The GdrD - GdrT range difference is not constant, but varies regionally. It is slightly reduced for regions with disturbed sea states (around Indonesia), as shown on right side of figure 28. This is related to the MQE setting.

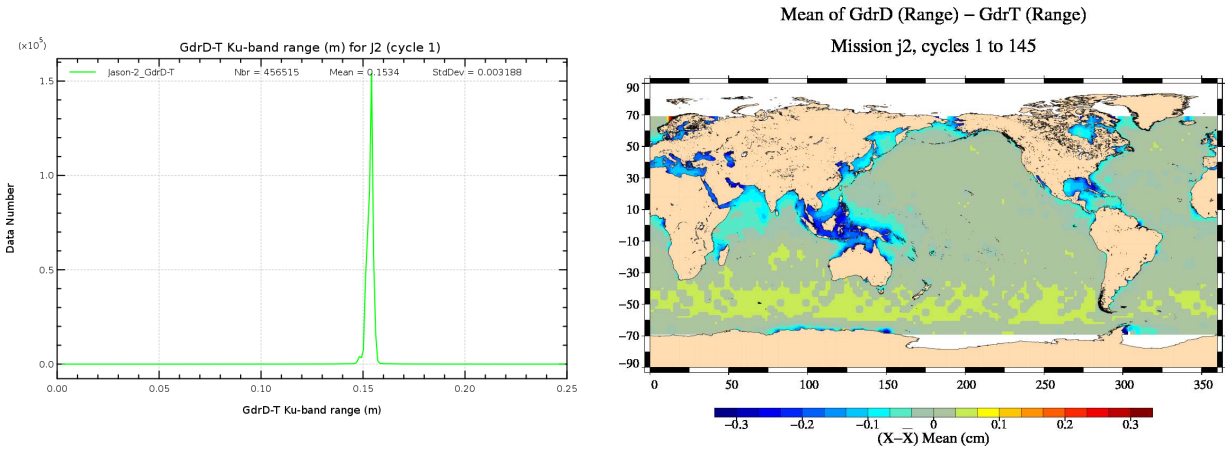

Figure 28: ***Left:*** *Histogram (for valid data) of differences of GdrD and GdrT Ku-band range for Cycle 001.* ***Right:*** *Difference between GdrD - GdrT range on the right (only measurements with (GdrD /GdrT) time differences less than 0.01 s). The map is centered around 15.3 cm.*

5.4.3. Mispointing from waveforms

Due to the use of a new antenna aperture angle (at 3 dB), which is 1.29 deg, the histogram of the Jason-2 GdrD mispointing is more centered around zero, as shown on left side of figure 29. The right of figure 29 shows that this value stays very stable, though mostly slightly negative, over the 145 cycles.

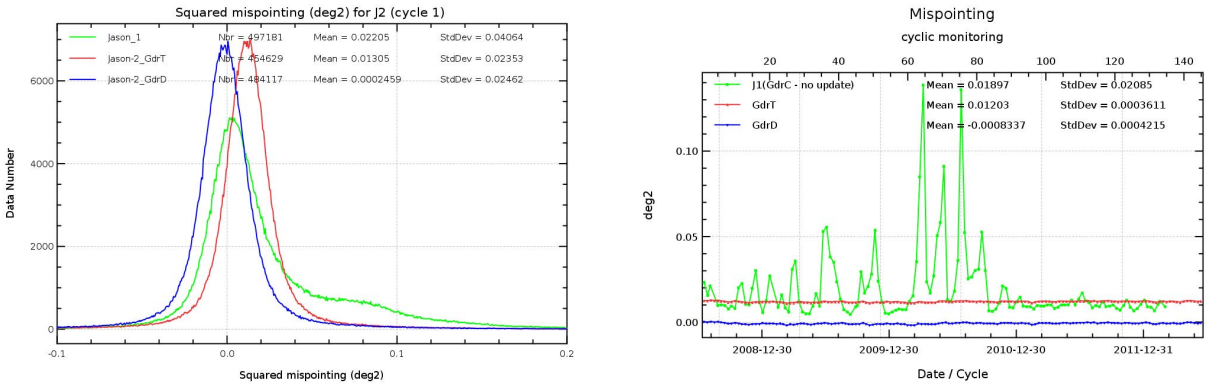

Figure 29: ***Left:*** *Histogram of GdrD and GdrT off nadir angles for Cycle 001.* ***Right:*** *Cycle per cycle monitoring of mispointing for Jason-2 GdrT, GdrD, and Jason-1 GdrC.*

5.4.4. Dual-frequency ionosphere correction

As range and sea state bias have changed between GdrT and GdrD versions, the dual-frequency ionosphere correction is also modified. The mean bias between GdrD and GdrT is around 0.6 cm. This means that Jason-2 GdrD dual-frequency ionosphere correction is now closer to Jason-1 than it was the case for Jason-2 GdrT version. Note that a global bias of around 3 mm remains between Jason-1 and Jason-2 dual-frequency ionosphere correction.

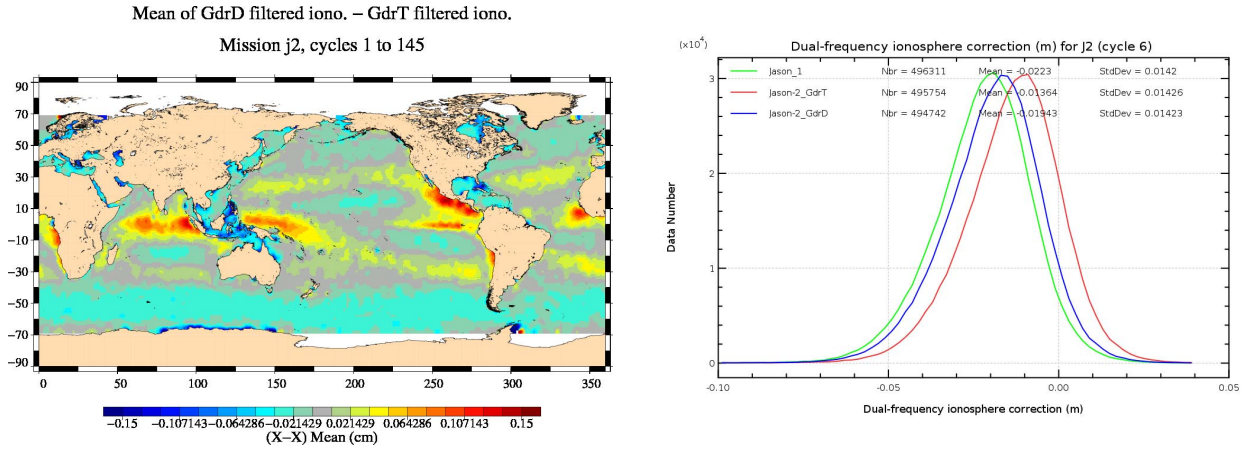

Figure 30: ***Left:*** *Difference between GdrD - GdrT filtered ionosphere. The map is centered around the mean of -0.57cm.* ***Right:*** *Histogram (for valid data) dual-frequency ionosphere correction of Jason-2 GdrD, GdrT, and Jason-1 GdrC for cycle 006.*

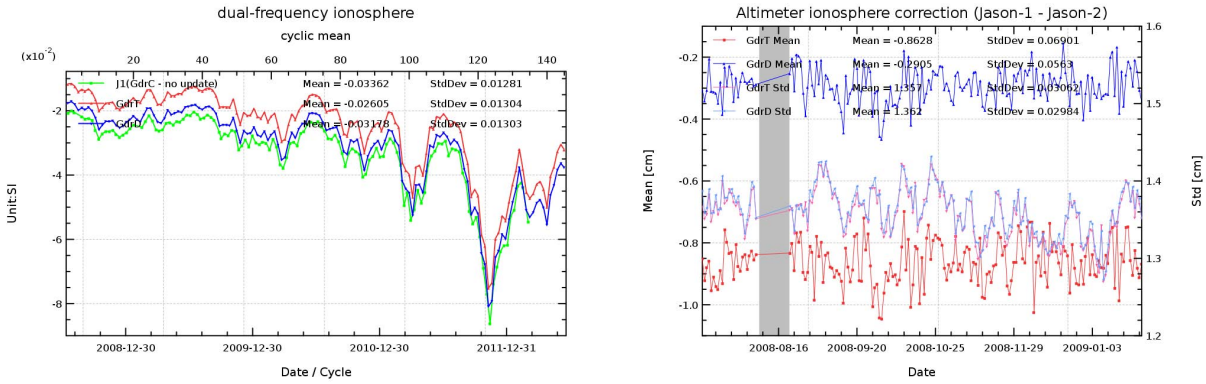

Figure 31: ***Left:*** *Cycle per cycle monitoring of mean of dual-frequency ionosphere correction for Jason-2 GdrD, GdrT, and Jason-1 GdrC.* ***Right:*** *Daily mean and standard deviation of Jason1-Jason2 dual-frequency ionosphere correction difference over the formation flight phase.*

5.4.5. Ku-band sigma0

There is a bias of about -0.15 dB between GdrD and GdrT Ku-band backscattering coefficient. This is likely related to the modified value of the antenna aperture. The regional differences (left side of figure 32) are correlated to the atmospheric attenuation differences (see figure 26) as the Ku-band backscattering coefficient is corrected for the atmospheric attenuation. Compared to Jason-1 data (bottom panel of figure 32), the differences are increased with Jason-2 GdrD. Note that prior to the altimeter wind speed computation for GdrD, a calibration bias of 0.32 dB has been added to the Ku-band backscatter coefficient (as for Jason-2 the same wind speed look up table is used as for Jason-1).

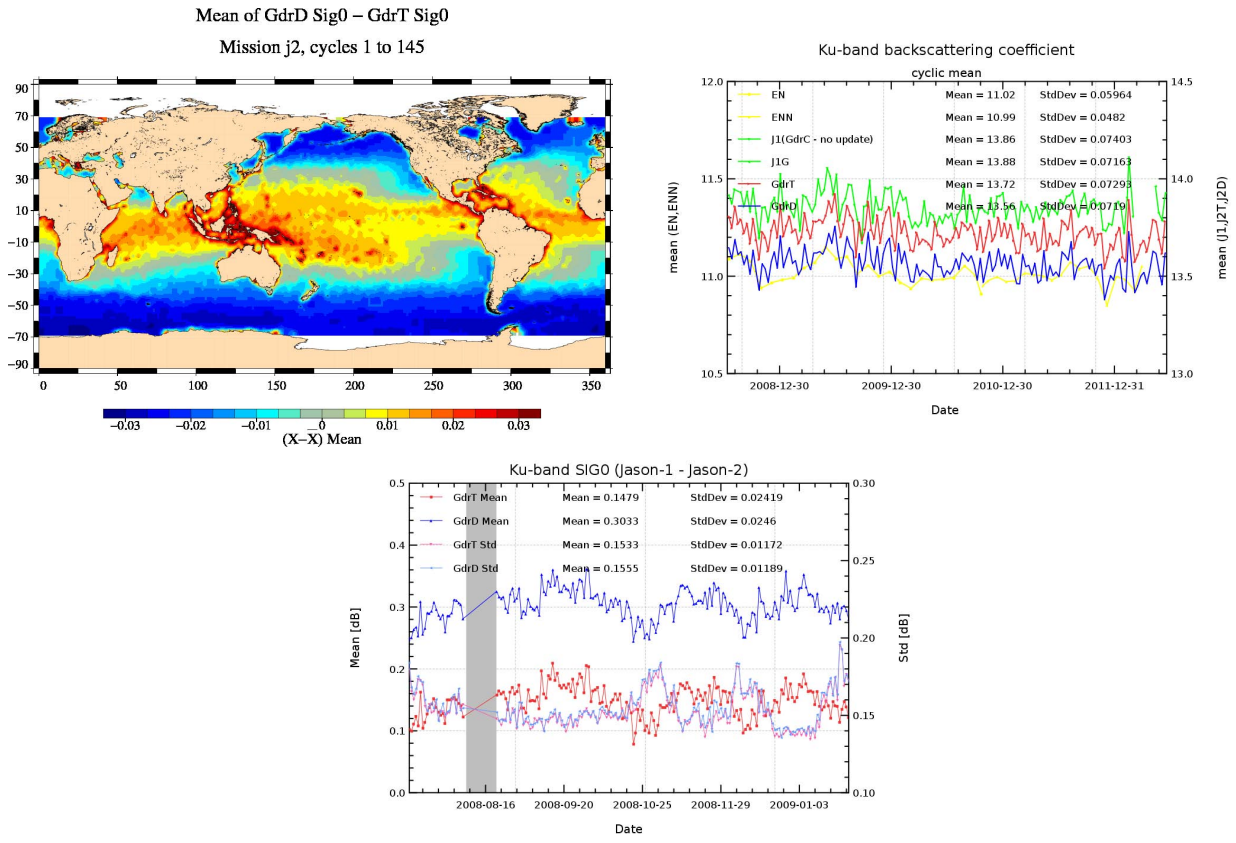

Figure 32: ***Top left:*** *Difference between GdrD - GdrT Ku-band backscattering coefficient. The map is centered around -0.15 dB.* ***Top right:*** *Cyclic mean of Envisat, Jason1, Jason2 GdrT and Jason2 GdrD Ku-band backscattering coefficient.* ***Bottom :*** *Daily mean and standard deviation of Jason1-Jason2 Ku-band backscattering coefficient difference over the formation flight phase.*

5.4.6. Ku-band significant wave height

The GdrD significant wave height (SWH) is only slightly different from the GdrT one. The regional differences are likely related to the MQE setting (applied for GdrD, not used for GdrT).

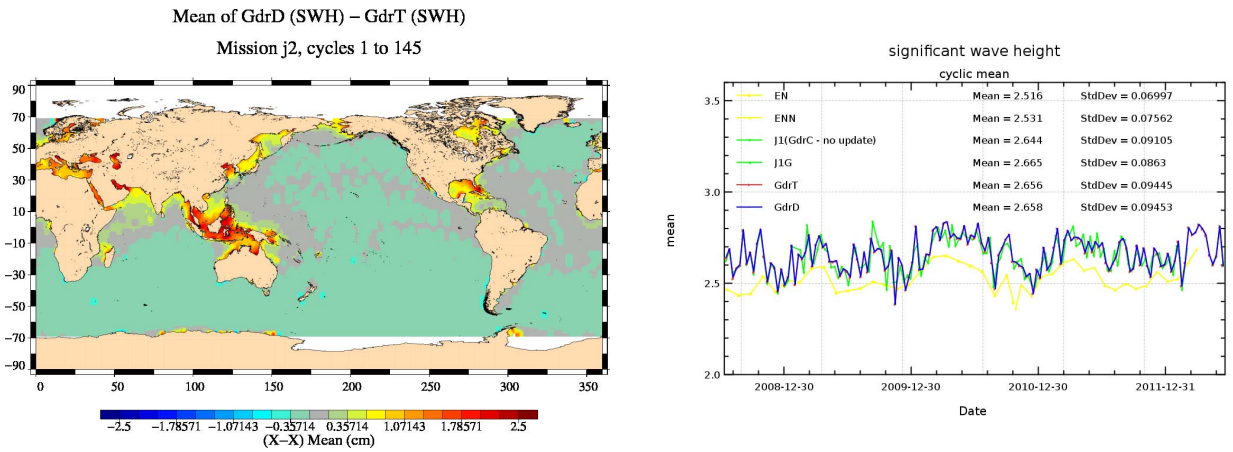

Figure 33: ***Left:*** *Difference between GdrD - GdrT SWH. The map is centered around 0.1 cm.* ***Right:*** *Daily mean of Envisat, Jason1, Jason2 GdrT and Jason2 GdrD Ku-band backscattering coefficient.*

5.4.7. Altimeter wind speed

In the GdrD product version, in order to compute the altimeter wind speed, a bias of 0.32 dB is applied to the Ku-band backscattering coefficient. The mean difference between Jason-2 GdrD and GdrT altimeter wind speed is -0.5 m/s. This difference varies regionnally (see left side of figure 34), especially in low latitudes. The shape of the Jason-2 GdrD wind speed histogram is now closer to the shape of Jason-1 wind speed histogram (see right side of figure 34), than in GdrT version. Jason-2 GdrD and Jason-1 wind speed are now more homogeneous, than previously. Regional biases are reduced with GdrD (see top right side of figure 35). Also, the global bias between Jason-2 and Jason-1 altimeter wind speed is reduced (bottom of figure 35).

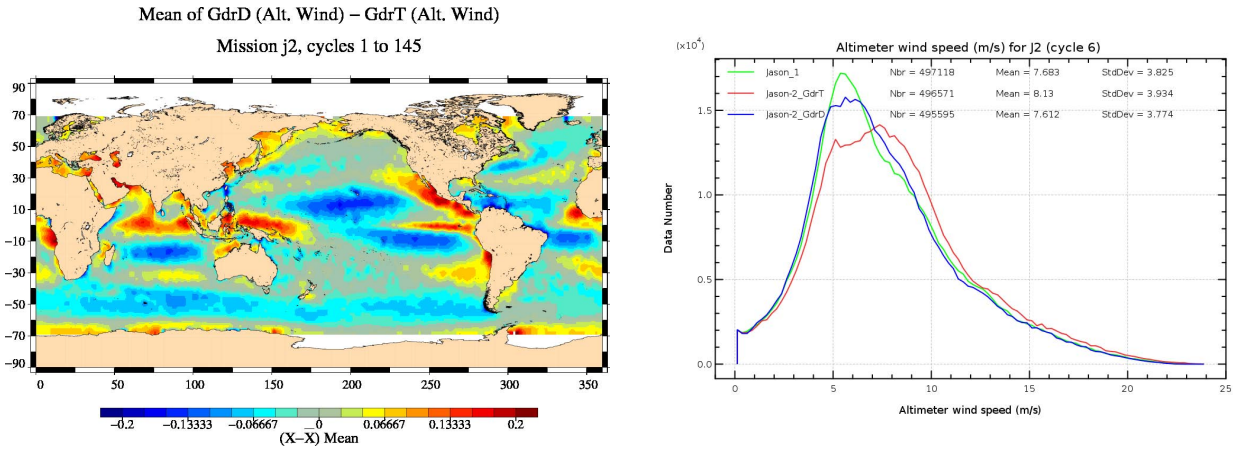

Figure 34: ***Left:*** *Map of differences of wind_speed_alt between GdrD and GdrT over cycle 001 to 145 (the map is centered around -0.51m/s).* ***Right:*** *Histogram (for valid data) of GdrD and GdrT of wind_speed_alt for cycle 006.*

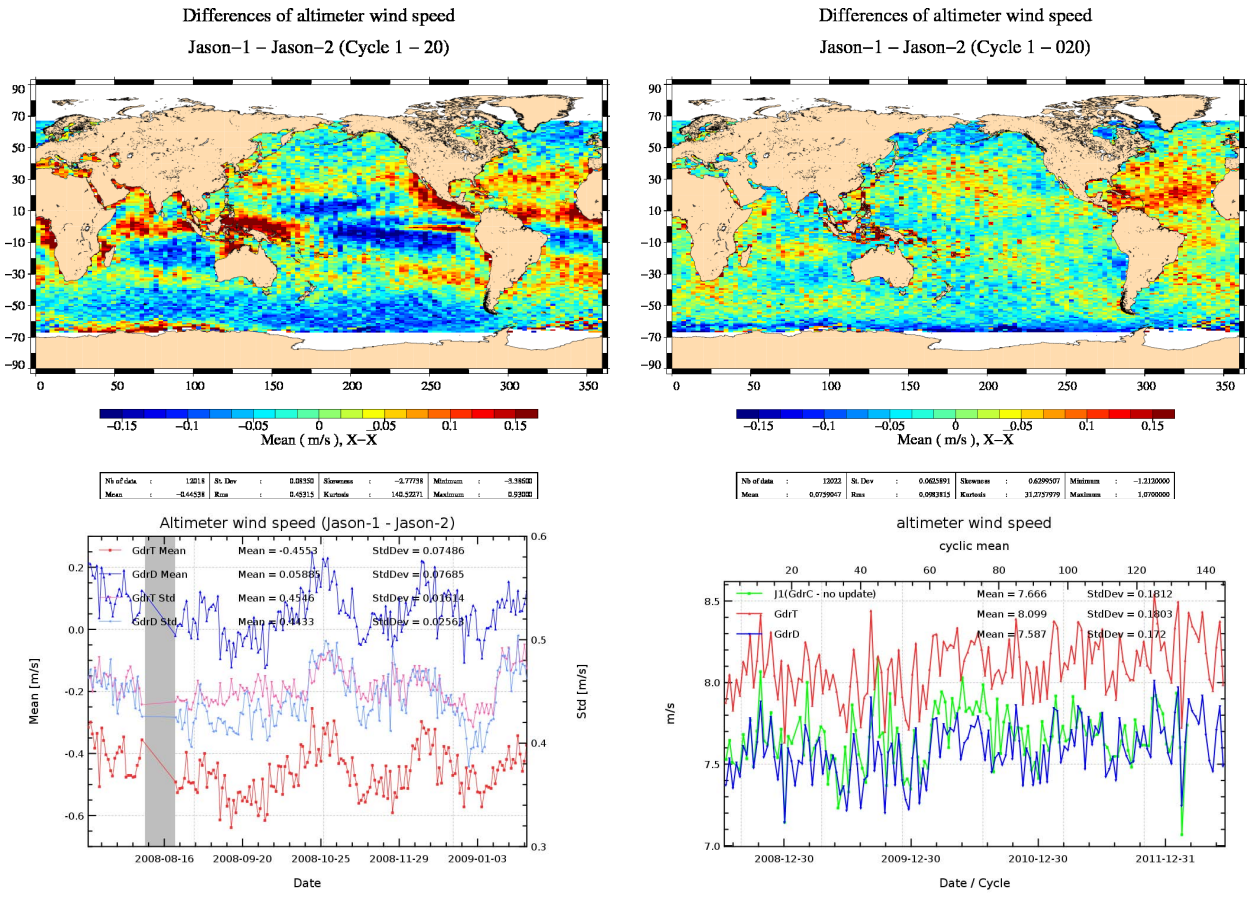

Figure 35: ***Top:*** *Map of mean differences of wind_speed_alt between Jason-2 and Jason-1 over cycle 001 to 020: using Jason-2 GdrT* ***(left)*** *or Jason-2 GdrD* ***(right)****.* ***Bottom left:*** *Daily mean and standard deviation of Jason-1 minus Jason-2 altimeter wind speed differences.* ***Bottom left:*** *Daily mean of alimeter wind speed for Jason-1, Jason-2 GdrT and Jason-2 GdrD over the 145 cycles.*

5.4.8. Sea State Bias

A new sea state bias look-up table was furnished for the GdrD reprocessing. It was computed using Jason-2 data from internal reprocessing which were as close as possible to the GdrD standards. The GdrD sea state bias differs by about 3 cm from the GdrT sea state bias (which used the same look up table as used in Jason-1 GdrC), see also figure 37. This difference is not a bias, as can be seen from the different shapes of the histograms (right side of figure 36) and the map of the mean GdrD - GdrT sea state bias difference (left side of figure 36). The regional differences are correlated with significant wave height values. There is a quite important class of SSB data near 0 for GdrD. It comes from measurements with very small significant wave height. Differences between Jason-1 and Jason-2 sea state bias increase using Jason-2 GdrD (figure 38), as the methods (as well as data) used for the SSB model computation are different. In the case of left side of figure 38, the SSB model was the same for Jason-1 GdrC and Jason-2 GdrT data, only the input values (altimeter wind speed and significant wave height) differed. For the right side of figure 38, the input values (wind, wave) have evolved for Jason-2 (from GdrT to GdrD version). Furthermore the method of computing the SSB model has also changed (see [17]). Indeed, GdrD sea state model is calculated with a different approach for low sea states. In these areas, the editing method has changed so that differences are mainly observed here.
At OSTST 2012 meeting, Tran et al. [18] presented a new SSB model computed using one year of GdrD data. This model seems slightly better than the SSB model used for the GdrD product. Though the SSB model used for the GdrD products was computed on Jason-2 data from an internal reprocessing which was as close as possible to the GdrD standard, there were nevertheless some differences with the GdrD data. Indeed, the wind speed (necessary for SSB computation) from the internal reprocessing was tuned with a preliminary bias on sigma0, whereas the wind speed of the GdrD product uses a fine-tuned bias (which takes into account additionally a correction from LTM and corrected atmospheric correction from S. Brown in sigma0).

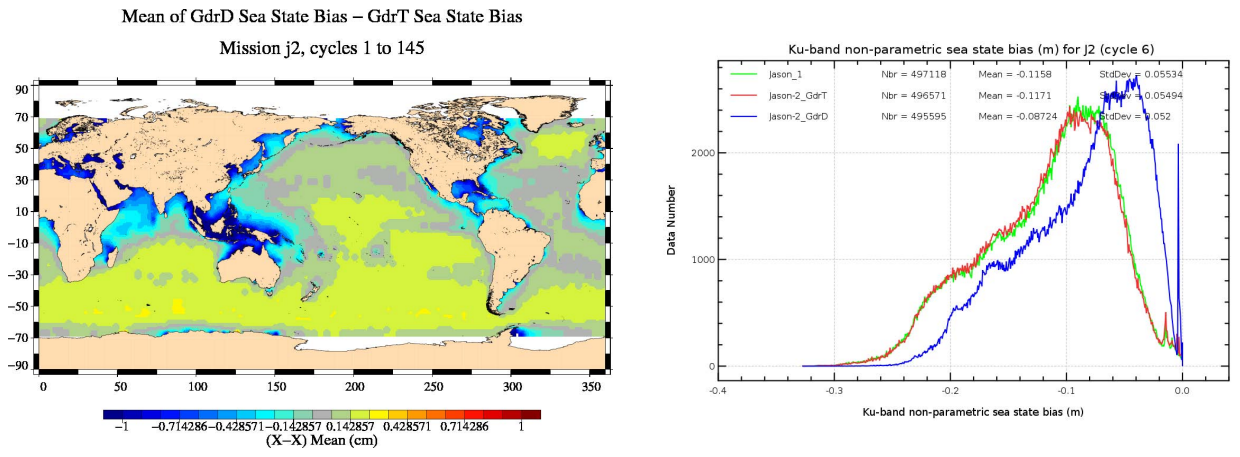

Figure 36: ***Left:*** *Difference between GdrD - GdrT Sea State Bias. The map is centered around a mean of 2.97cm.* ***Right:*** *Histogram of Jason-2 GdrT and GdrD, as well as Jason-1 (GdrC) sea state bias for cycle 006. Only valid data are used.*

When using the updated sea state bias proposed by Tran et al. [18] for both missions, the Jason-1 minus Jason-2 differences are much more homogeneous (see bottom of figure 38). Note that this

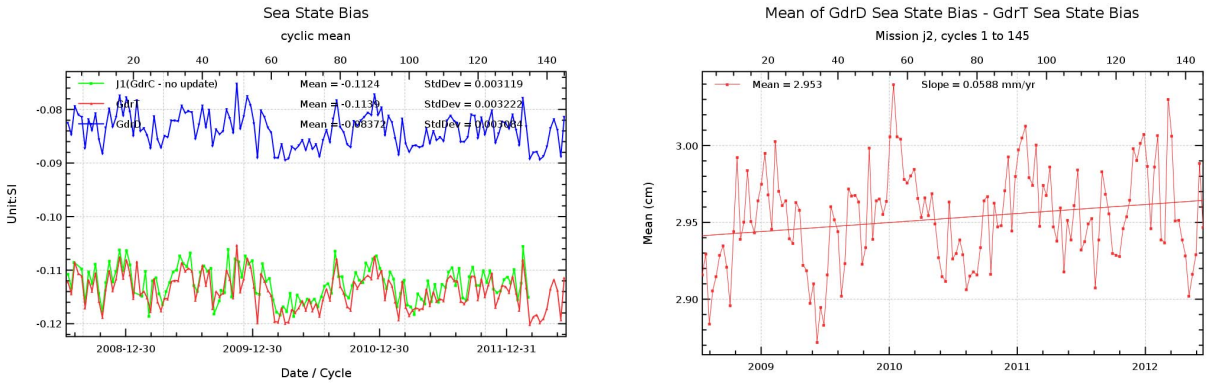

Figure 37: ***Left:*** *Cycle per cycle monitoring of mean of Jason-2 GdrD, GdrT, and Jason-1 GdrC sea state bias.* ***Right:*** *Mean of GdrD-GdrT difference of Sea State Bias (mean weighted by latitude)*

homogenization is mainly due to the updated Jason-2 SSB and to a lesser extent due to the updated Jason-1 SSB.

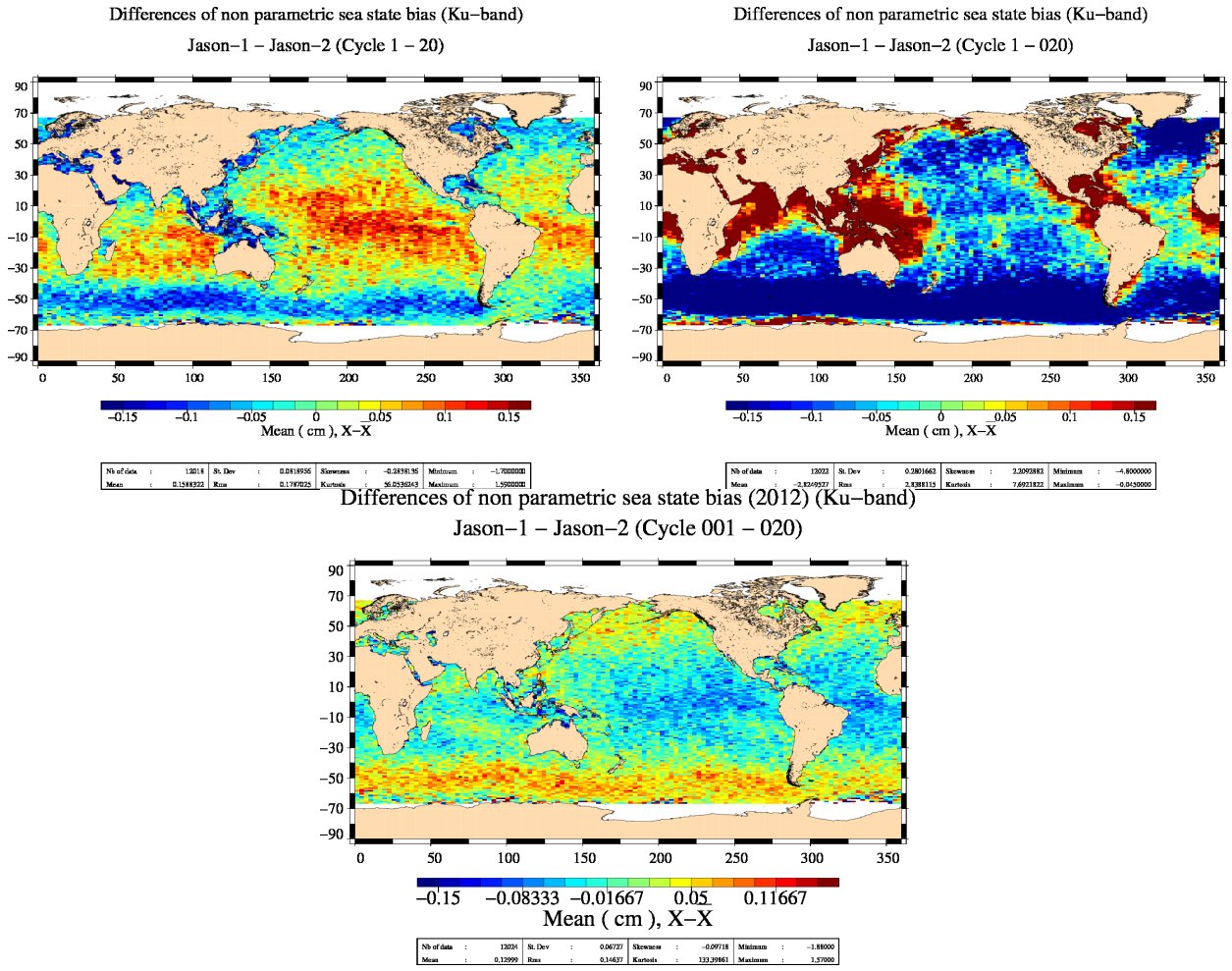

Figure 38: *Map of mean differences of sea state bias between Jason-2 and Jason-1 over cycle 001 to 020. [**Left:** Jason-2 GdrT , **Right:** Jason-2 GdrD], **Bottom:** using updated sea state bias ([18]) for both Jason-1 and Jason-2. (Note that maps are centered around a mean: 0.16cm for GdrT, -2.82cm for GdrD, and 0.13cm for updated SSB)*

5.5. Concerning other corrections

5.5.1. New global tide model (GOT4.8)

For GdrD, the global tide model GOT4.8 has replaced the GOT00V2 model available in GdrT products. Averaged over the 145 analyzed cycles, there is no global bias between the two ocean tide standards (see left side of figure 40). Nevertheless an approximatively 59 days signal is visible on the global ocean tide differences (bottom of figure 40). Using the GOT4.8 instead the Got00V2 tide standard reduces slightly this signal. The signal of the tide standard differences is correlated with the signal of SLA differences (GdrD - GdrT), see bottom of figure 40. Using the GOT4.8 global tide model instead of the GOT00V2 one improves the coherence between ascending and descending passes. The right side of figure 40 shows the reduction of SSH crossover variance when using GOT4.8, instead of GOT00V2. The global variance reduction has a value of about 0.5 cm^2. This is the second strongest variance reduction of the GdrD variables/corrections (the strongest variance reduction comes from the new POE-D orbit standard). The SSH crossover variance reduction is especially important for regions of continental shelfs (see left side of figure 39). The GOT4.8 global model compared to the GOT00V2 global model, is indeed especially improved in coastal areas. This is also visible on the right side of figure 39, showing that the SLA variance is strongly reduced for coastal areas.

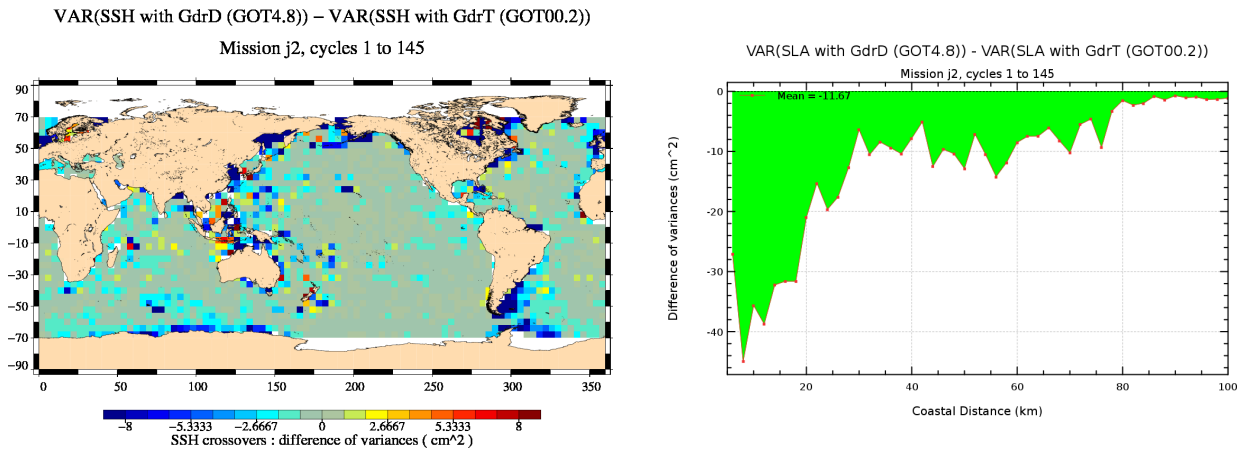

Figure 39: ***Left:*** *Map of differences of SSH variances (SSH variance using GOT4.8 - SSH variance using GOT00V2).* ***Right:*** *Difference of SLA variances - computed by using successively GdrD GOT4.8 and GdrT GOT00.2 tide model - plotted in function of coastal distances between 0 and 100 km.*

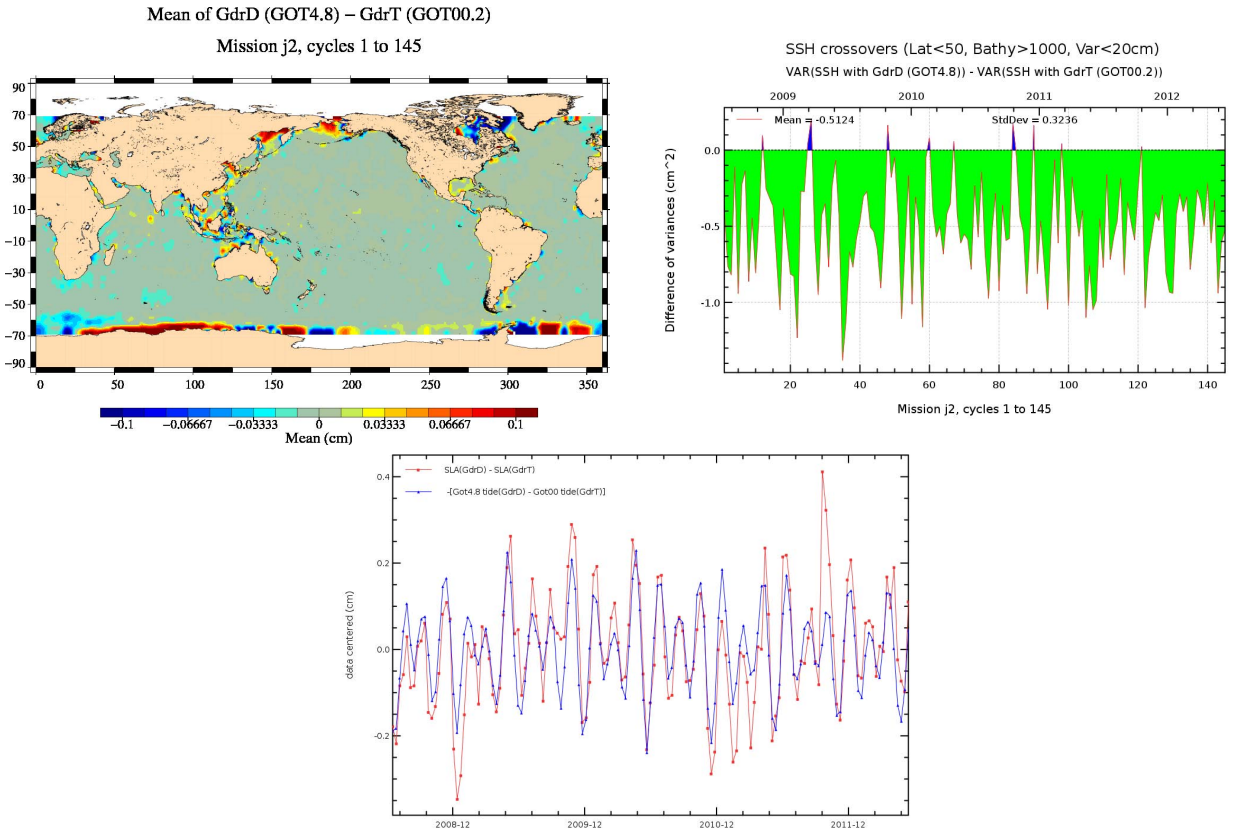

Figure 40: ***Left:*** *Difference between GdrD - GdrT global tide model (GOT4.8 - GOT00V2).* ***Right:*** *Cycle per cycle monitoring of difference of SSH crossover variances using GdrD data, using GOT4.8 or GOT00V2 model (SSH variance using GOT4.8 - SSH variance using GOT00V2). Only crossover points with |latitude| < 50°, bathymetry < -1000m and oceanic variablity less than 20 cm are chosen.* ***Bottom:*** *Cycle per cycle difference of GdrD (GOT4.8) and GdrT (GOT00V2) global ocean tide superimposed with cycle per cycle GdrD minus GdrT SLA. The curves are centered around zero.*

5.5.2. Pole tide correction

An error in the calculation of the pole tide correction has been corrected. Over lakes and enclosed seas, the pole tide is now calculated using h2*He (h2 = 0.609 and He = equilibrium pole tide). On the figure 41, main differences are therefore visible over these regions (lakes and enclosed seas).

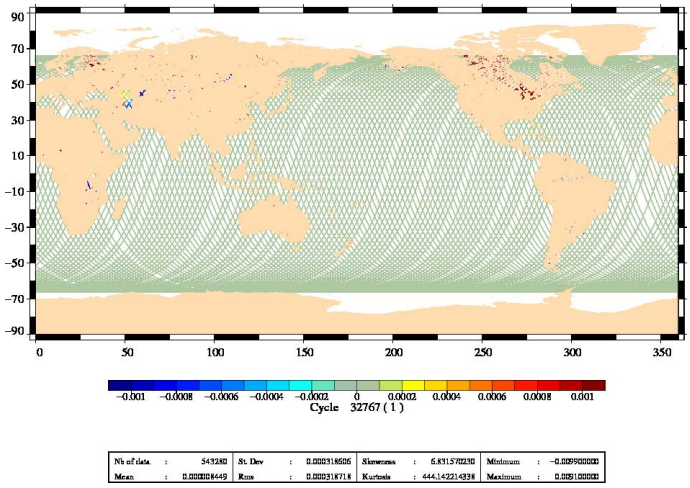

Figure 41: *Differences of pole tide correction (pole_tide) between GdrD and GdrT for cycle 001. Only measurements with time differences less than 0.01 s are shown on the difference map, but otherwise no other selection was used*

5.5.3. Long period non equilibrium tide

The long period non equilibrium tide has been corrected in Jason-2 GdrD products. The global differences between the corrected one (GdrD) and the one which had an anomaly (GdrT), is shown on figure 42.

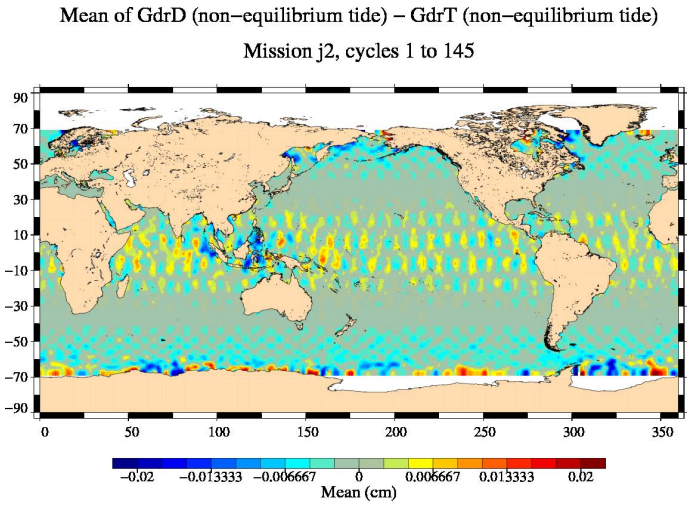

Figure 42: *Difference between GdrD - GdrT non equilibrium long period tides over cycles 001 to 145*

5.5.4. Mean sea surface and mean dynamic topography

The mean sea surface of GdrD contains the CNES/CLS 2011 version (instead of 2001 for GdrT) (see also Schaeffer&al. in [16]). The global mean bias between GdrD MSS (CNES/CLS 2011) and GdrT MSS (CLS 2001) is around 0.44 cm. There are also some regional biases, shown on left of figure 43. Using the MSS CNES/CLS 2011 instead of MSS CLS 2001 reduces the standard deviation of the SLA (see right of figure 43).

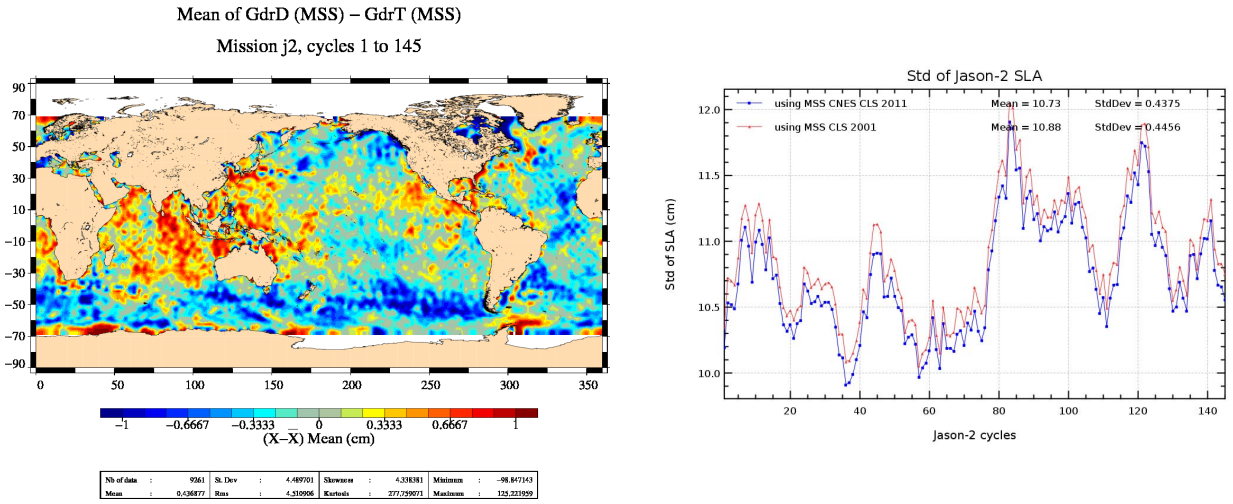

Figure 43: ***Left:*** *Difference of MSS 2011 and MSS 2001 over Jason-2 cycles 1 to 145. The map is centered around a mean of 0.44cm.* ***Right:*** *Cycle per cycle standard deviation of along-track SLA of Jason-2 GdrD using either MSS CNES/CLS 2011 (blue) or MSS CLS 2001 (red).*

The mean dynamic topography of Jason-2 GdrD contains the CNES/CLS 2009 version (instead of 2005 for GdrT).

5.5.5. Unchanged corrections between GdrD and GdrT versions

For the analyzed period, the following corrections are the same in GdrD and GdrT versions :

- Dry troposphere correction
- Model wet troposphere correction
- Earth tide
- Dynamic Atmosphere correction
- GIM ionosphere correction

6. Long Term Monitoring

The global mean sea level is one of the most important indicators of climate change as it incorporates the reactions from several different components of the climate system.

External data sources such as tide gauges allows to assess the altimeter MSL evolution and detect potential MSL drift. The changes concerning the MSL trends are presented here.

6.1. Global and Regional Mean Sea Level Trend

The description of the method and particular studies on this subject are detailed in [20]. The aim of this part is to synthesize how it was impacted by the reprocessing.

Figure 44 shows the difference of MSL trends of Jason-2 computed by separating ascending and descending passes. Normaly these trends should be very close, as the same ocean is sampled. Nevertheless for GdrT, there were trend differences of about 0.7mm/yr between odd and even passes (when removing annual and semi-annual signals). For GdrD, there is a very good improvement as the odd/even pass MSL trend difference is reduced to less than 0.1mm/yr. Note that a 120-days signal still remains (which is probably related to the orbit computation).

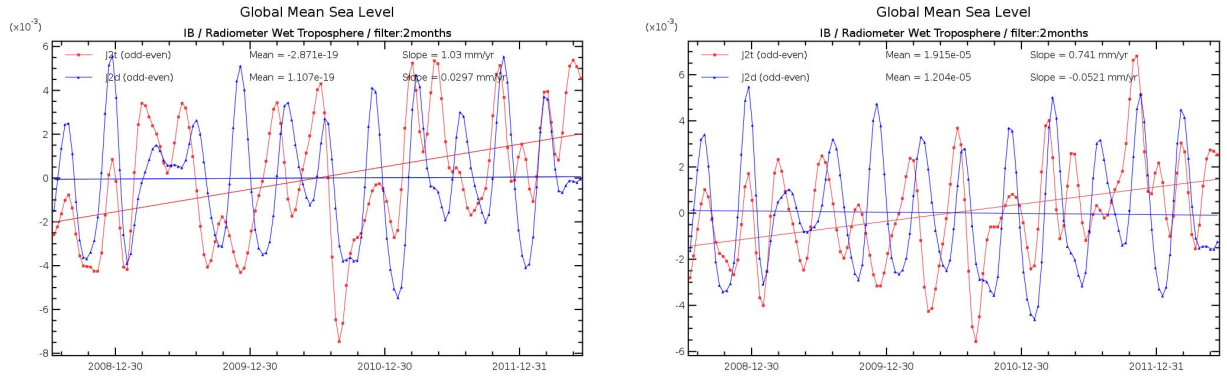

Figure 44: *Global MSL difference of trends with selection on odd and even passes, GdrT versus GdrD (**Left:** no ajustment, **Right:** semi-annual and annual signals removed)*

On figure 45, the global mean sea level is calculated after removing the annual and semi-annual signals. A 2-month filter is applied to the points to draw the curves. In order to take into account the postglacial rebound, a correction of +0.3 mm/year has to be added (not applied on the figures). The global MSL trend using Jason-2 GdrD increases by 0.2mm/yr compared to GdrT GMSL when using radiometer wet troposphere correction, but decreases by almost 0.2mm/yr when using model wet troposphere correction. The main contributor to the trend modification between GdrD and GdrT data is the radiometer wet troposphere correction (+0.35 mm/yr when using the GdrD radiometer wet troposphere correction) and to a lesser extend the POE-D orbit standard (-0.1 mm/yr when using the POE-D orbit standard).

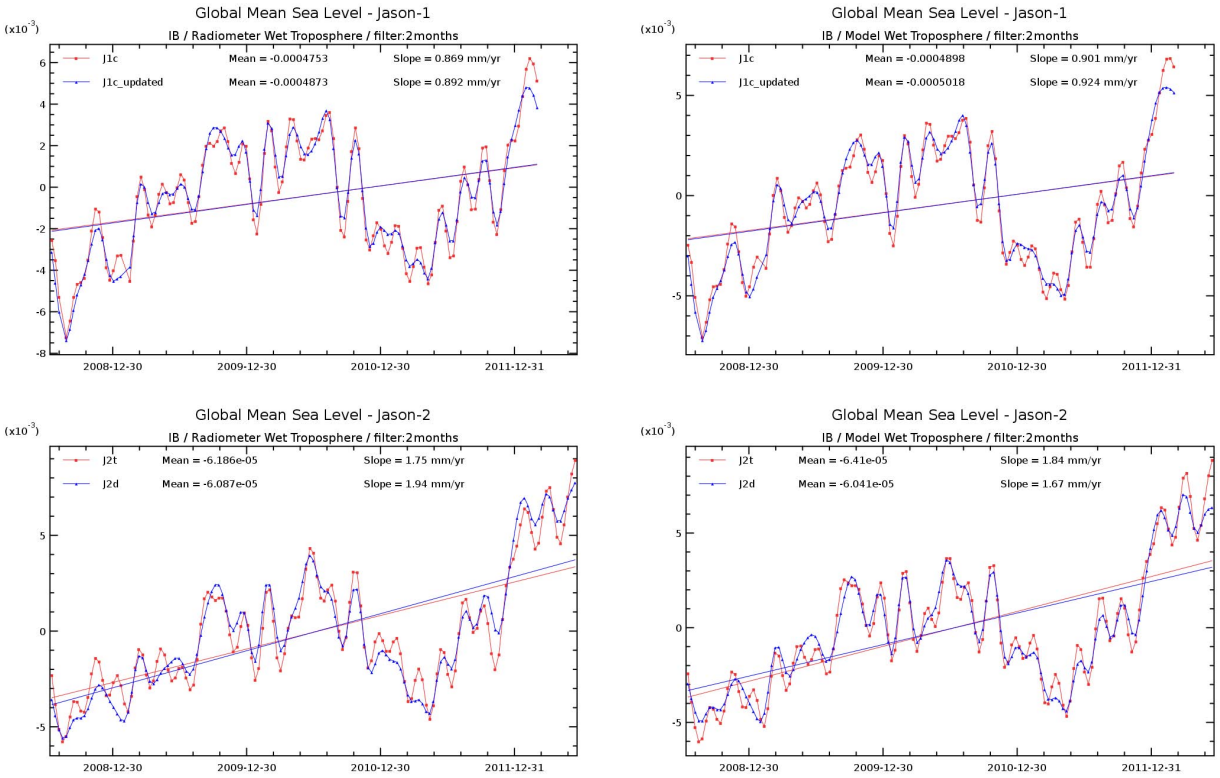

Figure 45: *Global MSL trends for J1 and J2 (2months filtered, semi-annual and annual signals removed):* ***Top:*** *Jason-1 ,* ***Bottom:*** *Jason-2;* ***Left:*** *radiometer wet troposphere,* ***Right:*** *model wet troposphere.*

Figure 46 represents the differences between Jason-1 and Jason-2 mean sea level trend before (left) and after (right) reprocessing. Blue curves are computed using radiometer wet troposphere, whereas red curves are computed using ECMWF wet troposphere model. The difference between Jason-1 and Jason-2 when using model wet troposphere is lower with GdrD (-0.25mm/yr) than with GdrT (-0.41mm/yr). On the contrary, the difference between Jason-1 and Jason-2 when using radiometer wet troposphere is greater with GdrD (-0.53mm/yr) than with GdrT (-0.36mm/yr). Note that the comparison can only be done until february of 2012, as Jason-1 entered a safe hold mode at the beginning of 2012. Consequently, these trends have been computed over a period of less than 4 years, which is a short period to conclude about long term monitoring and MSL trend calculation.

Concerning regional differences of Mean Sea Level trends between GdrD and GdrT data, hemispheric east ($longitudebetween - 180^{\circ} and 0^{\circ}$) / west ($longitudebetween 0^{\circ} and 180^{\circ}$) differences up to ±3mm/yr are observed, mainly related to the change of orbit solution (see chapter 5.2.). The Jason-2 reprocessing has therefore a large impact on the Jason-2 regional mean sea level trends. In order to analyse if this change is an improvement or not, comparisons with T/S Argo profiles should be performed (by separating analysis for eastern and western hemisphere, as described in [21]). Though this particular analysis is not yet done, global comparison of GdrT and GdrD Jason-2 data with external in-situ data, such as tide gauges or temperature/ salinity (T/S) Argo profiles were performed and results are presented in the following.

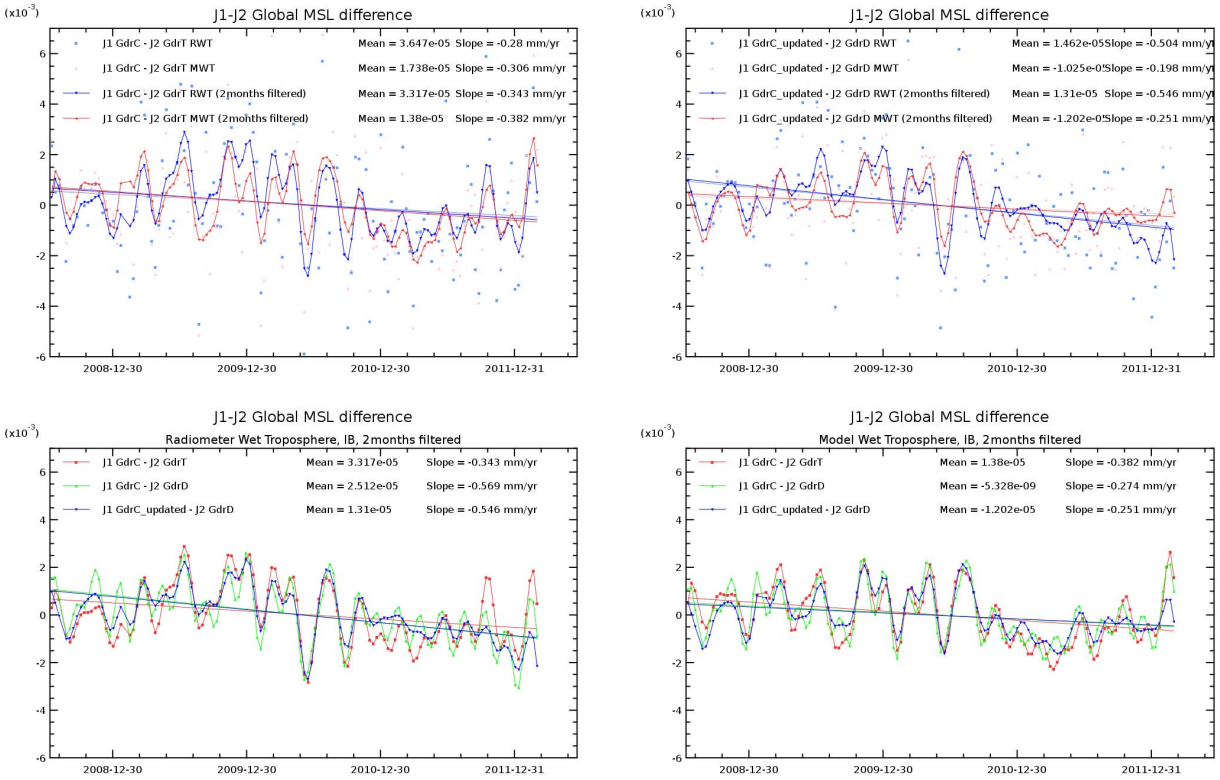

Figure 46: *Global MSL difference of trends between J1 and J2:* ***Top left:*** $J1_{GdrC}$ - $J2_{GdrT}$, ***Top right:*** $J1_{GdrC+updates}$ - $J2_{GdrD}$. ***Bottom left:*** *Radiometer Wet Troposphere,* ***Bottom right:*** *Model Wet Troposphere.*

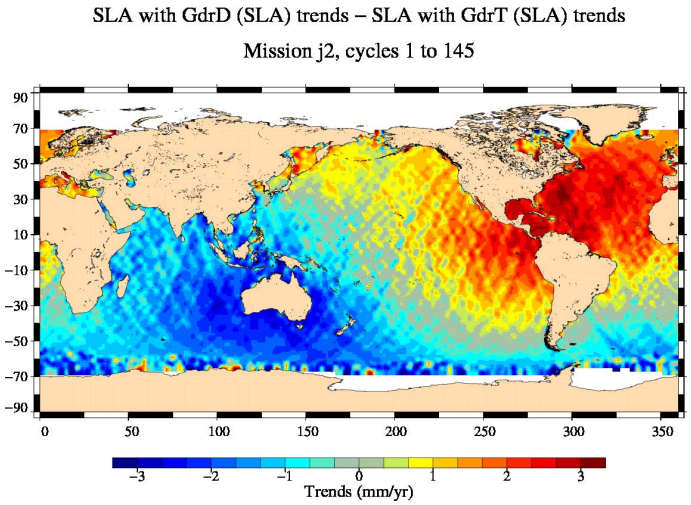

Figure 47: *Regional MSL difference of trends between GdrD and GdrT data*

6.2. Tide Gauges Comparison

While the main benefit is to estimate the performance of the GDR-D reprocessing through in-situ independent datasets comparison, the drawback of this method is that each correction can't be individually assessed in the global reprocessing. Concerning the long-term trend differences (figure 48 left), results displayed show a change in the behavior of the drift observed on Jason-2 time series, with a mean value of 0.1 mm/yr using GDR-D while it was -0.3 mm/yr considering GDR-T products. Although this result seems to be in better agreement with the trends observed on the other on-flight missions, the formal adjustment error is still very high (close to 0.5 mm/yr) due to the short period considered. This result would have to be confirmed with the computation of the 2013 Jason-2 data. Concerning the histogram of the difference of variances (figure 48 right), the mean value is close to zero, which demonstrates that the improvement of the reprocessing concerning Jason-2 data don't affect the behavior of the temporal variability of the signal. Therefore, residual signal of the difference between altimetry and tide gauges are neither increased nor reduced, which means that the temporal consistency between both datasets is the same when comparing to tide gauge measurements.

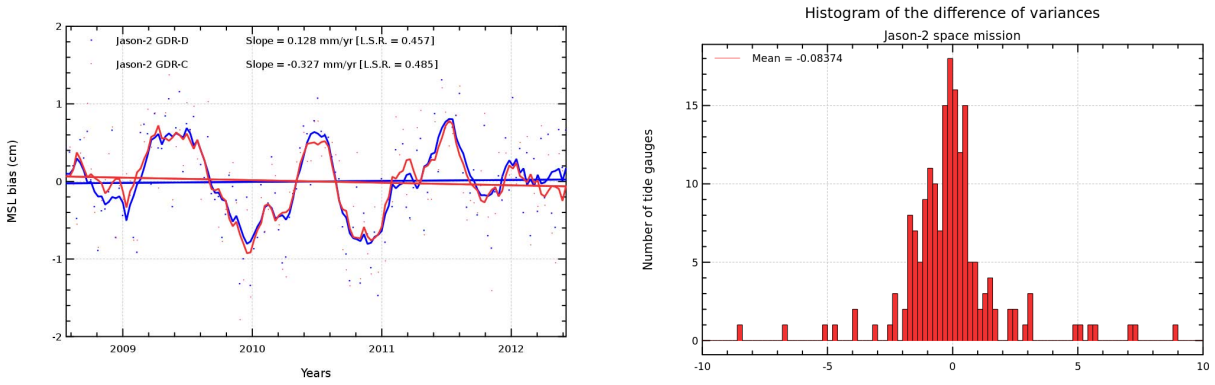

Figure 48: ***Left:*** *Monitoring of SSH trend differences computed with GDR-D and GDR-T for Jason-2 and using tide gauge measurements.* ***Right:*** *Histogram of the variance differences between altimetry and tide gauges considering both GDR-D and GDR-C Jason-2 altimeter products.*

6.3. T/S Argo profiles comparisons

The Argo+GRACE data have been used to estimate the impact of the reprocessed data on the quality of the altimeter SLA. The spatial distribution of the mean differences obtained with both versions (figure 49, top left) displays hemispheric (East/West) differences of ±1 cm as an east-west hemispheric bias has been corrected in the GDR-D orbit solution (see 5.2.). The impact of other GDR-D standards are masked by the dominant effect of the orbit. The global correlation between altimetry and the external reference is unchanged with the GDR-D version (74.1% vs 74.2%). The global standard deviation of the differences is unchanged (5.2 cm) and the map of the variances difference (figure 49, top right) shows the spatial distribution of this statistic, and thus, only the temporal evolution of the variability is taken into account (contrary to the previous global estimate where both spatial and temporal scales are included). Higher values observed in

regions of high ocean variability are associated with the higher uncertainty of the method due to the colocation of the data in these regions. Except these regions, a relatively homogeneous distribution of the variance difference is observed. Concerning the impact on the altimeter MSL drift referenced to the independent in-situ measurements, figure 49 (bottom) indicates that it is increased by 0.1 mm/yr with the use of the GDR-D standards over the studied period. This evolution is mainly associated with the updated wet troposphere correction and the GDR-D orbit solution.

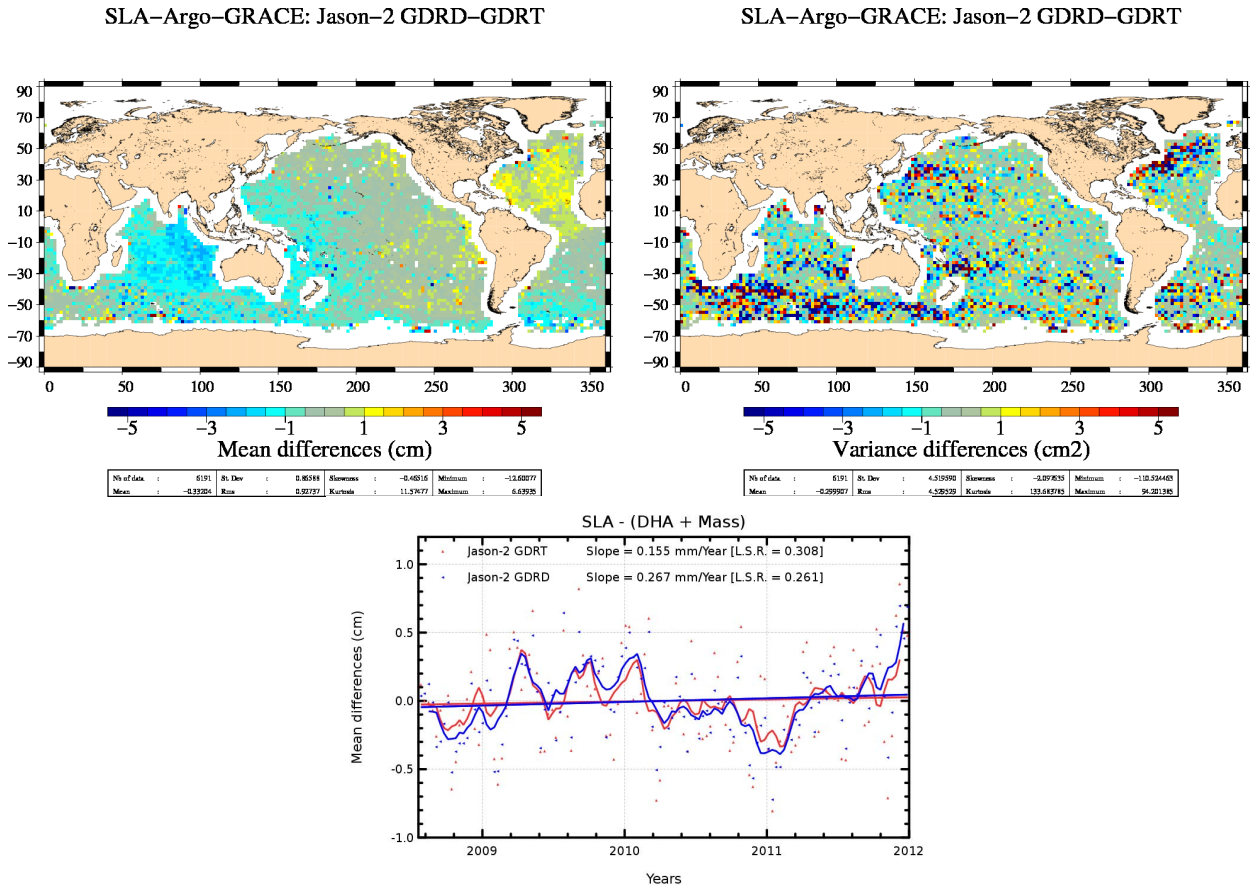

Figure 49: ***Left:*** *Mean of the sea level differences (altimeter - T/S) with Jason-2 derived from GDR-T and GDR-D standards.* ***Right:*** *Spatial distribution of the variance differences between Jason-2 GDR-D and GDR-T sea level differences (altimeter - T/S).* ***Bottom:*** *Monitoring of the sea level differences (altimeter - T/S) with both altimeter standards, where annual and semi-annual signals are removed and the curves are the 2-months filtered signal.*

7. MLE3 retracking parameters analysis - Comparisons with MLE4 retracking parameters.

The aim of this chapter is to compare the performances of two retracking algorithms based on the same least square principle (MLE is the acronym of Maximum Likelihood Estimator but in our case, the MLE has been degraded in a LSE solution): the MLE3 algorithm provides the estimations of three parameters (range, significant wave height, and power from which is derived the backscatter coefficient) whereas MLE4 provides the estimations of four parameters (the three previous ones and the slope of the waveform trailing edge).
Because Jason-1 star tracker system had shown abnormal behavior leading to mispointing angles out of the limit of validity of the model that is used in the MLE3 algorithm (0.3 deg) a new model has been developed, valid up to 0.8 deg. With this model, the mispointing angle cannot be estimated anymore with a regression of the waveform trailing edge and a retracking algorithm (MLE-4) solving for the four parameters at the same time has to be used. Amarouche and al. explain in details the differences between MLE3 and MLE4 in [25]. The impact of retracking on Jason-1 data has been presented several times by P.Thibaut at the OSTST meetings (since 2004) and also analysed in [24] by Ablain and al. in 2006. In 2010, Thibaut and al. studied in [23] the relative performance of the MLE3 and MLE4 retracking algorithms on Jason-2 altimeter waveforms. They concluded on the very good performances of the MLE4 algorithm for range and significant wave height estimates especially when return echoes do not conform to the Brown model, but highlighted two drawbacks: a small increase of the range noise level and a degraded estimation of the sigma naught coefficient (that impacts the determination of the presence of rain, the wind speed estimation and the SSB correction). Finally, Dibarboure and al. studied in [26] the differences between MLE3 and MLE4 when investigating short wavelength correlated errors.

7.1. Data coverage impact

In this paragraph, the objective is to analyze the data coverage of valid Sea Surface Height (SSH) measurements using successively MLE4 and MLE3 data. The same validation method (described in part 3.2.) is applied to the two datasets, in order to derive comparable statistics.

7.1.1. Differences in valid SSH measurements

In the following description, valid measurements will refer to points that are not rejected during the validation process. The annual signal on both curves (on figure 50) is linked to the sea ice and ice cycle.
There are globally 0.7% more valid measurements in the MLE3 dataset than in the MLE4 dataset (the reasons of this difference will be detailed in part 7.1.3.). The difference between the number of rejected measurements in MLE3 or MLE4 validation process (green curve on figure 51) is not constant and shows an annual signal ($\pm 0.1\%$) that is also related to the sea ice coverage. In order to highlight this relationship, we have superimposed the percentage of measurements that are rejected because of ice and sea ice (figure 51). The numbers of rejected measurements in case of MLE3 or MLE4 retracking are closer during winter, showing a different behaviour of the two retracking methods according to the sea ice coverage in the northern hemisphere.

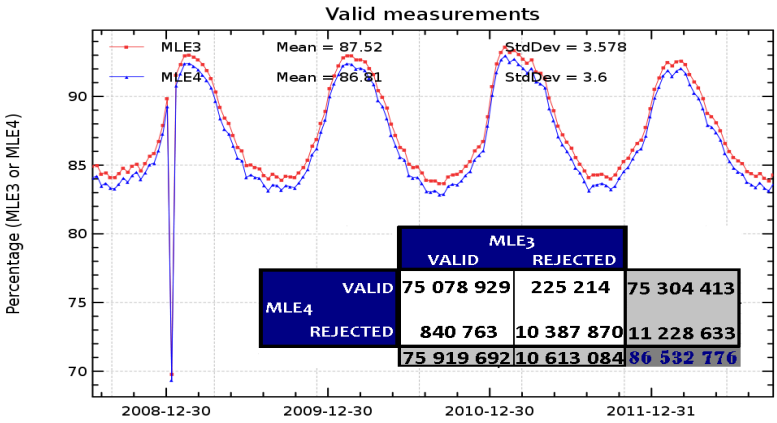

Figure 50: *Percentage of valid measurements per cycle.* ***inside box:*** *Total number of rejected measurements versus retracking method over cycle 001 to 145.*

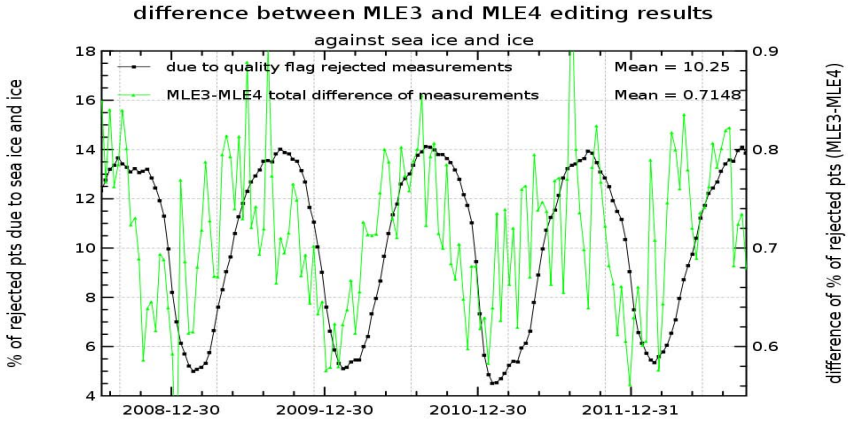

Figure 51: *MLE3 minus MLE4 difference of percentage of valid measurements per cycle against percentage of rejected measurements due to sea ice and ice over cycles 001 to 145.*

Figure 52 shows the location of rejected measurements with each validation process. The bottom map of the figure shows the percentage of measurements that are rejected in both cases. The top line of the figure shows the local percentage of points that are rejected in one validation process but validated in the other: on the top left, 0.97% of available points are only rejected in case of editing process with MLE4 data, on the top right, 0.26% of available points are only rejected in case of editing process with MLE3 data. These maps highlight a different behavior in high latitudes (which is coherent with the result presented previously (figure 51)), in near coast areas and in wet areas.
In part 7.1.3., the reasons of these differences are studied parameter by parameter.

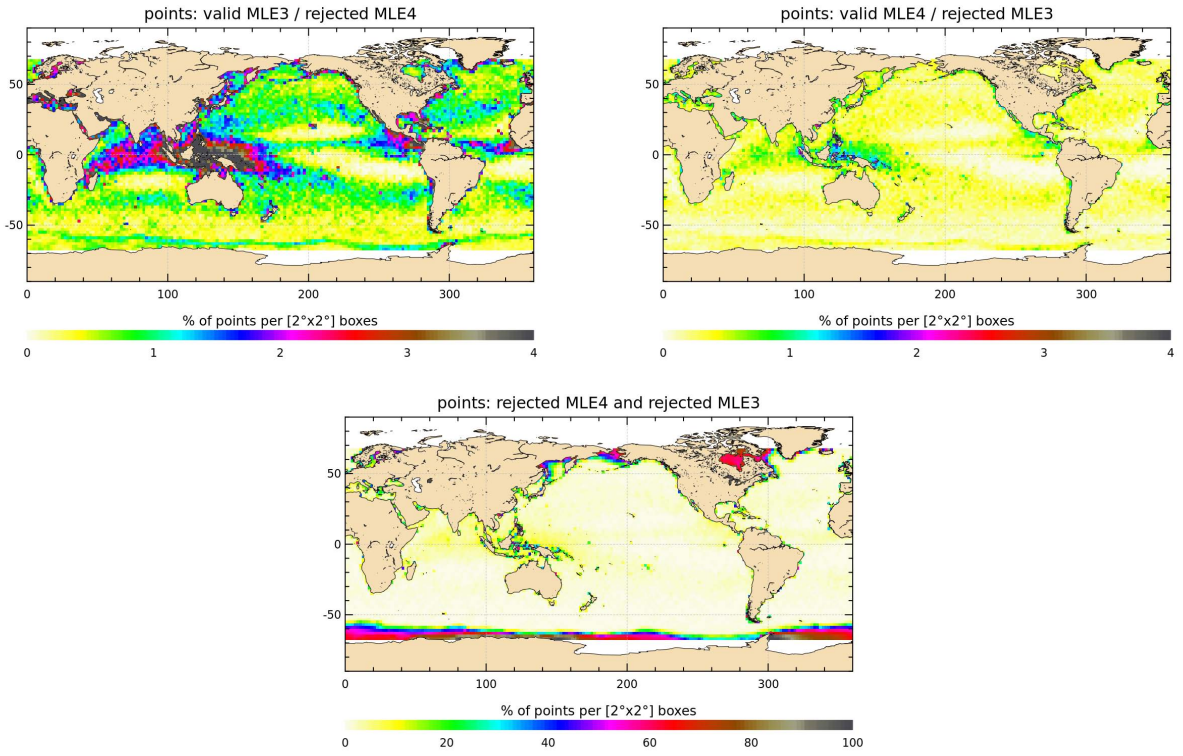

Figure 52: *Location of rejected measurements versus retracking methods.* ***Top-left:*** *Points that are rejected in the MLE4 validation process but not in the MLE3 validation process (0.97% of total measurements).* ***Top-right:*** *Points that are rejected in the MLE3 validation process but not in the MLE4 validation process (0.26% of total measurements).* ***Bottom:*** *Measurements rejected in both cases (12.00% of total measurements).*

7.1.2. A new parameter estimated in the retracking algorithm: the slope of the trailing edge

Regarding the slope of the trailing edge that is estimated by the MLE4 algorithm, it is important to keep in mind that this slope can be modified by two different causes: the first one is the real mispointing of the antenna axis with respect to the nadir. The second one is linked to the backscattering properties of the surface. As a consequence, the fourth parameter solved by the retracker must be considered as the slope of the trailing edge rather than an effective mispointing angle. The difference in rejected measurements versus the retracking method is strongly correlated with the absolute value of the square of the off-nadir angle (see figure 53). Nevertheless, the number of measurements that have been rejected directly by this criterion is the same on both validation processes: in order to be as close as possible to the MLE4 validation process, the square of the off-nadir angle obtained by the MLE4 retracking has been used in the MLE3 validation process, so that the same measurements are removed due to the square of the off-nadir angle thresholds in both cases. In the following parts, we will focus on how estimating the slope of the trailing edge in the MLE4 retracking impacts the estimation of the other parameters.

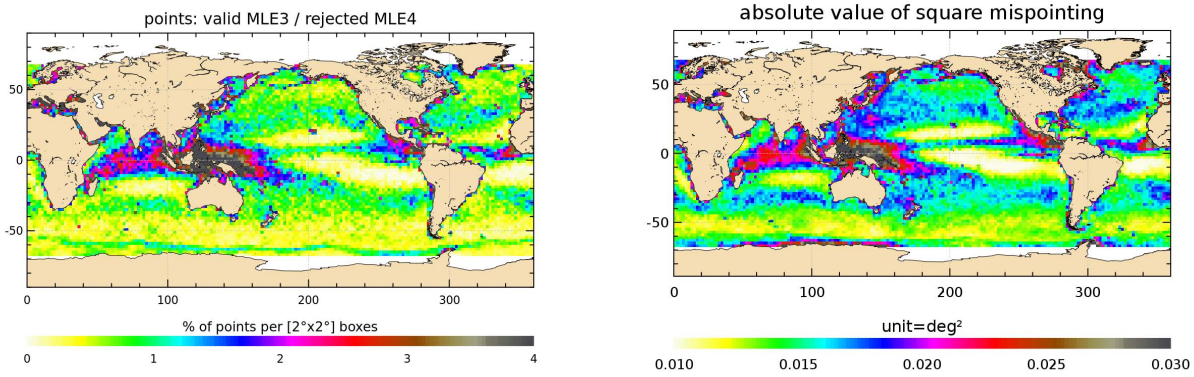

Figure 53: ***Left:*** *Points that are rejected by the MLE4 validation process but not by the MLE3 validation process.* ***Right:*** *Mean of absolute value of the square of the off-nadir angle (deg^2) over cycles 1 to 145*

7.1.3. Impact by parameter

This part details the origin of the differences in the number of rejected measurements in case of MLE3 or MLE4.

Table 5 indicates the percentage of rejected measurements due to each threshold criterion (percentages are calculated after removing data corrupted by sea ice and ice (the same measurements are rejected in both validation processes)).

Except for the standard deviation of backscatter coefficient criterion, the percentages of rejected measurements are nearly the same in both cases. Differences are not significant. The main difference in the number of rejected measurements due to thresholds is for **the standard deviation of backscatter coefficient criterion** (There are 0.53% measurements edited for MLE3 and 1.93% measurements edited for MLE4). This increase of standard deviation of backscatter coefficient in MLE4 retracking (see map on figure 54) is due to the strong correlation between the slope of the trailing edge and the sigma naught coefficient.

There are globally more validated measurements with MLE3 dataset than MLE4 dataset, nonetheless these additional measurements are valid in case of this specific validation process (adapted in case of MLE4 retracking), and the interest of keeping them in the valid dataset will be discussed in part 7.3.5..

Parameter	Threshold: min	Threshold: max	Rejected points with MLE4	Rejected points with MLE3
Orbit - $range_{MLE3 or MLE4}$	-130.000 m	100.000 m	0.76 %	0.67 %
SLA (with MLE3 or MLE4 parameters)	-2.000	2.000	1.04 %	1.06 %
Number of valid points for Ku band range (MLE3 or MLE4)	10.000	DV	1.03 %	0.89 %
RMS of the Ku band range (MLE3 or MLE4)	0.000	0.200m	1.39 %	1.50 %
Square of the off nadir angle (MLE4)	-0.200 deg^2	0.640 deg^2	0.59 %	0.59 %
Wet troposphere correction	-0.500 m	-0.001 m	0.23 %	0.23 %
Dual frequency ionosphere correction (MLE3 or MLE4)	-0.400 m	0.040 m	1.18 %	1.10 %
Ku band corrected significant waveheight (MLE3 or MLE4)	0.000 m	11.000 m	0.65 %	0.84 %
Sea state Bias (MLE3 or MLE4)	-0.500 m	0.000 m	0.62 %	0.50 %
Backscatter coefficient (MLE3 or MLE4)	7.000 dB	30.000 dB	0.60 %	0.55 %
Number of valid points for Ku band backscatter coefficient (MLE3 or MLE4)	10.000	DV	1.02 %	0.88 %
RMS of the Ku band backscatter coefficient (MLE3 or MLE4)	0.000 dB	1.000 dB	**1.93 %**	**0.53 %**
Got4.8 tide	-5.000 m	5.000 m	0.01 %	0.01 %
Altimeter wind speed (MLE3 or MLE4)	0.000 m/s	30.000 m/s	1.01 %	0.89 %
Total			3.23 %	2.37 %

Table 5: *Percentage of rejected measurements versus retracking method over cycles 001 to 145*

7.2. Parameters monitoring

In the following part, the differences between MLE3 and MLE4 parameters are detailed plotting the mean value per cycle of parameters and maps of this mean value over cycles 1 to 145. Cyclic mean values have been computed using respectively MLE3 valid measurements for MLE3 monitoring, and MLE4 valid measurements for MLE4 monitoring. Concerning the maps of differences over cycles 1 to 145, only common valid points are used.

7.2.1. Parameters not directly used in SSH computation

In this part, we will focus on parameters that are not directly used in Sea Surface Height estimation.

Backscatter coefficient *(SIG0)*: *For more information about backscatter coefficient, see part 5.4.5.*
Concerning the backscatter coefficient, the top left of figure 55 only shows a small difference between the MLE3 and the MLE4 solutions (less than 0.01dB in average). A maximal difference value of about 0.1dB can be reached in areas of low significant wave height (top left of figure 54). As expected, the standard deviation of elementary 20Hz sigma naught coefficients is lower for MLE3 (there is a bias of 0.31dB between rms of backscatter coefficient deduced from the two retracking solutions), and differences of global standard deviation of elementary 20Hz sigma naught between cycles in diode/DEM mode and those in median mode are higher in case of MLE4 (see top right of figure 55). As it is the origin of the main differences in the validation process (see validation with thresholds criteria on part 7.1.3.), we can see that the map on the top right panel of figure 54 is strongly correlated with the top left side of figure 52. That shows the location of valid measurements in MLE3 validating process that are rejected in MLE4 validating process. This increase of the sigma naught noise level is in accordance with what is presented in [23], and is due to the strong correlation between the slope of the trailing edge and the sigma naught coefficient.

Significant Wave Height *(SWH)*: *For more information about significant wave height, see part 5.4.6.*
The two pictures on the middle line of figure 55 and figure 54 show respectively the mean per cycle (figure 55) and the regional mean (figure 54) of significant wave height and significant wave height rms. Concerning the SWH, there is only about 1cm difference between MLE3 and MLE4 solution in average. The standard deviation is higher with MLE4 data than with MLE3 data because of the addition of a fourth parameter in the estimation process.

Altimeter Wind Speed: *For more information about altimeter wind speed, see part 5.4.7.*
The altimeter wind speed monitoring is similar using both MLE3 and MLE4 solutions (see bottom left of figure 55). Temporal cyclic mean (figure 55) and spatial mean over cycles 1 to 145 (figure 54) stay bellow 0.1m/s. The bottom left map of figure 54 is strongly correlated with the top left and middle left panels of figure 54 as the backscatter coefficient and significant wave height are used to compute the wind speed.

C-band sea state bias: The C-band sea state bias (bottom right of figures 54 and 55) is slightly modified by the retracking method with regional differences strongly correlated with the absolute value of square of the off-nadir angle. The bias of -6.6cm in average from MLE4 to MLE3 is due to the computation method and does not represent a real geophysical bias.

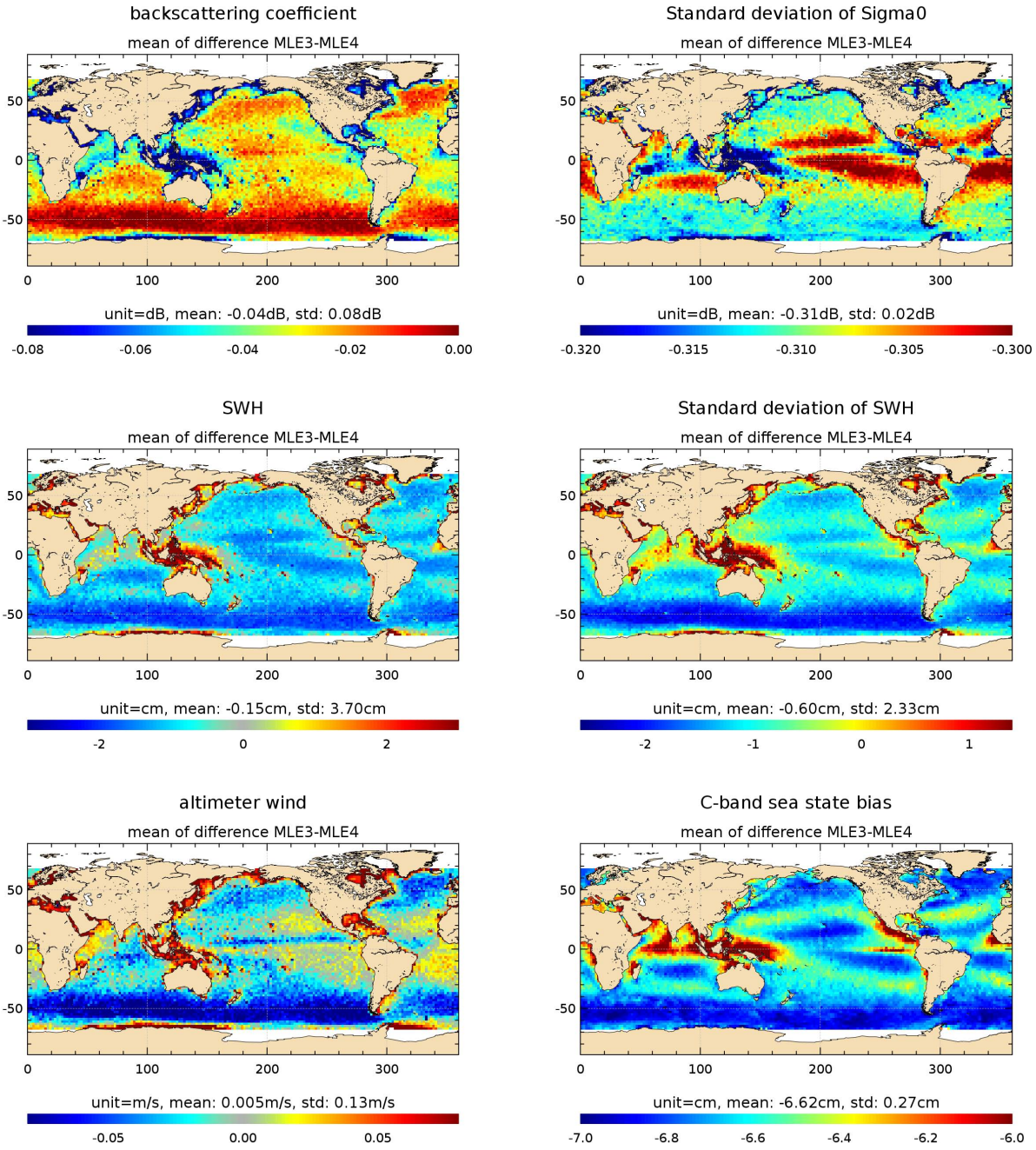

Figure 54: *Regional mean of parameters over cycles 1 to 145. Map of the mean of MLE3 minus MLE4 difference of the parameters over cycles 001 to 145. sig0_ku_mle3 - sig0_ku (top left), sig0_rms_ku_mle3 - sig0_rms_ku (top right), swh_ku_mle3 - swh_ku (middle left), swh_rms_ku_mle3 - swh_rms_ku (middle right), wind_speed_alt_mle3 - wind_speed_alt (bottom left), sea_state_bias_c_mle3 - sea_state_bias_c (bottom right)*

7.2.2. Parameters directly used in SSH computation

Sea Surface Height represents orbit minus range, taking into account some corrections, and particu-

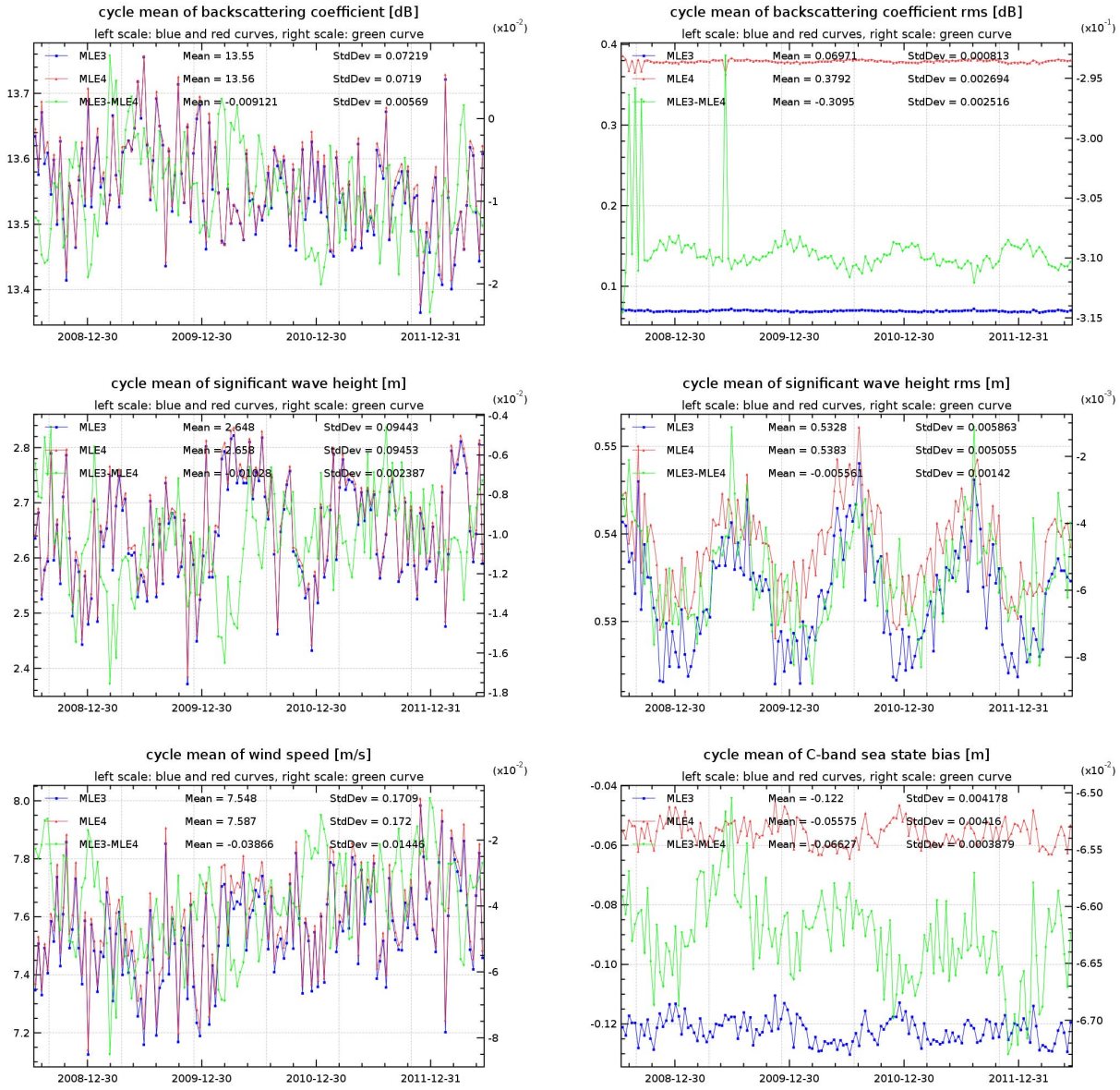

Figure 55: *Global cyclic mean monitoring of parameters over cycles 1 to 145. Monitoring of the mean of MLE3 minus MLE4 difference of the parameters from cycle 001 to 145. sig0_ku_mle3 - sig0_ku (top left), sig0_rms_ku_mle3 - sig0_rms_ku (top right), swh_ku_mle3 - swh_ku (middle left), swh_rms_ku_mle3 - swh_rms_ku (middle right), wind_speed_alt_mle3 - wind_speed_alt (bottom left), sea_state_bias_c_mle3 - sea_state_bias_c (bottom right)*

larly sea state bias and ionospheric corrections. The choice of retracking method impacts range, sea state bias and dual-frequency ionospheric corrections. *For more information about sea state bias, see part 5.4.8.*, and *for more information about ionospheric correction, see part 5.4.4.*. Sea state bias with MLE3 solution differs of about 3.2cm with respect to SSB with MLE4 solution (right of figure 57), and there is a difference of about 6 mm in average between MLE3 and MLE4 ionospheric correction (left of figure 57). Concerning the amplitude of the geographical evolution of these differences, geographical differences are less than 1mm and are not significant in case of ionospheric correction (see right of figure 56). Sea state bias spatial differences can reach 0.4cm. Regarding

range, local differences between MLE3 and MLE4 estimations can reach more than 0.6cm between Indonesia and areas in latitudes between -30° and -50°. This will impact the regional estimations of sea surface height (see part 7.3.3.)

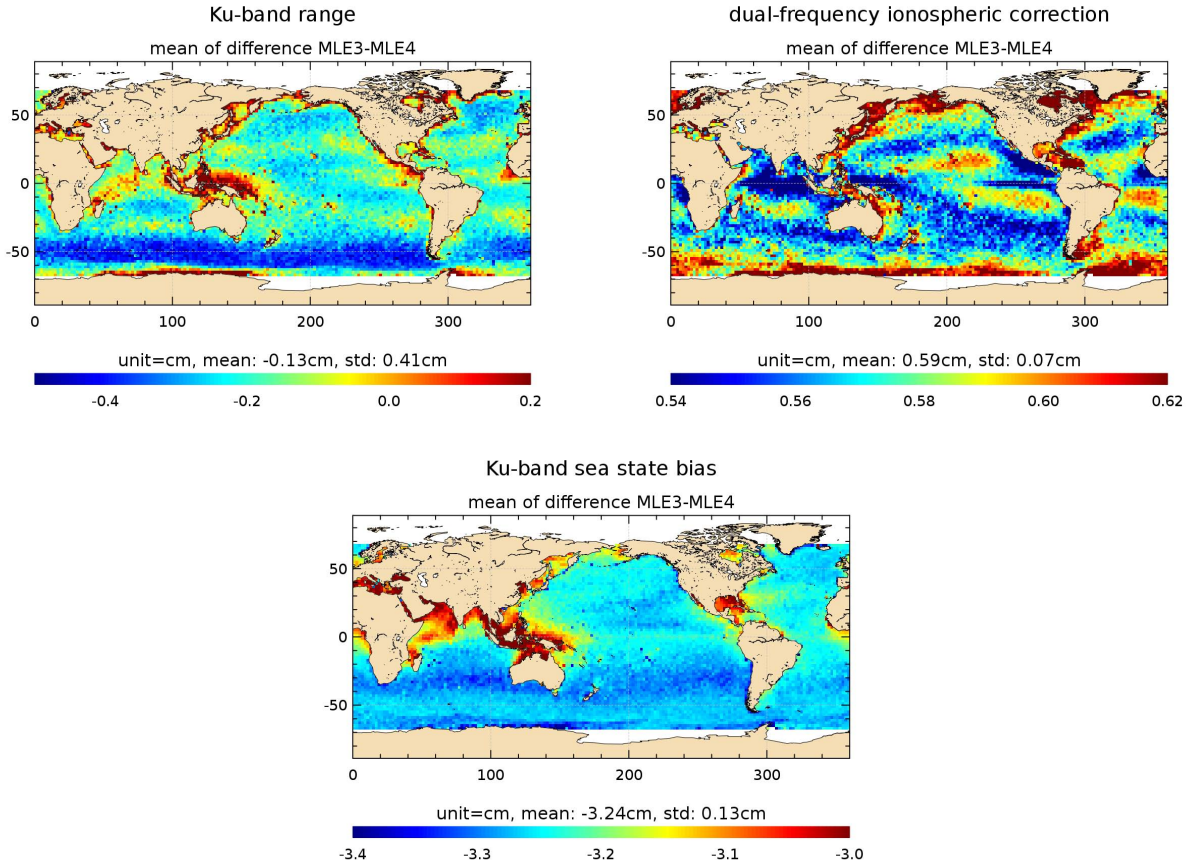

Figure 56: *Regional mean of parameters over cycles 1 to 145.* ***Left:*** *Range* ***Right:*** *Dual-frequency ionosheric correction.* ***Bottom:*** *Ku-band Sea State Bias.*

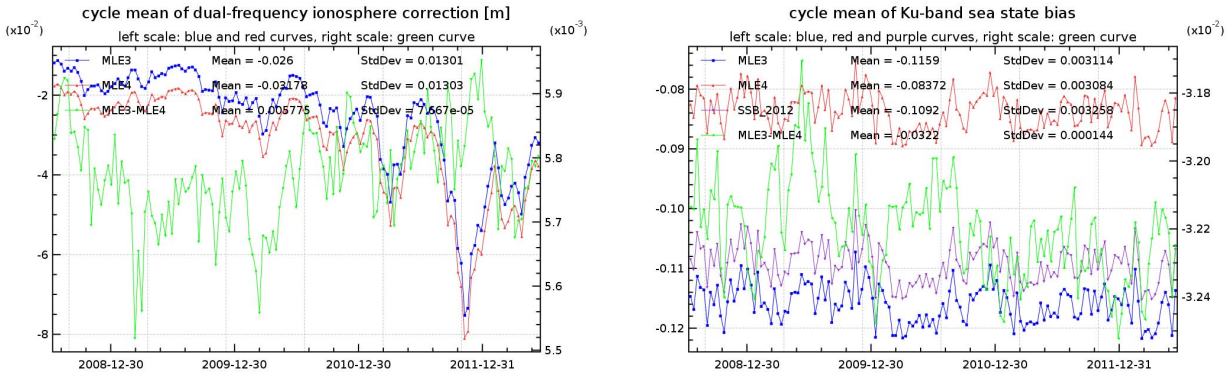

Figure 57: *Monitoring of Global cyclic mean over cycles 1 to 145.* ***Left:*** *Dual-frequency ionosheric correction.* ***Right:*** *Ku-band Sea State Bias.*

7.3. Sea Surface Height *(SSH)*

The system performances can be analyzed looking at the SSH differences at crossover points or Sea Level Anomaly (SSH - Mean Sea Surface(MSS)) from an along-track analysis with temporal or spatial averaging. In order to assess the system performance depending on retracking solution, Sea Surface Height has been computed using MLE3 or MLE4 parameters as defined below:

SSH = Orbit - Altimeter Range$_{MLE3 or MLE4}$ - $\sum_{i=1}^{n} Correction_i$

$\sum_{i=1}^{n} Correction_i$	=	Dry troposphere correction
	+	Dynamical atmospheric correction
	+	Radiometer wet troposphere correction
	+	Dual frequency ionospheric correction$_{MLE3 or MLE4}$ (filter 250km)
	+	Non parametric sea state bias correction$_{MLE3 or MLE4}$
	+	GOT4.8 ocean tide correction
	+	Earth tide height
	+	Pole tide height

Contrary to what was done in [23] and [24] where the impact of altimeter range was only taken into account, all the parameters that are available in one of the two retracking solutions are used in the SSH computation (range$_{MLE3 or MLE4}$, dual frequency ionospheric correction$_{MLE3 or MLE4}$ and sea state bias correction$_{MLE3 or MLE4}$). As these parameters are strongly correlated, it is important to keep a coherent trio of parameters in order to compute better statistics. Performance indicators have been computed taking into account the same points in both SSH estimates (common valid points from MLE3 and MLE4 validation processes).

7.3.1. Spectrum Analysis

Dibarboure and al. explain in [26] that computing the SLA spectra explains the two significant effects of adding a fourth parameter in the retracking process:

- The level of energy of the spectral hump of the MLE4 SLA PSD spectrum is lower than the one observed for the MLE3 by a factor of 2, departing from the linear ocean spectrum approximately at 50 km in case of MLE4 instead of the 70 km with MLE3.
- The 20Hz white noise level observed on the SLA PSD spectrum is slightly higher in MLE4 because there is one more degree of freedom when adjusting the Brown model.

This implies that MLE4 has a different and much more moderate response to waveform corruption on SSH thanks to the estimation of a fourth parameter.
The SLA 20Hz spectrum in figure 58 shows a stronger bump in case of MLE3 than in case of MLE4 data. This result is in accordance with what was presented in the analysis of the impact of retracking on Jason-1 data (see OSTST poster [24] about differences between Jason-1 Gdr-B and GDR-A), a 20Hz spectrum is also presented in [23] and in [26].

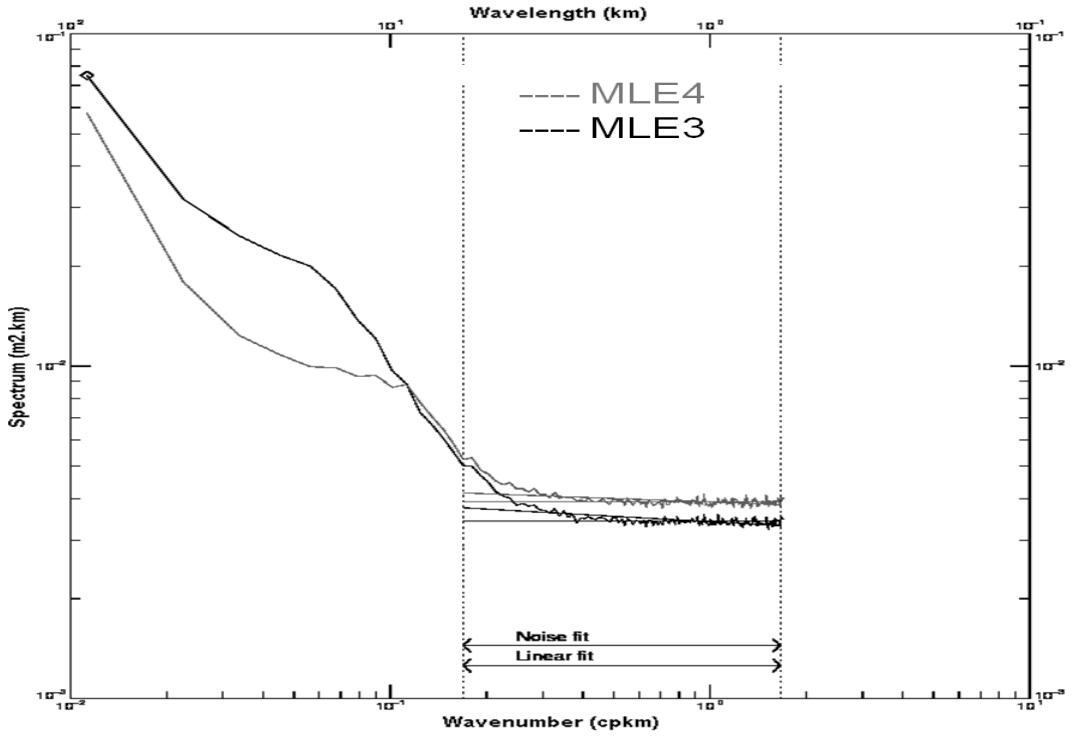

Figure 58: *Spectrum of SLA*

In the following, we will study the consequences of these differences on the performance of the system.

7.3.2. Sea Surface Height differences at crossover points

For more information about Sea Surface Height differences at crossover points, see part 4.1.
Ascending / descending SSH differences are computed at crossover points. These differences are computed for time differences inferior than 10 days between ascending and descending tracks. This allows us to minimize the contribution of the oceanic variability (mesoscale). The variance of the SSH differences at crossover points gives an information of the performance of the altimeter system. Computing the differences of variances of the SSH difference at crossovers (using on the one hand MLE3 data and on the other hand MLE4 data), allows to measure the improvement of the SSH estimation depending on the retracking solution.
On Figure 59, a selection on $|latitude| < 50deg$, $bathy < -1000m$ and low variability areas has been done on points that are valid in both MLE3 and MLE4 edited data set. The mean of SSH crossovers is globally equivalent in both cases. Standard deviation at SSH crossovers is largely higher using MLE3 data than using MLE4 data which means that **an important improvement of the performances at time scales less than 10 days is obtained with the MLE4 retracking with respect to the MLE3 retracking**.

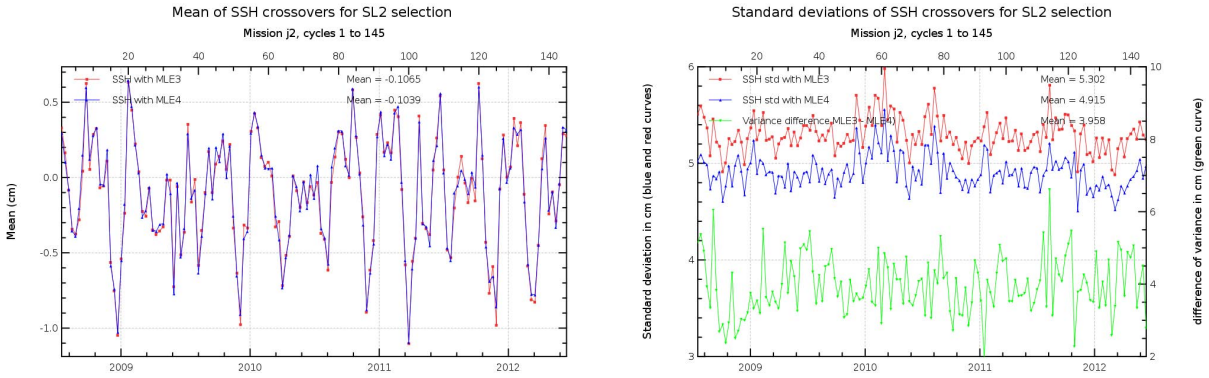

Figure 59: *Mean **(left)** and standard deviation **(right)** of SSH differences at crossover points. Only crossover points with $|latitude| < 50^{\circ}$, bathymetry < -1000m and oceanic variablity less than 20 cm are chosen. Only points valid with MLE3 AND MLE4 validation processes are taken into account.*

For Figure 60, only the points that have been validated with both validation processes (common valid measurements with MLE3 and MLE4 validation process) are taken into account. The mean value of the difference of variance between MLE3 and MLE4 SSH crossovers is $3.75cm^2$, which represents **a great improvement**. The global SSH variance difference is positive **everywhere** (yellow and red points on the map), meaning a reduction of variance from MLE3 to MLE4. This suggests again that the MLE4 algorithm performs better than the MLE3 **everywhere**, in agreement with SLA PSD spectrum shown in (figure58) .

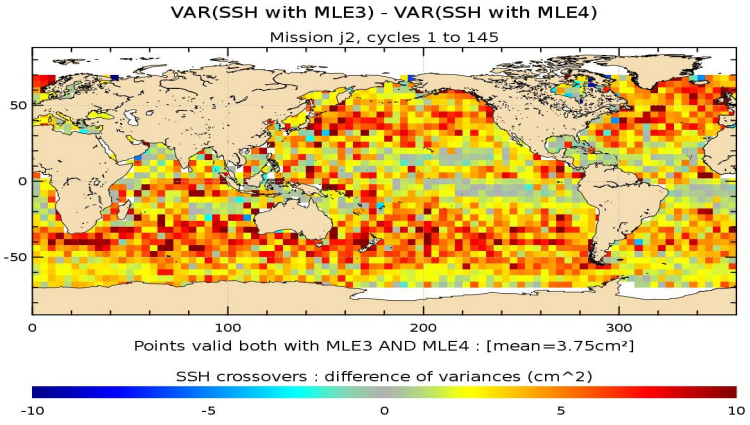

Figure 60: *Differences between SSH crossover variances (variance SSH_{MLE3} - variance SSH_{MLE4}) for data from cycle 1 to 145. MLE3 AND MLE4 valid points : $[mean = 3.75cm^2]$.*

7.3.3. Along-track performances of Sea Level Anomaly

The Sea Level Anomaly (SLA) corresponds to the sea surface height (SSH) minus the mean sea surface (SLA = SSH - MSS). *For more information about Sea Level Anomaly, see part 4.2.* The second classical method to quantify the altimeter performances consists in a spatial averaging of the sea level anomaly measurements over N cycles (here from cycle 1 to 145).
The difference between SLA computed with MLE4 data and MLE3 data is 2.8 cm in average. It is mainly due to the differences in sea state bias (-3.2cm from MLE4 to MLE3) and ionospheric correction (+0.6cm from MLE4 to MLE3). The right part of figure 61 shows the regional distribution of this bias which is lower near the coasts.

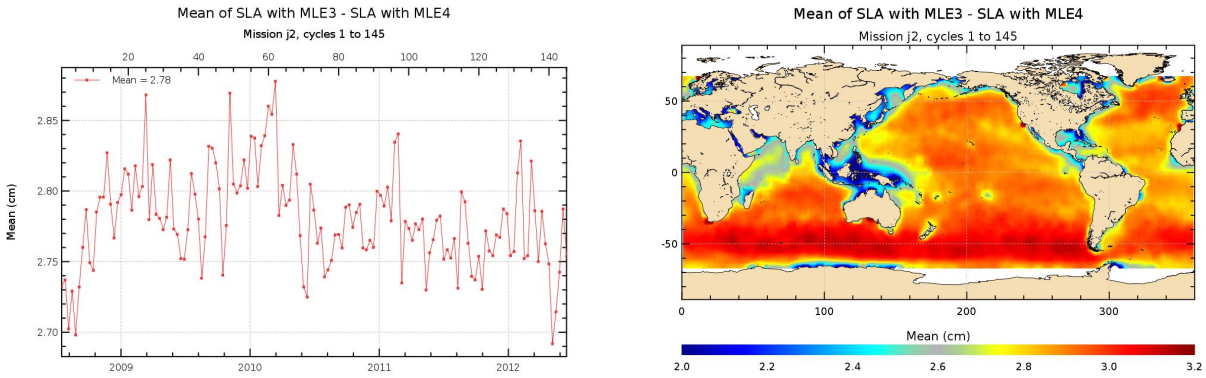

Figure 61: ***Left:*** *Monitoring of mean value of the Sea Level Anomaly.* ***Right:*** *Map of Sea Level Anomaly mean over cycles 001 to 145*

The impact of the choice of dataset on global mean sea level trend over the 145 cycles is less than 0.1mm/yr, which is not significant (see figure 62).

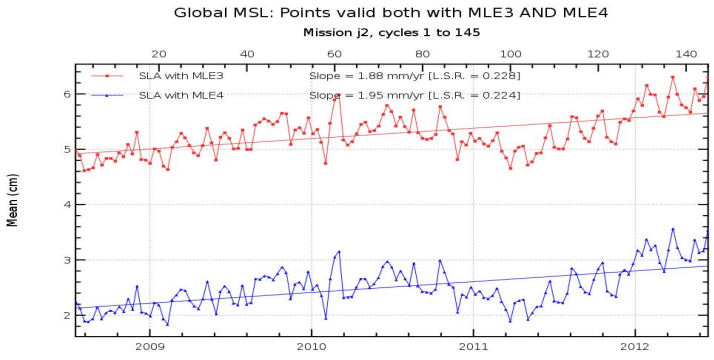

Figure 62: *Impact on Global MSL trend*

Figure 63 allows to evaluate the origin of the regional differences of sea level anomaly. These differences are mainly due to range differences, particularly for areas with latitudes between -30° and -60° and around Indonesia. The contribution of the Sea state bias differences is also important around Indonesia and near the coasts.

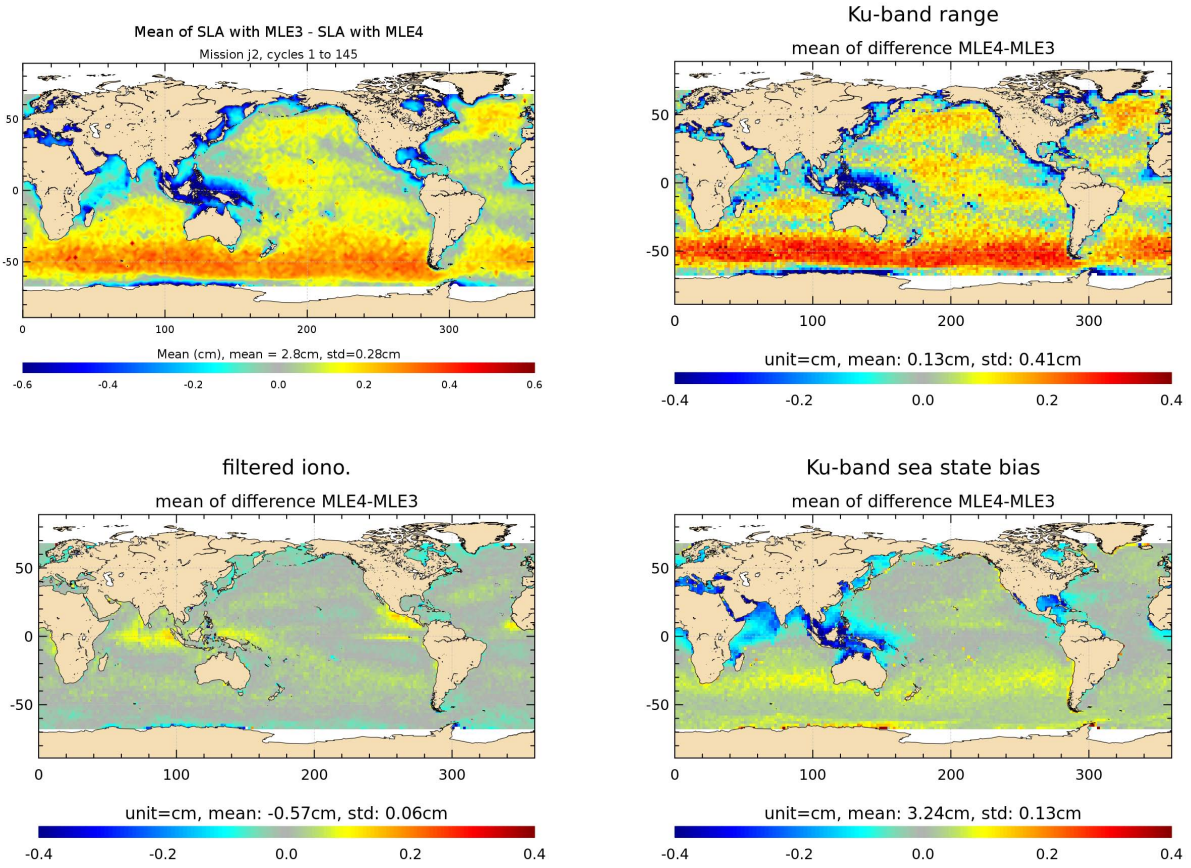

Figure 63: *Centered maps of MLE3-ML4 differences over cycles 1 to 145.* ***Top-Left:*** *Sea Level Anomaly.* ***Top-Right:*** *Range.* ***Bottom-Left:*** *filtered ionospheric correction.* ***Bottom-Right:*** *sea state bias.*

The global Sea Level Anomaly standard deviation is higher using MLE3 data than using MLE4 data (see figure 64) with a difference of variance of SLA of 2.72cm^2 between the two datasets.

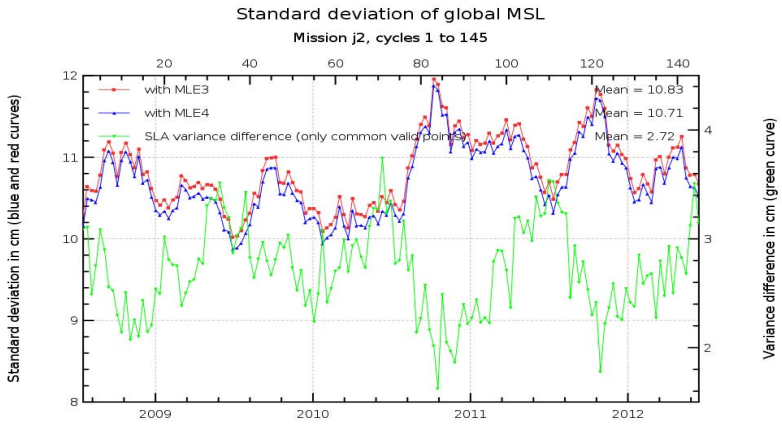

Figure 64: *Monitoring of Sea Level Anomaly standard deviation. MLE3 AND MLE4 valid points .*

On the top map of figure 65 that only takes into account the points that have been validated with both validation processes (common valid measurements with MLE3 and MLE4 validation processes) the total SLA variance reduction is equal to $2.85cm^2$. This result is consistent with the previous one (temporal averaging on collocated measurements). The map of the along-track SLA variance differences shows that the gain (in red) is strongly correlated with the absolute value of the square of the off-nadir angle value on the bottom panel of figure 65. Knowing that globally, the real Jason-2 platform mispointing angle is close to zero, the slope of the trailing edge on the map mainly varies mainly in regions where geophysical effects like sigma0 bloom events and rain cells occur (as explained in [23]). **In conclusion, MLE4 performs better than MLE3 with a reduction of the variance of SLA in the regions where the waveforms do not conform to the theoretical Brown's model**.

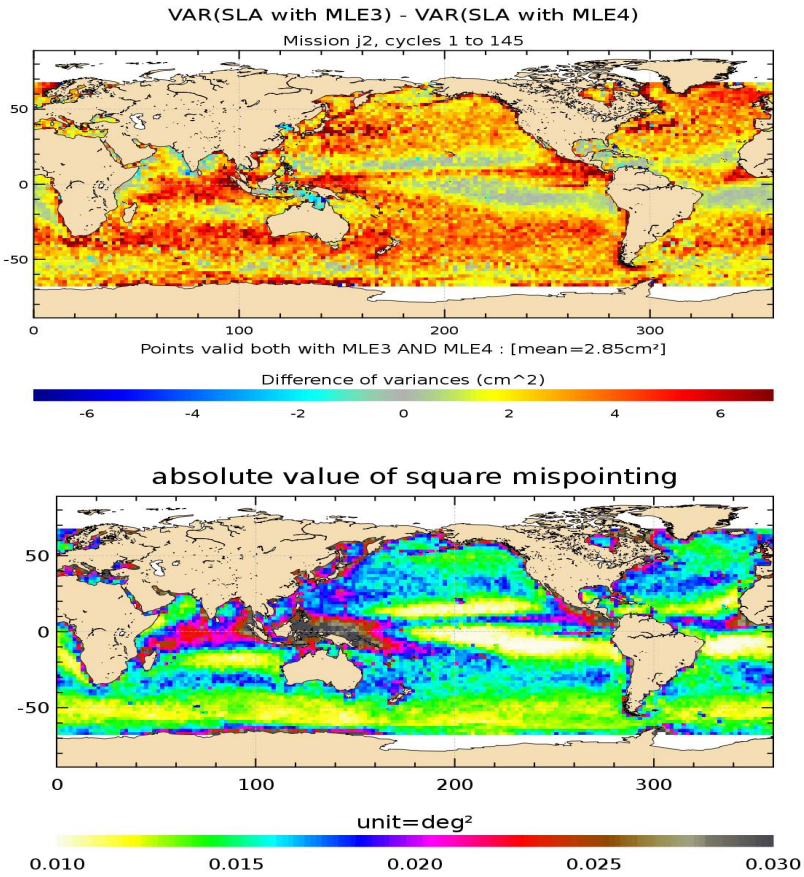

Figure 65: ***Left:*** *Map of difference of Sea Level Anomaly variances. MLE3 AND MLE4 valid points .* ***Right:*** *Mean of absolute value of square of the off-nadir angle (deg^2) over cycles 1 to 145*

7.3.4. Analysis

The analysis of variance for SSH difference at crossovers points or SLA gives information of the performance of the altimeter system. The total SLA variance reduction is $2.85cm^2$. The difference of variance between MLE3 and MLE4 SSH crossovers at time scales less than 10 days is $3.75cm^2$, as errors on Sea Surface Height are on both tracks (ascending and descending), dividing by 2 gives

the gain in explained variance in Jason-2 final Sea Surface Height about $2cm^2$. These two results show that the gain in variance is mainly observed for lower that 10days signals. This is coherent with the SLA spectrum differences (as there is a bump of energy for MLE3 signals for wavelenghts between 10 and 70 km).
The analysis of the regional differences allows to locate the main improvements in the regions where geophysical effects like sigma0 bloom events and rain cells occur.
In conclusion MLE4 always performs better than MLE3, and particularly in the regions where the waveforms do not conform to the theoretical Brown's model.

7.3.5. Investigation on additional valid measurements in MLE3 validation process

As mentioned in part 7.1.1. there are globally 0.7% more validated measurements in the MLE3 dataset than in the MLE4 dataset. Nonetheless, the validation process used has been adapted in case of MLE4 retracking, and these additionnal valid points with MLE3 dataset have to be analysed. In order to understand how these additional MLE3 validated measurements impact the system performances, the previous study has been done with another approach, by taking into account:

- all validated points from MLE3 validation process in case of SSH calculation with MLE3 parameters
- all validated points from MLE4 validation process in case of SSH calculation with MLE4 parameters.

On maps of figure 66, the global SSH crossovers variance reduction is $7.55cm^2$ when taking into account only valid measurements from each own validation process (MLE3 or MLE4), whereas when taking into account only the points that have been validated with both validation processes (common valid measurements with MLE3 and MLE4 validation process), the difference of variance is lower ($3.75cm^2$).

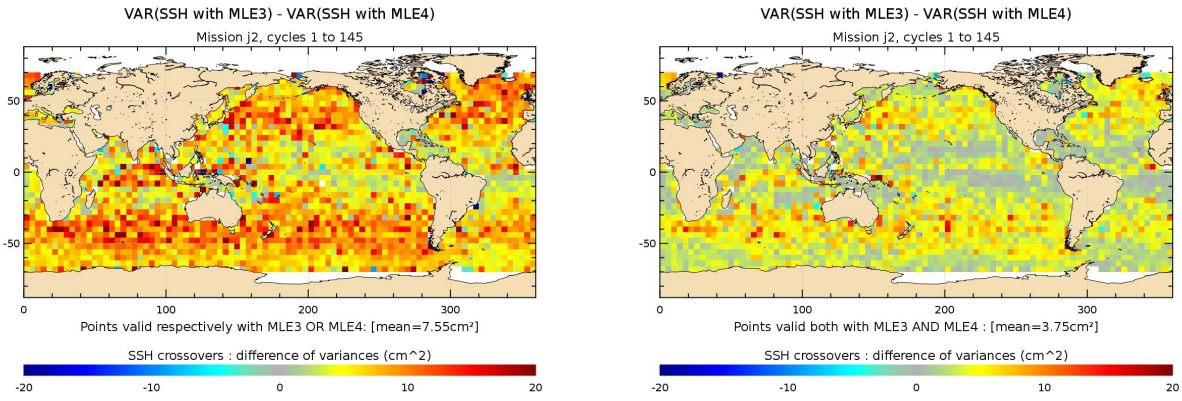

Figure 66: *Differences between of SSH crossover variances (variance SSH_{MLE3} - variance SSH_{MLE4}) for data from cycle 1 to 145.* ***Left:*** *Points valid respectively with MLE3 OR MLE4: [$mean = 7.55cm^2$].* ***Right:*** *Points valid both with MLE3 AND MLE4: [$mean = 3.75cm^2$].*

As the red curve is under the blue curve on figure 67, the MLE3 minus MLE4 difference of SLA variance is lower when taking into account only the common valid points in both validation processes

(2.72cm^2 with common points, 4.51cm^2 when taking into account additional points in case of MLE3 data).

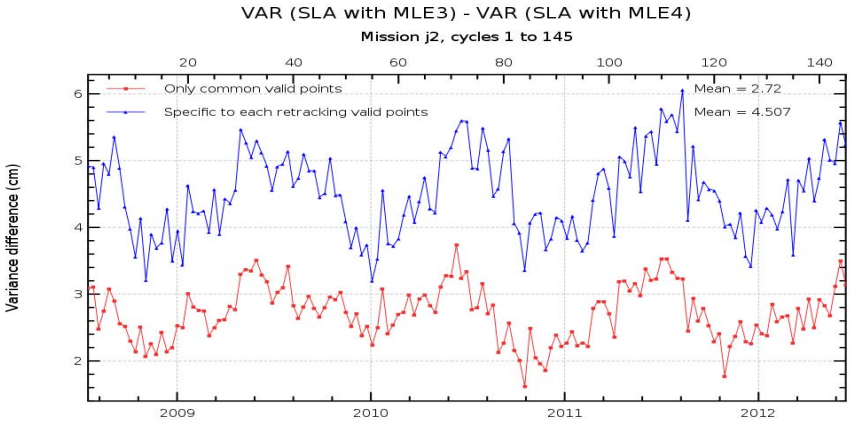

Figure 67: *Difference of global variance with and without taking into account points that are valid in MLE3 validation process.* ***Blue:*** *Points valid respectively with MLE3 OR MLE4.* ***Red:*** *Points valid both with MLE3 AND MLE4.*

Finally, on maps of figure 68, the global SLA variance reduction is 4.93cm^2 when taking into account only valid measurements from their own validation process (MLE3 or MLE4). When only taking into account the common valid measurements, the difference of variance drops to 2.85cm^2. This result is consistent with the previous one (temporal averaging on collocated measurements).

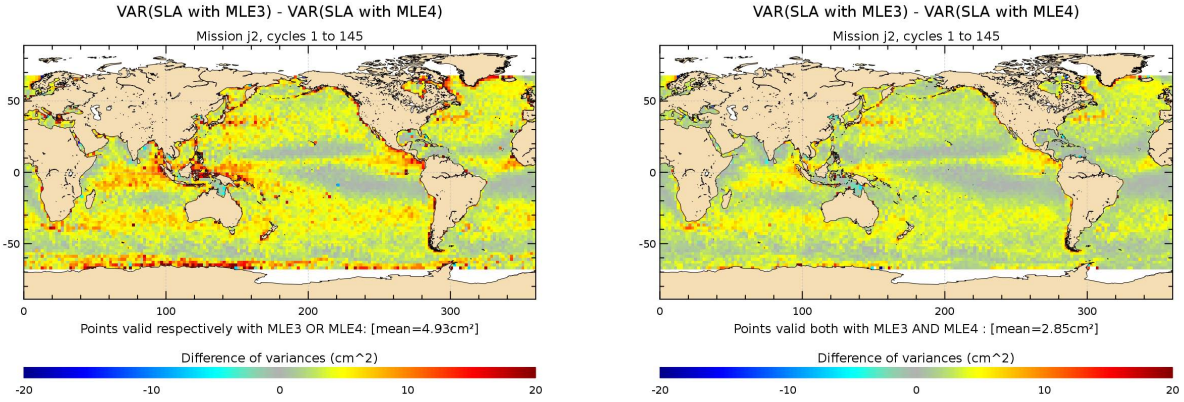

Figure 68: ***Top:*** *Map of difference of Sea Level Anomaly variances.* ***Left:*** *Points valid respectively with MLE3 OR MLE4.* ***Right:*** *Points valid both with MLE3 AND MLE4.*

All these results allow to conclude that when taking into account the points that have not been rejected during MLE3 validation process in the SLA calculation, the variance at SSH crossovers and SLA increase, meaning a degraded performance of the system. These 0.7% of points which are kept after the validation process in case of MLE3 data contain a level of variance of about 300 cm^2 (three times more than normal global SLA variance that is about 100 cm^2).

7.4. Conclusion

The main objective of this study was to check in the last J2 GDR-D release the good quality of MLE3 and MLE4 parameters and to compare their respective performances. All the performed analyses have shown that we obtain similar results to those obtained on Jason-1 ([24]).

Concerning the system performance, the two diagnostics that are commonly used in Calval studies show similar results, namely a variance of SSH crossovers and along-track SLA greater with the MLE3 output than with the MLE4 output.

Concerning the validation process, more measurements are rejected with MLE4 parameters, but the additional data kept with MLE3 have bad performances. This highlights that the validation process is not strict enough in case of MLE3 data.

This study confirms on Jason-2 data the results already presented and published: the MLE4 retracking performs better than the MLE3 one. It allows an improvement of the physical content of SLA for along track scales between 10 and 70 km.

8. Conclusion

8.1. Conclusion on the data quality

An overview of the impact of the GdrD version of Jason-2 altimeter system over ocean has been presented in this report. Comparisons have been done with previous version data (GdrT). Taking advantage that Jason-2 and Jason-1 flew on the same ground track with only 55 seconds apart during the formation flight phase (from 12th of July 2008 to 26th of January 2009), particular comparisons with Jason-1 data have been done over this period. From 10th of February 2009 to 3rd of March 2012, Jason-1 flew on an interleaved ground track with a time shift of 5 days compared to Jason-2 ground track, so that comparisons with Jason-1 data have also been done over this period. Furthermore comparisons between Jason-2 and Envisat data are also included in this report.

The **reprocessing** of the Jason-2 altimetric mission allows several modifications that correct some problems and improve several standards, following the OSTST community's requests.
- In terms of available and valid data, the coverage is at least as good as in GdrT version. A few missing measurements in previous version are added in GdrD version. Slightly more data are edited in the GdrD version than in the GdrT version (as due to the MQE setting more measurements than previously are at default value).
- In terms of performance at crossovers, the quality is also improved : the average of mean ascending/descending SSH differences at crossovers is more centered, and the standard deviation is reduced. The gain on global SSH variance was estimated to around $1.7cm^2$ with some maximums of $3cm^2$. The GdrD data improve also the coherence of ascending/descending SSH differences as geographic patterns are reduced (which is due to the new orbit solution).

Finally, the analysis of the data from the MLE3 retracking confirms that MLE4 always performs better than MLE3, and particularly in the regions where the waveforms do not conform to the theoretical Brown's model.

8.2. Particular warnings

Several (especially) ascending passes have a time tag shifted (compared to GdrT version) by about 0.051 seconds. Nevertheless, this has no impact on the quality of the data.

8.3. Main evolutions

Note the following evolutions:

- The main improvement in GdrD version is its new orbit. This solution very much improves the coherence of ascending/descending SSH differences. It also improves the coherence between Jason-2 and Envisat as there are no longer east/west biases
- The pseudo time-tag bias mean (-0.29ms for Jason-2 GdrT) has been corrected and is now close to zero. Consequently, the small north/south hemispheric differences on Jason-2 SSH crossovers differences are reduced.
- Radiometer parameters have been enhanced in coastal regions, and an anomaly in 34GHz

channel has been corrected. New AMR calibration coefficients are also used.

- The expected modifications with the update of the altimeter characterization file, corrected pole tide solution, altimeter wind speed, global tide model are observed.
- GdrD sea state bias is calculated with a different approach for low sea states. Main differences are observed in these areas (as the editing method has changed). Note that an updated version of SSB model (based on Gdr-D data) was presented at OSTST2012.

8.4. Conclusions

In conclusion, the reprocessed dataset is improved compared to the original GdrT time series. However, when compared to Jason-1 data, the differences increase with GdrD data. This is mainly due to the sea state bias.
As concerned the long term impact of the GdrD version, such as mean sea level trend impact, the completion of the reprocessing of the whole Jason-2 mission (4 years of data) allows to improve the coherence between Jason-2 odd and even passes results, and between Jason-2 and Jason-1 trends.

9. Bibliography

References

[1] AVISO and PODAAC User Handbook. IGDR and GDR Jason-1 Products. Edition 4.1, October 2008. SMM-MU-M5-OP-13184-CN (AVISO), JPL D-21352 (PODAAC). Available at http://www.aviso.oceanobs.com/fileadmin/documents/data/tools/hdbk_j1_gdr.pdf.

[2] Boy, François and Jean-Damien Desjonqueres. 2010. Note technique datation de linstant de reflexion des échos altimètres pour POSEIDON2 et POSEIDON3 *Reference: TP3-JPOS3-NT-1616-CNES*

[3] S. Brown. 2010. A Novel Near-Land Radiometer Wet Path-Delay Retrieval Algorithm: Application to the Jason-2/OSTM Advanced Microwave radiometer. *IEEE TGRS vol. 48 n ° 4*. Available at ftp://podaac.jpl.nasa.gov/allData/ostm/preview/L2/AMR/docs/Brown_TGARS_2010.pdf

[4] S. Brown, S. Desai, and A. Sibthorpe. 2011. Improvements to the Radiometer Processing for GDR-D. *Oral presentation at OSTST meeting, San Diego, USA*. Available at http://www.aviso.oceanobs.com/fileadmin/documents/OSTST/2011/oral/02_Thursday/Splinter5IP/04_Brown.pdf

[5] Cerri, L., A. Couhert, S. Houry, F. Mercier. 2011. Improving the long-term stability of the GDR orbit solutions. *Oral presentation at OSTST meeting, San Diego, USA*. Available at http://www.aviso.oceanobs.com/fileadmin/documents/OSTST/2011/oral/02_Thursday/Splinter3POD/05_Cerri.pdf.

[6] Dumont, J.-P., V. Rosmorduc, N. Picot, S. Desai, H. Bonekamp, J. Figa, J. Lillibridge, R. Sharroo, 2011: OSTM/Jason-2 Products Handbook. CNES: SALP-MU-M-OP-15815-CN. EUMETSAT: EUM/OPS-JAS/MAN/08/0041. JPL: OSTM-29-1237. NOAA/NESDIS: Polar Series/OSTM J400. Issue 1 rev 8. Available at http://www.aviso.oceanobs.com/fileadmin/documents/data/tools/hdbk_j2.pdf

[7] Jason-2 Version T Geophysical Data Records : Public Release, August 2009. Available at : http://www.aviso.oceanobs.com/fileadmin/documents/data/products/Jason-2_GDR_T_disclaimer.pdf

[8] MSEs (CNES, NASA, NOAA, EUMETSAT). 2011. GDR Status. *Oral presentation (by N. Picot) at OSTST meeting, San Diego, USA*. Available at http://www.aviso.oceanobs.com/fileadmin/documents/OSTST/2011/oral/03_Friday/Plenary/GDRProducts/02PicotGDR_status_2011.pdf.

[9] Ollivier et al., JASON-2 / ENVISAT CROSS-CALIBRATION *Oral presentation at OSTST meeting, Venice, Italy.*

[10] Ollivier et al., Assessment of Orbit Quality through the SSH calculation *Oral presentation at OSTST meeting, Venice, Italy.*

[11] Ollivier and M. Guibbaud, Envisat RA2/MWR reprocessing impact on ocean data. SALP-RP-MA-EA-22083-CLS. CLS.DOS/NT/12.064. Available at http://www.aviso.oceanobs.com/fileadmin/documents/calval/validation_report/EN/EnvisatReprocessingReport.pdf

[12] Ollivier and M. Guibbaud, Envisat RA2/MWR ocean data validation and cross-calibration activities. Yearly report 2012.

[13] S. Philipps, G. Valladeau, J.F. Legeais and M. Ablain, 2012: Jason-2 validation and cross calibration activities 2011. SALP-RP-MA-EA-22042-CLS.

[14] S. Philipps, H. Roinard and M. Ablain, 2012: Jason-2 reprocessing impact on ocean data (cycles 001 to 020). Comparison of Jason-2 Gdr-D with Gdr-T, as well as with Jason-1 Gdr-C. SALP-RP-MA-EA-22118-CLS. ftp://avisoftp.cnes.fr/AVISO/pub/jason-2/documentation/gdr_d_calval_report/JA2_GDR_D_validation_report_cycles1to20_V1_1.pdf

[15] Philipps S., H. Roinard, M. Ablain and N. Picot. Global Jason-2 Data Analysis of Reprocessed Gdr-D Products. Poster OSTST 2012, Venice.

[16] Schaeffer P., Y. Faugère, JF Legeais, A. Ollivier, T. Guinle and N. Picot. The CNES-CLS11 Global Mean Sea Surface computed from 16 years of satellite altimeter data. Marine Geodesy, in press.

[17] Tran N. , Labroue S. , Philipps S. , Bronner E. and Picot N. (2010) Overview and Update of the Sea State Bias Corrections for the Jason-2, Jason-1 and TOPEX Missions, *Marine Geodesy*,**33:1, 348 - 362**. Avialable at http://pdfserve.informaworld.com/804727__925502357.pdf

[18] Tran N. , Philipps S. , Bronner E. and Picot N. (2012) Impact of GDR_D standards on SSB corrections,*Oral presentation at OSTST meeting, Venice, Italy.*

[19] Valladeau, G., 2012: Validation of altimeter data by comparison with tide gauge measurements for TOPEX/Poseidon, Jason-1, Jason-2 and Envisat (Annual report 2011). SALP-NT-MA-EA-22046-CLS, CLS.DOS/NT/12-016.

[20] http://www.aviso.oceanobs.com/msl

[21] Legeais, JF. 2012: Validation of altimeter data by comparison with in-situ T/S Argo profiles for Jason-1, Jason-2 and Envisat (Annual report 2012).

[22] OSTST2010, San Diego. Splinter: "60-day variations in J1 & J2" http://www.aviso.oceanobs.com/fr/courses/sci-teams/ostst-2010/ostst-2010-presentations.html

[23] P.Thibaut, J.C.Poisson, E.Bronner, N.Picot: "Relative Performance of the MLE3 and MLE4 Retracking Algorithms on Jason-2 Altimeter Waveforms" (Marine Geodesy, 33(S1):317-335, 2010.)

[24] S. Philipps, M. Ablain, J. Dorandeu, P. Thibaut, N. Picot and J. Lambin. SSALTO CalVal performance assessment Jason-1 Gdr-B/GDR-A. Poster OSTST 2006, Venice.

[25] L.Amarouche, P.Thibaut, O.Z.Zanife, J.P.Dumont, P.Vincet, N.Steunou (2004): "Improving the Jason-1 Ground Retracking to Better Account for Attitude Effects." Marine Geodesy. Vol. 27,Iss 1-2,2004.

[26] G.Dibarboure, F.Boy, J.D.Desjonqueres, S.Labroue, Y.Lasnes, N.Picot, J.C.Poisson, P.Thibaut. "Investigating short wavelength correlated errors on low-resolution mode altimetry". Submitted to the Journal of Atmospheric and Oceanic Technology Submitted in April 2013.